JATROPHA WASTE MEAL AS AN ALTERNATIVE ENERGY SOURCE:

COMPLETE ANALYSIS FOR ITS ENERGY PRODUCTION

A Dissertation

by

JINJUTA KONGKASAWAN

Submitted to the Office of Graduate and Professional Studies of
Texas A&M University
in partial fulfillment of the requirements for the degree of

DOCTOR OF PHILOSOPHY

Chair of Committee,	Sergio C. Capareda
Committee Members,	Mahmoud M. El-Halwagi
	Gerald L. Riskowski
	Patricia K. Smith
Head of Department,	Stephen W. Searcy

December 2016

Major Subject: Biological and Agricultural Engineering

ABSTRACT

Agricultural waste is considered an alternative energy resource, in addition to raw biomass. Besides serving as an energy source, agricultural waste is environmental friendly and cost-effective. This study provided a complete analysis and conversion process of Jatropha de-oiled cake. Starting from the pyrolysis of the Jatropha waste, the pyrolysis products (liquid and solid) were upgraded into more valuable energy products using thermo-chemical and physico-chemical treatments.

Atmospheric pyrolysis of Jatropha residue yielded 12% of bio-oil, 24% of aqueous product, 38% biochar, and 15.7% syngas. The heating values of bio-oil, biochar, and gaseous product were obtained at 33, 28, and 1.2 MJ/kg, respectively. The properties of liquid product suggested the possibility to use it as biofuel but further upgrading process would be needed to improve the quality. Likewise, biochar, a carbon-rich material, was considered a precursor for the activated carbon production.

The response surface method was used to identify the effects of activation parameters (impregnation ratio, activation temperature, and time) on activated carbon yields and characteristics. Highest yield (69.8%) was achieved with the highest ratio between biochar and KOH (1.8) and lowest activation temperature (600^{o}C). The surface area of activated carbon was significantly improved from pyrolysis biochar (1.51 m^2/g). The optimum surface area of 285 m^2/g was achieved. The adsorption ability analysis showed that the activated carbon with highest surface area could remove 90.3% of Acetaminophen from the solution.

Fractional distillation of bio-oil revealed the effectiveness of removing the water from the bio-oil. The qualities of organic distillate fractions were significantly improved from the original bio-oil such as low moisture content, low acidity, and high heating value. However, the separation of aqueous phase indicated that the major compounds in the aqueous phase were water, oxygenates and nitrogenates. The catalytic hydrotreatment of bio-oil distillate using Pd/C as a catalyst showed an improvement in product qualities. The optimum condition was achieved at 200^{o}C with the highest upgraded bio-oil yield of 64.9%. The upgraded products from both fractional distillation and catalytic upgrading suggested a potential useful source of fuels.

The overall mass and energy conversion efficiencies for energy conversions process of Jatropha waste were achieved at 74.3% and 54.5%, respectively. The CO_2 emissions due to the electricity consumed during the productions of activated carbon, bio-oil distillate (BD1), and the hydrotreating distillate were found at 4.3, 0.43, and 1.8 g CO_2 de-oiled cake, respectively. The obtained positive NER and NEB values referred to the effectiveness and sustainability of the energy production system.

DEDICATION

To my ‘Owkusumsirisakul’ family, I could never have done this without your faith, support, and constant encouragement…

ACKNOWLEDGEMENTS

This dissertation would not have been completed without the support of many people. First of all, I would like to thank my advisor and committee chair, Dr. Sergio Capareda, for giving me the inspiration for this work and his helpful suggestions, guidance, and support throughout the course of this research. I also appreciate and thank my committee members, Dr. Mahmoud El-Halwagi, Dr. Gerald Riskowski, Dr. Patricia Smith and Dr. Calvin Parnell, for their valuable feedback and comments.

Deepest gratitude is also due to the Royal Thai Government for granting me financial support throughout my study. Special thanks also to my BETAzoids family for guiding me on all laboratory facilities and having patience answering my questions. I would be remiss without thanking my truly great friends in Thailand and here in College Station, especially for their encouragement and assistance in a number of ways. I am very much grateful to Detchat Samart for taking time to proofread an early version of this manuscript.

I would like to convey my thanks to the department faculty and staff, for making my time at BAEN and Texas A&M University a memorable experience. I also want to extend my gratitude to all teachers and students who were willing to participate in the study.

Last but not least, I wish to express a sense of gratitude and love to my beloved Owkusumsirisakul family for their understanding, encouragement, and endless patience when it was most required…

NOMENCLATURE

ANOVA	Analysis of Variance
DOD	Degree of Deoxygenation
FC	Fixed Carbon
GHG	Greenhouse Gas
HHV	Higher Heating Value
KOH	Potassium Hydroxide
MC	Moisture Content
NEB	Net Energy Balance
NER	Net Energy Ratio
TAN	Total Acid Number
VCM	Volatile Combustible Matter

TABLE OF CONTENTS

Page

LIST OF FIGURES

Page

LIST OF TABLES

1. INTRODUCTION

Energy is a crucial factor for the development of human civilization. It is the main input to almost all production and consumption activities [1]. With the rapid population and economic growth, the energy demand has been dramatically increasing year by year but not the energy resources [2]. Fossil fuels (i.e., oil, coal, natural gas) act as the main source to meet world energy consumption over other energy sources for many decades [3]. The replenishment rate of fossil source is significantly slower than the extracted rate, so it is predicted to be completely exhausted in the near future [4]. Due to the limited fossil fuel resources, the development of renewable energy is essential, as it is an alternative way for a fossil fuel substitution. Furthermore, renewable energy not only helps to fulfill the deficiency of fossil fuel but it is also environmental friendly and cost-effective [5,6].

Biomass is one source of renewable energy. Three main products can be obtained from biomass conversion process including transport fuel, power/heat generation, and chemical feedstock [7]. As of 2015, biomass meets around 10-14% of the global energy supply. Both purpose-grown biomass and waste-biomass can be considered for energy production [8]. The biomass-based fuel has been considered a better alternative because it is a clean, non-pollutant and renewable [9]. Nevertheless, the growth in agricultural production has been associated with many environmental problems. There are a lot of residues left behind after crop harvesting and processing, and this can pollute the environment if the waste is not managed properly. Utilization of by-products is

substantially required because it reduces waste products that may be harmful to the environment, increases the economic profit from the use of whole product chain, and is appropriate for the development of bio-based economies [10].

Agricultural and industrial residues such as husk, rice bran, rice straw, corn straw, corncob, bagasse, and de-oiled seed cakes can be utilized by the biomass-to-energy conversion processes [11-13]. There are many ways to turn biomass into energy products such as thermochemical process, biochemical process, and mechanical extraction. Different conversion technologies convert biomass into different energy products. Pyrolysis is one option among thermochemical conversion processes that turns biomass into three energy products i.e., biochar, bio-oil, and gaseous product. Researchers are still keeping on improving the biomass conversion system so that it could be used more widely and effectively.

Jatropha is a drought-resistant tropical tree with a minimum necessity of water compared to other fruit trees. It can be grown easily under various soil conditions with a capability to survive drought. It is spread in the wild and agricultural tropical zone of Central America, South America, Africa, India, South Eastern Asia, and Australia. The fruits can be harvested in the second year from establishment. The seed yields do not change a lot after the fourth or fifth year and the tree can live up to 50 years [14]. The annual seed production ranges from 0.1 t/ha to more than 8 t/ha depending on growing conditions. The toxins contained in Jatropha plant, such as phorbol esters, curcin, lectins, phytates, and trypsin inhibitors, make it unable to serve as food or feed animal without detoxification process [15].

Thailand is one of the agricultural producers which has a high potential for energy crop production. Although most of biodiesel production in Thailand comes from palm oil, Jatropha curcas L. is also considered as another promising oil seed plant [16]. The use of Jatropha as an alternative energy source was also investigated in many countries such as India [17], Malaysia [18], and China [19]. Jatropha seed has a very high oil content, which can be around 35-55 wt % of non-edible oil compared to other fruit seeds. In contrast with other oil plants, Jatropha oil has low acidity, good oxidation stability compared to soybean oil, low viscosity compared to Caster oil, and well cooling properties compared to palm oil [20,21]. The major fatty acids in Jatropha oil such as oleic and linoleic acids make it suitable for biodiesel production. The biodiesel produced from Jatropha oil via transesterification process had high qualities that passed the standards for vegetable oil-based fuels. It can be used directly or blended with the commercial diesel fuel in the diesel engine without any engine modification. Previous studies showed that Jatropha has a potential to serve as a fossil fuel substitute [22-28].

2. CHARACTERIZATION OF PRODUCTS FROM ATMOSPHERIC PYROLYSIS OF JATROPHA DE-OILED CAKE*

2.1. Introduction

Pyrolysis is a thermal cracking process that decomposes the organic feedstock in the absence of oxygen. The process temperature for pyrolysis ranges between 300 to 1200^{o}C. Pyrolysis turns biomass into three main products, the liquid bio-oil, solid biochar, and gaseous products [29]. This thermal conversion process is considered to be a potential option for waste management. The products obtained from pyrolysis can be used as feedstock to produce hydrocarbons which are the primary energy source for petroleum refineries or bio-refineries [30]. Moreover, pyrolysis has become an innovative option among the thermochemical methods due to its simple operation, its suitability as fuel for energy production and its uncomplicated reproduction [10,31-33].

After the oil extraction process, the remaining seedcake of Jatropha was found to be more than 50 wt% of input biomass. The residue still has a high value of volatile combustible matter and gross energy. Moreover, the Jatropha meal is a good source of protein and carbohydrates, but it cannot be used to feed animal because of some toxins remained in the seedcake. Therefore, pyrolysis is an interesting option for the waste utilization in order to turn it into the energy products [11,34-36].

---

*Part of this chapter is reprinted with permission from "J. Kongkasawan, H. Nam and S. C. Capareda. Jatropha waste meal as an alternative energy source via pressurized pyrolysis: A study on temperature effects," Energy, vol. 113, p. 631-642, October 2016" [37]

In previous work, the pyrolysis of Jatropha de-oiled cake was performed under elevated pressure [37]. However, the pyrolysis system for the pressurized condition needed an appropriate pressure sealing, which led to higher cost. In this paper, the pyrolysis was done under atmospheric condition using the operating temperature at the optimum condition from the previous study. The pyrolysis products obtained from atmospheric pyrolysis were investigated for their physical and chemical properties and compared with those from pressurized pyrolysis to determine the possibility of serving as an alternative energy source.

2.2. Materials and Methods

2.2.1. Jatropha de-oiled cake preparation and its characterization

Jatropha de-oiled cake used in this study was a residue left from the oil extraction process from the previous study. Jatropha curcas L. seeds were received from the farm in the Mexico. A screw press machine (HFG 505 WN) with 7 mm discharge nozzle diameter was used to extract the oil from Jatropha seeds. The extracted oil was recovered at 44 wt% of the input raw seed and converted into biodiesel [28]. The remaining de-oiled cake (54 wt%) was used as feedstock for the pyrolysis experiment. The Jatropha de-oiled cake was ground through a Wiley mill (Arthur A. Thomas Co., Philadelphia, PA) using 1.0 mm screen filter prior to pyrolysis. The ASTM E 1756 Standard Test Method for Determination of Total Solids in Biomass was selected to determine the moisture content. Jatropha de-oiled cake was also analyzed for its properties including heating value, proximate analysis and ultimate analysis. Gross heating value was

determined according to ASTM D 2015 using PARR Isoperibol Bomb Calorimeter Model 6200, made by Parr Instrument Company, Moline, IL. Proximate analysis was done in accordance with ASTM D 3172 and ASTM E 1755. The ultimate analysis of the sample was also determined based on ASTM D 3176 using Vario MICRO Elemental Analyzer manufactured by Elementar Analysemsysteme GmbH, Germany. The compositional analysis was also done according to NREL procedures such as (1) Preparation of samples for compositional analysis, (2) Determination of extractives in biomass, (3) Determination of structural carbohydrates and lignin in biomass, and (4) Determination of acid soluble lignin concentration curve by UV-Vis spectroscopy. The prepared biomass and extractives free biomass samples were sent to Soil, Water and Forage Testing Laboratory, Texas A&M University, for a protein content analysis.

2.2.2. Pyrolysis set-up

Pyrolysis runs were carried out using a bench-scale batch pressure reactor (Series 4580 HP/HT Reactors, Parr Instrument Company, Moline, IL) with automatic temperature controller (Series 4848, Parr Instrument Company, Moline, IL) as illustrated in Figure 2.1, which was previously used in the pyrolysis of rice straw study [38]. The batch reactor was equipped with a condenser connected directly to the head of the reactor. The condensed liquid products were collected in a cylinder, which was attached to the condenser. The condenser was equipped with an indirect heat exchange cooling jacket connected to a chiller containing $4^{o}C$ glycol water as a working fluid. The volume of the gas produced was measured using a gas flow meter (METRIS 250, Itron, Oweenton, KY) connected at the gas outlet of the reactor.

Approximately 200 g of the sample was placed in the reactor. Before starting each run, the reactor was purged with nitrogen for 15 min to make sure that the process operated in an absence of oxygen. The reactor controller and heater were then turned on along with an internal stirrer for mixing the sample in the reactor. The operating temperatures of pyrolysis for this study were chosen to be 500^{o}C. The reactor was heated until it reached the specified temperature. The run was performed under atmospheric condition, so the outlet valve of the reactor was fully opened during the run. When the desired temperature was achieved, the process continued to run for 20 min, and the gas produced was collected in a sampling bag for the gas composition analysis. After that, the reactor was allowed to cool down and the products were collected and weighed. The liquid product was collected from the cylinder below the condenser and the biochar was collected from the reactor for further analysis

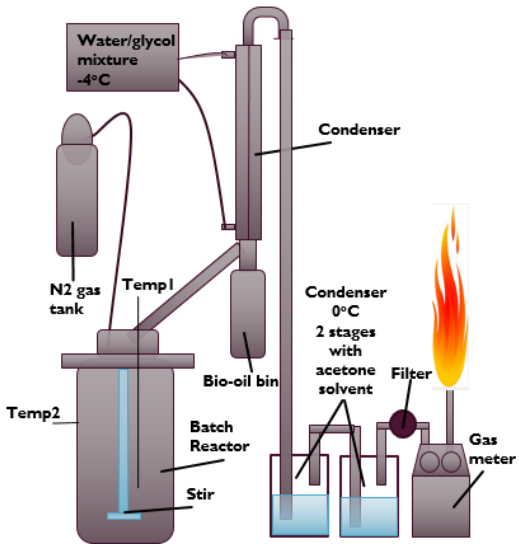

Figure 2.1. Pyrolysis set-up [38].

2.2.3. Pyrolysis products characterization

Pyrolysis products including bio-oil, biochar, and gaseous product were analyzed for their properties as described in the following sections:

2.2.3.1. Gross calorific value

The gross calorific values of bio-oil and biochar products were determined using PARR isoperibol bomb calorimeter in reference to ASTM D 2015. Solid products were ground with a Wiley mill using a 2 mm screen prior to the bomb calorimeter operation.

2.2.3.2. Proximate analysis and ash content

Proximate analysis is the measurement of moisture content (MC), volatile combustible matter (VCM), fixed carbon (FC), and ash content containing in biomass. Proximate analysis of the biochar was completed by following the ASTM standards (D 3172 and E 1755). The biochar obtained from pyrolysis experiment were hammer ground before conducting an analysis. The ash content of bio-oil was also determined according to ASTM D 0482-07.

2.2.3.3. Ultimate analysis

The ASTM standard (D 3176) was used to determine for the elemental composition of bio-oil and biochar using Vario MICRO Elemental Analyzer (Elementar Analysemsysteme GmbH, Germany). Then, the empirical formulas of bio-oil and biochar were calculated based on the elemental compositions (C, H, N, S, O) obtained from the ultimate analysis.

2.2.3.4. FTIR

A Shimadzu IRAffinity-1 FTIR (Fourier Transform Infrared) Spectrophotometer (Shimadzu, Inc.) was used to identify the existence of functional groups in the bio-oil.

2.2.3.5. Chemical composition (GC-MS)

The GC-MS analysis was used to identify the chemical composition of bio-oil. Dichloromethane (10%vol) was used to dilute the concentration of crude bio-oil before performing an analysis. The GC-MS system was performed on Shimadzu QP2010 with DB-5 ms column (25 m × 0.25 mm (i.d.), 0.25 mm film thickness). The injection temperature was 295^{o}C. Helium was used as a carrier gas with flow rate of 0.83 ml/min. The column temperature was held at 45^{o}C for 4 min, then heated up to 250^{o}C at rate of 5^{o}C/min and maintained at this temperature for 10 min. The ion source temperature was set at 250^{o}C with m/z ranging from 40 to 500.

2.2.3.6. Gas composition

The pyrolysis gas collected at different temperatures during the heating process was then analyzed for its composition by SRI Multiple Gas Analyzer #1 (MG#1) gas chromatograph (SRI GC, Torrance, CA). The detectors used in the analyzer were helium ionization detector (HID) and thermal conductivity detector (TCD). The columns for the syngas analysis were 60 Molecular Sieve 13X and 60 Silica Gel, with helium as the carrier gas. The calibration gas standard mixture consisted of H_2, N_2, O_2, CO, CH_4, CO_2 and C_2H_6 (Praxair Specialty Gases, Austin, TX) with an analytical accuracy of ±5%. The column temperature was initially set at 65^{o}C for 10 min before rising at a rate of 16^{o}C/min to 250^{o}C as a final temperature.

2.2.4. Mass and energy distribution

The product yields (wt%) from pyrolysis process were calculated using Equation 2.1. The amount of gas produced was measured in the form of gas volume; therefore, the mass of gas was calculated after the gas composition was determined. Equation 2.2 was used for mass of gas calculation under the assumption that the gas was collected at normal temperature and pressure (25^{o}C and 1 atm). The densities of each gas were obtained from the Handbook of Natural Gas Engineering [39]. Energy distribution of pyrolysis products were also determined using Equation 2.3.

$$\text{Product yield (\%wt)} = \frac{\text{Product weight}}{\text{Initial biomass weight}} \times 100 \quad (2.1)$$

$$\text{Mass of gas} = \frac{\text{Gas density} \times \text{Volume} \times \text{Gas fraction from GC}}{100} \quad (2.2)$$

$$\text{\%Energy recovery} = \text{Product yield (\%wt)} \times \frac{\text{HHV of product}}{\text{HHV of biomass}} \quad (2.3)$$

2.3. Results and discussion

2.3.1. Characteristics of Jatropha seed and de-oiled cake

The chemical properties of Jatropha seed and de-oiled cake are presented in Table 2.1 along with other non-edible de-oiled cakes. The HHV (higher heating value) of Jatropha de-oiled cake was lower than the raw seed, and higher than other non-edible seed cakes such as Pongamia and Neem. Moreover, the HHV was even higher compared to other waste biomass that can be used for energy conversion such as rapeseed oil cake (19.49) [36], corn stover (18.45) [40], sugarcane bagasse (15.08) [41], rice husk (16.8) [42], and cotton stalk (16.9) [43]. The results from proximate analysis showed an

increase in FC, and decrease in VCM and ash from raw seed to de-oiled cake due to the extracted Jatropha crude oil of 37.6 MJ/kg HHV [28]. The ultimate analysis also revealed the significant decrease in carbon content and increase in oxygen content, which resulted in lowering the heating value of the de-oiled cake. The heating value can also be calculated from elemental mass fractions in biomass (i.e., C, H, O, N, S) using Equation 2.4 (Boie's formula) [44]. The theoretical values were not much different from the values obtained from the experiment.

$$HHV\ (MJ/kg) = 0.3515C + 1.1617H + 0.06276N + 0.1046S - 0.1109O \quad (2.4)$$

The results from compositional analysis showed that the raw seed had high extractives (44.6%) due to a large amount of oil contained in the seed. The extractives of the de-oiled cake reduced to 20.4% after the oil extraction process. The inorganic compounds, nonstructural sugars, and nitrogen containing substances were present in water extractives whereas ethanol extractives contained chlorophyll, waxes, oils, and fats [29]. The sugar content was obtained by difference. The protein contents of the Jatropha seed and de-oiled cake were also high, which was related to the nitrogen content that existed in the biomass. The percent protein contents did not change much even after the oil extraction process.

Table 2.1. Characteristics of Jatropha raw seed and de-oiled cake, and other non-edible oil cakes.

Characteristics	Jatropha seed[a] [37]	De-oiled cake			
		Jatropha[a] [37]	Pongamia [45]	Mahua [46]	Neem [47]
Calorific value (MJ/kg)					
ASTM D 2015	24.0 ± 0.24	20.5 ± 0.40	17.65	21	18.2
Boie's equation	25.3 ± 0.78	18.2 ± 0.42	18.5[b]	19.8[b]	14.8[b]
Proximate analysis (wt%)					
Moisture	7.5 ± 0.12	6.5 ± 0.01	12.00	4.18	6.13
VCM	77.1 ± 0.95	73.0 ± 1.29	71.21	88.38	79.26
Fixed carbon	9.4 ± 0.53	11.3 ± 1.01	11.71	3.07	4.61
Ash	5.9 ± 0.55	9.2 ± 0.76	5.08	4.36	10.00
Ultimate analysis (wt%)					
C	53.7 ± 0.79	43.3 ± 0.56	47.11	49.65	42.5
H	8.0 ± 0.02	5.8 ± 0.04	5.63	5.71	4.5
N	4.5 ± 0.23	5.0 ± 0.46	0.27	3.34	1.9
S	-	-	-	0.61	1.3
O (by difference)	27.9 ± 0.69	36.7 ± 0.48	41.91	40.69	49.8
Chemical Formula	$CH_{1.79}O_{0.39}N_{0.07}$	$CH_{1.61}O_{0.63}N_{0.10}$	$CH_{1.43}N_{0.005}O_{0.67}$ [b]	$CH_{1.379}N_{0.0576}S_{0.004}O_{0.614}$	$CH_{1.275}N_{0.0375}S_{0.011}O_{0.878}$
Compositional analysis (wt%)					
Extractives	44.6	20.4	-	-	-
Water	15.5	13.5	-	-	-
Ethanol	29.1	6.9	-	-	-
Lignin	26.1	39.2	-	-	-
Acid insolubles	14.8	20.7	-	-	-
Acid solubles	11.3	18.5	-	-	-
Sugars	3.7	16.1	-	-	-
Protein	25.6	24.3	-	-	-

[a] From experiment

[b] Calculated from original work

2.3.2. Product yields

The pyrolysis yields in this study (atmospheric condition) were shown in Figure 2.2 in comparison with the yields from pressurized pyrolysis (100 psi) at 500^{o}C, as reported in the previous study [48]. Biochar yielded the highest amount among all products for both atmospheric (38.1%) and pressurized (40.3%) pyrolysis. Atmospheric pyrolysis yielded more liquid product (bio-oil and aqueous) than pressurized pyrolysis. On the other hand, the biochar and gaseous product yields from atmospheric condition were lower than ones from pressurized pyrolysis. More volatiles were apparently released at high pyrolysis temperatures (< 500^{o}C), which led to the reduction in biochar yield. However, under the pressurized condition, higher concentrations of pyrolytic volatiles could improve the secondary cracking of volatiles and residence time of tar vapors. This resulted in higher gas formation and enhancement of biochar production through the decomposition of vapors into carbonaceous material [49-50]. Mok and Antal [51] also supported the effect of operating pressure on pyrolysis biochar yield. The elevated pressure during pyrolysis of cellulosic biomass reduced the heat of reaction, thus increased biochar yield. In addition, the reduction in liquid product yield from pressurized pyrolysis could be due to the formation of incondensable gaseous components as it was held captive inside the reactor to maintain the pressurized condition. Previous studies on pressure effects on pyrolysis yields also showed the same trend such as *Nannochloropsis oculata* [52], scrap tire [53], and acacia wood [54].

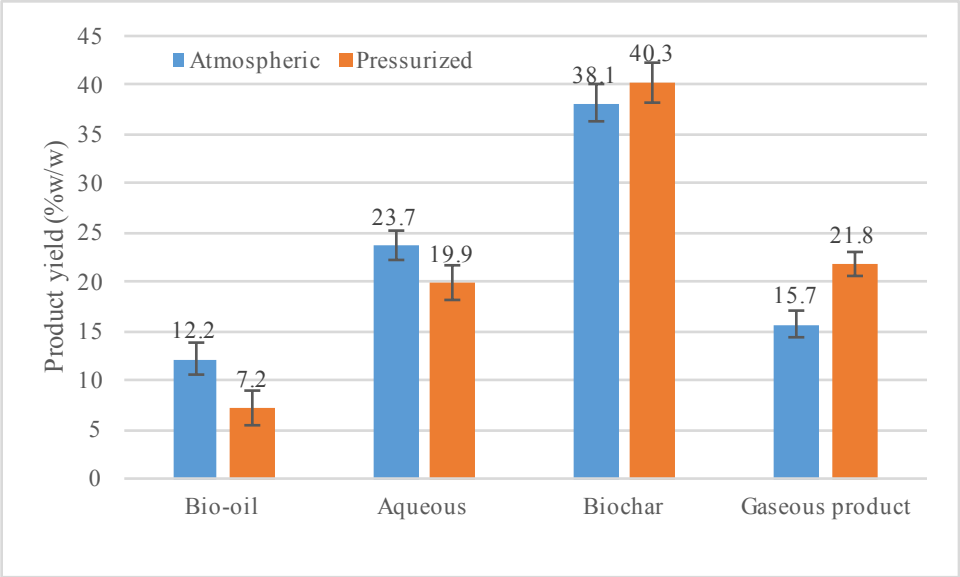

Figure 2.2. Product yields of atmospheric and pressurized pyrolysis.

2.3.3. Product properties

Bio-oil, biochar and gaseous products in this study were obtained from the pyrolysis experiment at atmospheric condition. All products were analyzed for their chemical properties such as energy content, moisture content, and component elements.

2.3.3.1. Biochar

After the pyrolysis process was completed, the solid product or biochar was collected from the reactor where the initial biomass was placed. The biochar was first analyzed for the proximate analysis (VCM, FC, and ash). VCM is strongly related to the thermal conversion process since it creates more combustible gases during the process while FC is the remaining solid combustible residues after the volatile matter is released. The proximate analysis of Jatropha de-oiled cake, biochar obtained at atmospheric condition and at 100 psi were compared as shown in Figure 2.3

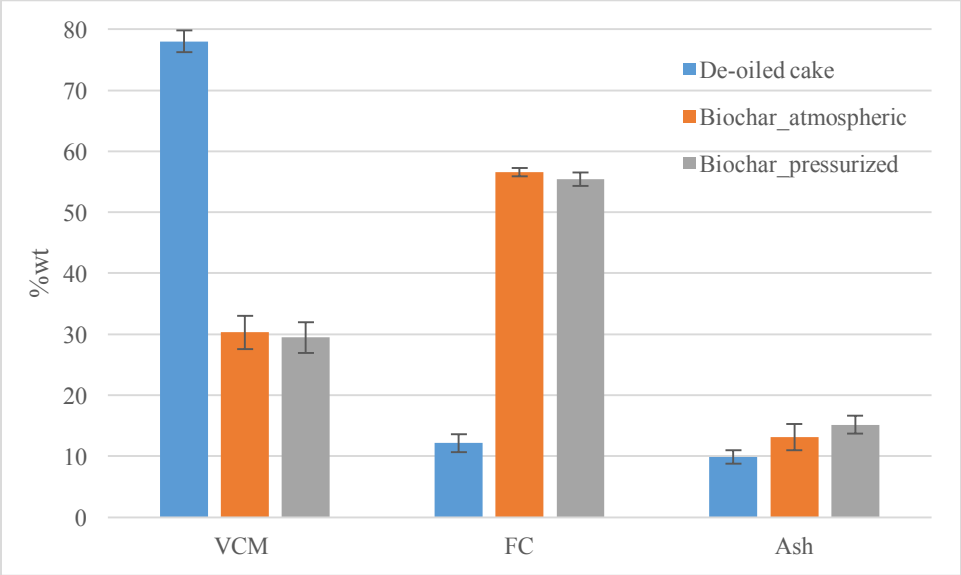

Figure 2.3. Proximate analysis of de-oiled cake and biochar from atmospheric and pressurized pyrolysis.

The decomposition of lignin started at relatively low temperatures of 200-275^{o}C and the significant decomposition occurred at around 400-500^{o}C. This led to the release of volatile components, which left behind the carbon-rich solid, biochar [55]. According to the graph, the VCM of the seedcake significantly dropped from 78% to around 30% with a substantial increase of FC from 12% to approximately 55% after the pyrolysis process. Biomass rather released more volatiles at higher temperatures, which led to the reduction in VCM from the de-oiled cake. Meanwhile, the FC was the remaining solid combustible residue after VCM was discharged. Therefore, the FC content in the biochar had a significant rise compared to the de-oiled cake.

The ash content significantly increased from de-oiled cake to biochar. Moreover, statistical analysis by ANOVA also confirmed that the operating pressure had an effect

on the ash content of biochar (p-value < 0.001) but not the VCM and FC. The biochar obtained at atmospheric condition had lower ash content than that from pressurized pyrolysis. The volatilization of sulfur, but not the inorganic compounds, during heating contributed to the increase of ash content [56]. Whitty et al. [57] also observed an increase of sulfur released with pressure during the pyrolysis experiment. High ash content is not preferable since it could result in the reduction of heating value of energy products.

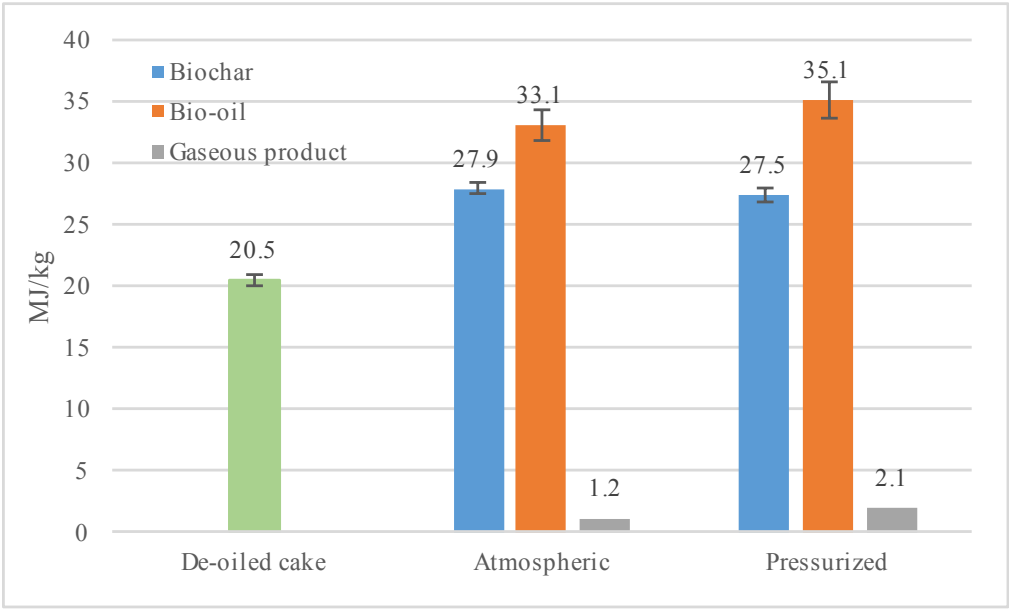

Figure 2.4. Energy content of de-oiled cake and products from atmospheric and pressurized pyrolysis.

Figure 2.4 shows the heating values of the Jatropha de-oiled cake and the pyrolysis products. The gross calorific value of the biochar was significantly improved

from the de-oiled cake (20.5 MJ/kg). This could be described by the carbonization during pyrolysis process that converted biomass into a solid residue abundant in carbon content (i.e., biochar). The heating value of biochar obtained from atmospheric pyrolysis was slightly higher than that from pressurized pyrolysis. This could be explained by more liberation of VCM occurred at elevated pressure, which lowered the HHV of the biochar. In addition, a small difference on the HHV of biochar and bio-oil according to the pressure effect can be supported by the chemical analysis discussed in the following sections.

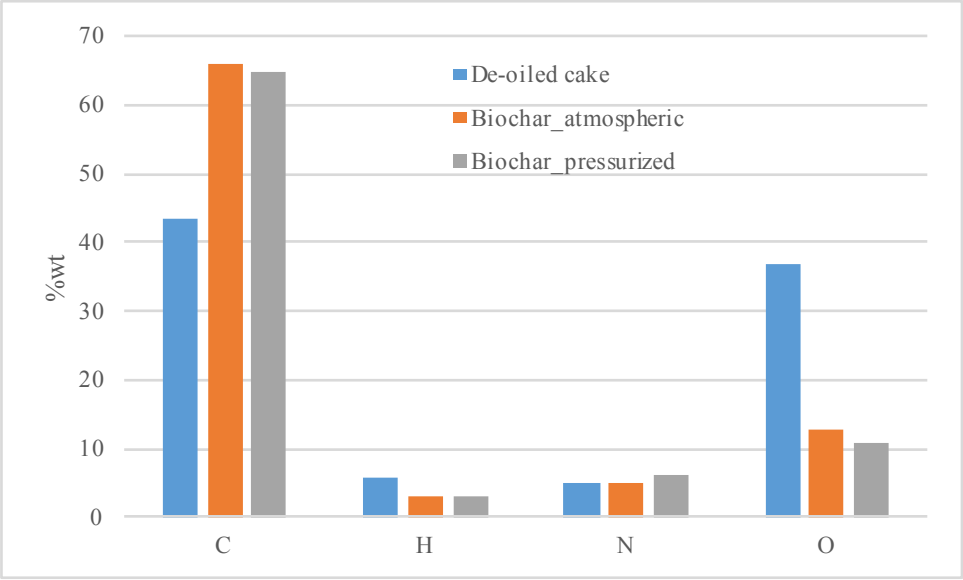

Figure 2.5. Ultimate analysis of de-oiled cake and biochar from atmospheric and pressurized pyrolysis.

The elemental compositions of the biochar obtained from atmospheric and pressurized pyrolysis were completed in comparison with the de-oiled cake as

demonstrated in Figure 2.5. The major differences between the de-oiled cake and biochar were carbon and oxygen contents, while nitrogen content was a minor difference, as shown in the graph. The oxygen and hydrogen content of the de-oiled cake diminished with the rise in carbon content after pyrolysis. The carbon content of the de-oiled cake increased from 43% to around 65%, while the oxygen content reduced from 37% to around 10%. The results proved that the deoxygenation occurred during the thermal decomposition of biomass, which relates to an increase in carbon content from the de-oiled cake to the biochar.

Biochar obtained from non-pressurized pyrolysis had higher carbon and oxygen content, and lower nitrogen content than that from pressurized pyrolysis. The trend of carbon content also corresponded to the amount of FC found from the proximate analysis as described earlier. The empirical formulas of de-oiled cake and biochar from atmospheric and pressurized pyrolysis were calculated to be $CH_{1.61}O_{0.63}N_{0.10}$, $CH_{0.55}O_{0.15}N_{0.06}$, and $CH_{0.57}O_{0.13}N_{0.08}$, respectively. The empirical formulas of biochar showed the reduction of H, O, and N components from the de-oiled cake. This could be explained by the secondary reactions and thermal decomposition of the pyrolysis process, which led to the release of nitrogen components into the gases of HCN, NH_3, and HNCO [58,59]. The HHV of biochar at different pressure conditions can also be explained by the elemental compositions according to Boie's formula (Equation 2.4). High amounts of carbon content led to an increase of HHV. On the other hand, high amounts of oxygen content resulted in a reduction of HHV. However, the coefficient of carbon (0.35) was higher than oxygen (0.11). Therefore, the biochar obtained from non-

pressurized pyrolysis with higher carbon and oxygen contents still had higher HHV than one from pressurized pyrolysis.

The Van Krevelen diagram can be constructed by calculating the H:C and O:C ratios of each sample as demonstrated in Figure 2.6. The Jatropha de-oiled cake fell into the region where most biomass was found, while biochar obtained from both atmospheric and pressurized pyrolysis was located in the coal area. The H:C and O:C ratios of the biochar were found to be around 0.6 and 0.1, respectively. Similar results of the biochar characteristics were also found with pyrolysis of different feedstock such as corn stover [60], wheat straw [61]*, and Pongamia pinnata* de-oiled cake [62]. Nam et al. [38] also reported similar ranges of O:C and H:C ratios of rice straw pyrolysis from a batch reactor. The bio-oil and biochar regions indicated in Figure 2.6 were based on different feedstocks of rice straw, sorghum, switchgrass, algae, and corncob. They also reported that the O:C ratios varied depending on reactor types of a batch, an auger, and a fluidized bed. The carbon to carbon bonds had greater energy than carbon-oxygen and carbon-hydrogen bonds. The lower O:C ratio was preferable to obtain a higher energy value [8]. Therefore, the reduction in the O:C ratio of the biochar led to an increase in heating values. The properties of biochar such as high carbon content and reasonable heating value made it appropriate for making an activated carbon or using as a fuel substitute.

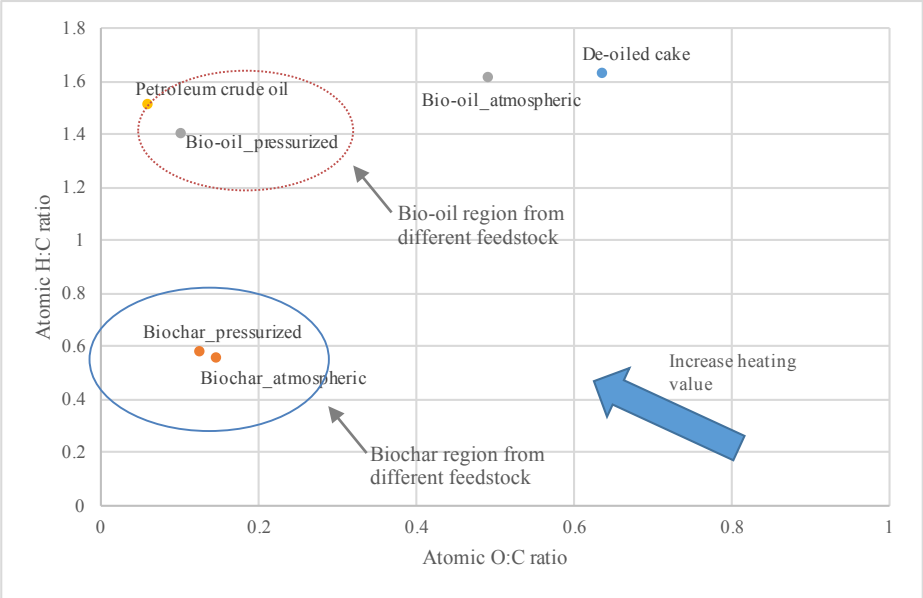

Figure 2.6. Van Krevelen diagram of de-oiled cake and pyrolysis products from atmospheric and pressurized pyrolysis, petroleum crude oil adapted from [63], and the bio-oil and biochar region from a batch reactor adapted from [38].

2.3.3.2. Liquid product

The produced heavy volatiles were condensed and formed into a liquid product, which comprised of two phases in separated layers (bio-oil and aqueous phases). The bio-oil was a black viscous smoky oil with a very strong irritating smell, while the aqueous phase was a slightly cloudy yellow-brown solution. The amount of aqueous phase presented in liquid product affected its energy content. Thus, the separation of bio-oil from liquid product resulted in a greater heating value.

The gross heating values of the bio-oil obtained from atmospheric and pressurized pyrolysis are illustrated in Figure 2.4. The bio-oil produced from atmospheric pyrolysis had a heating value of 33.1 MJ/kg which was significantly lower

than the one from pressurized pyrolysis (35.1 MJ/kg). However, the heating value of the bio-oil was considerably greater than the Jatropha de-oiled cake and was the highest among all pyrolysis products. The gross heating values of bio-oil obtained from the current experiment (slow pyrolysis) were much higher than the reported heating values of pyrolysis from Jatropha residue using a fluidized bed [30,64]. These experimental values were also higher than the pyrolytic oil from other biomass residues such as sunflower cake [35], sesame cake, mustard cake [47], and olive waste [65]. The ash content of the bio- oil was found to be around 0.2%.

Figure 2.7 compares the elemental composition of liquid product from atmospheric and pressurized pyrolysis. Carbon content was the major composition found in bio-oil from both conditions. However, the carbon content of bio-oil from atmospheric was found at around 52% which was considerably lower than the bio-oil from pressurized pyrolysis (71%). Moreover, the oxygen content of bio-oil from atmospheric condition (34%) was a lot higher than that from the pressurized condition (9.7%). Moisture contents of bio-oil were obtained at 8.2% for atmospheric condition and 0.6% for the pressurized condition, which related to the amount of oxygen content found in bio-oil.

Higher carbon content with lower oxygen content found in bio-oil resulted in higher heating value of bio-oil from pressurized pyrolysis than that from atmospheric condition. High oxygen content in the bio-oil was undesirable since it would lower the energy content and lead to the instability of the bio-oil. The results from the ultimate analysis showed that more than 70% of oxygen was contained in the aqueous layer of the

liquid product from both pyrolysis conditions. This suggested a high amount of water present in the aqueous phase. The moisture content of the aqueous phase was found to be around 67%.

A high amount of carbon content is preferable since it results in higher heating value. Therefore, the heating value of bio-oil from pressurized pyrolysis was higher than that from atmospheric pyrolysis. Maguyon [52] also reported similar trends of carbon content and the heating values of bio-oil obtained from both pressurized and atmospheric pyrolysis. The elevated pressure during the pyrolysis process could lead to the secondary reactions. This might eliminate more heteroatoms (O and N) from the bio-oil. The chemical formulas of the bio-oil and aqueous products were found to be $CH_{1.61}O_{0.49}N_{0.10}$ for atmospheric bio-oil, $CH_{1.39}O_{0.10}N_{0.12}$ for pressurized bio-oil, $CH_{16.3}O_{6.10}N_{0.48}$ for atmospheric aqueous product, and $CH_{21.1}O_{11.1}N_{1.16}$ for pressurized aqueous product.

According to the Van Krevelen diagram (Figure 2.6), the O:C ratio of the bio-oil obtained from pressurized pyrolysis was notably lower than that from atmospheric pyrolysis, which indicated the better heating value of the product. The bio-oil from pressurized pyrolysis was located near the petroleum crude oil area and in the same area where a bio-oil region produced from a batch type reactor as reported by [38]. However, the bio-oil obtained from atmospheric pyrolysis was located out of those ranges. The result from the ultimate analysis showed the significant differences of carbon and oxygen content between bio-oil from atmospheric and pressurized pyrolysis. Therefore, this suggested the further upgrading process to improve the quality of bio-oil to be used as fuel replacement by reducing the oxygen content.

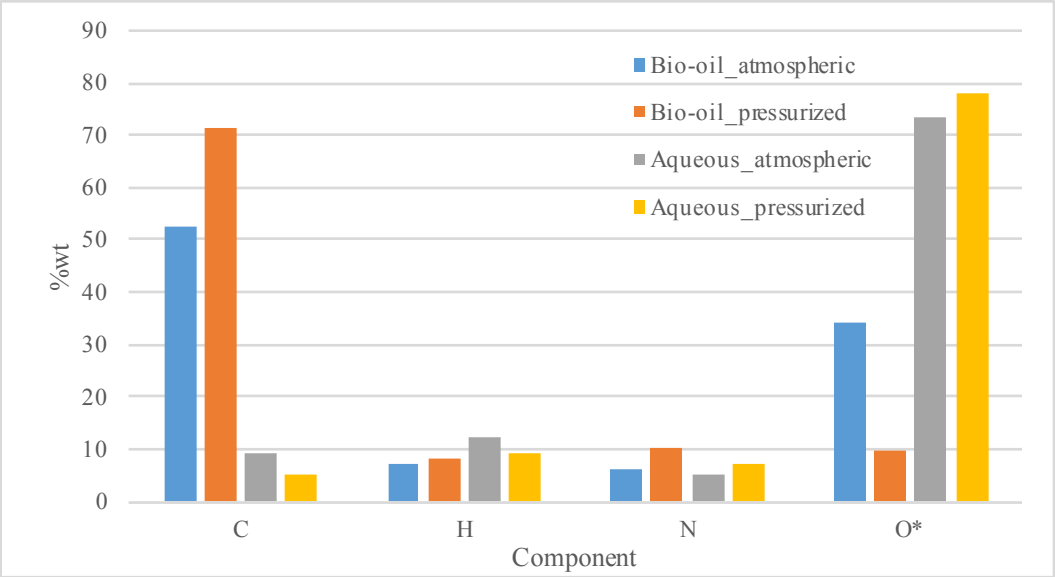

Figure 2.7. Ultimate analysis of liquid product from atmospheric and pressurized pyrolysis.

The functional groups presented in liquid product from atmospheric pyrolysis were analyzed using FTIR spectroscopy and compared with that from pressurized pyrolysis as demonstrated in Figure 2.8. According to the diagram, the FTIR spectra of the liquid product (i.e., aqueous and bio-oil phases) at different operating pressures appear to be similar. The dominant peak of the aqueous fraction at 3640-3200 cm^{-1} referred to the O-H stretching vibrations and H-bonded, which suggested the presence of phenols, alcohols, or water. High absorbance intensity of this peak supported a large amount of water present in the aqueous phase. The peaks within this range were also observed in bio-oil phases with a small absorbance intensity. In the bio-oil phase, it can be observed the absorbance peak at 3000-2850 cm^{-1}, which indicated alkanes group for C-H stretching vibrations. Furthermore, C-H stretch off C=O vibrations at 2850-2800

cm^{-1} suggested the existence of aldehydes. The peak observed in the 2300-2200 cm^{-1} range suggested the presence of nitrile compounds. C=O stretching vibrations found in the range of 1760-1665 cm^{-1} can be due to carbonyls, carboxylic acids, esters, aldehydes and ketones. The C-C stretching vibrations at 1600-1400 cm^{-1} designated the presence of aromatics. The peak at 1000-900 cm^{-1} for =C-H bending indicated the alkene group and the peak observed at 725-720 cm^{-1} specified the alkane group existed in bio-oil.

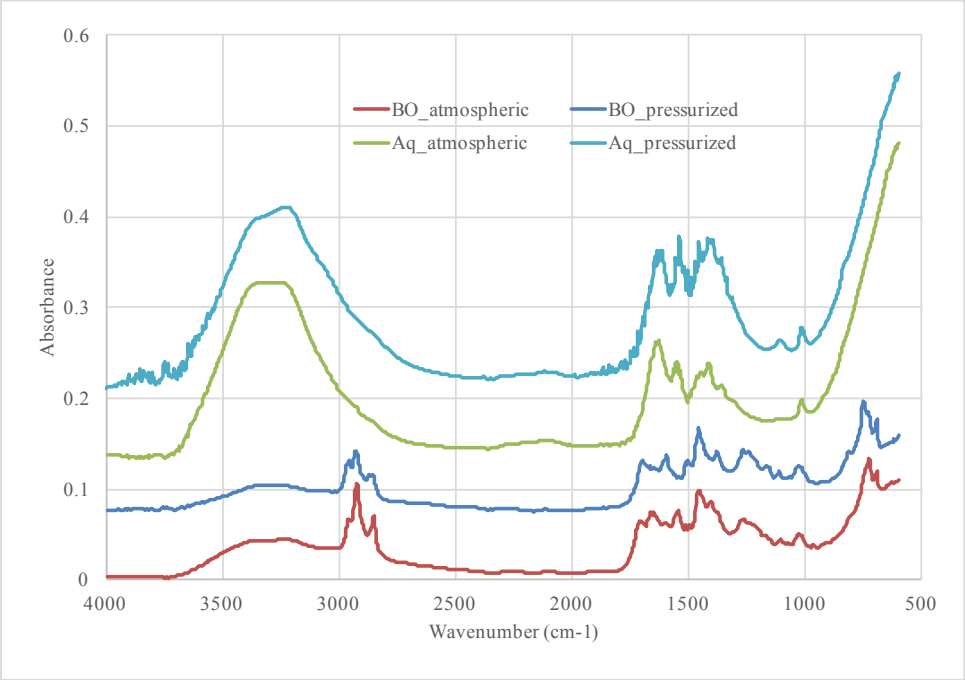

Figure 2.8. FTIR spectra of aqueous (Aq) and bio-oil (BO) from atmospheric and pressurized pyrolysis.

Liquid product obtained from atmospheric pyrolysis were then analyzed for the chemical compositions using GC-MS. Figure 2.9 demonstrates the percent relative

content of chemical compounds present in liquid product (bio-oil and aqueous phase) obtained from atmospheric pyrolysis and compares with the bio-oil obtained from pressurized pyrolysis. The compounds were classified into each chemical groups. The bio-oil from atmospheric pyrolysis consisted of 42.6% of hydrocarbons, which were mostly paraffin (15.9%) and aromatics (14.7%). The amount of hydrocarbons contained in atmospheric bio-oil was higher than that from pressurized pyrolysis (34.8%). The oxygen and nitrogen containing compounds in atmospheric bio-oil were also lower than the pressurized bio-oil.

Phenol was one of the main compounds found in the liquid product. The phenolic compounds found in the bio-oil was a result of a lignin contained in the de-oiled cake. Murata et al. [66] also reported phenols as the main compounds found in the Jatropha bio-oil. Bio-oil containing high amounts of phenolic compounds had become an interest because of the introduction of petroleum-based phenol after the segregation of phenols from bio-oil [67]. On the other hand, high oxygen content in the bio-oil would reduce the energy density, increase the acidity, and lower the miscibility with hydrocarbon fuel [68]. According to the aqueous product, the major components found were nitrogen-containing aromatic rings, oxygen and nitrogen containing compounds with some small amount of hydrocarbons. The presence of nitrile group in the liquid product was due to high amount of protein contained in Jatropha de-oiled cake (24.3%). The high amount of oxygenated compounds (phenols, ketones, carboxylic acids, and aldehydes) and some nitrogenous substances indicated bio-oil required further upgrading process to remove these un- wanted compounds and make it suitable to use as transport fuel.

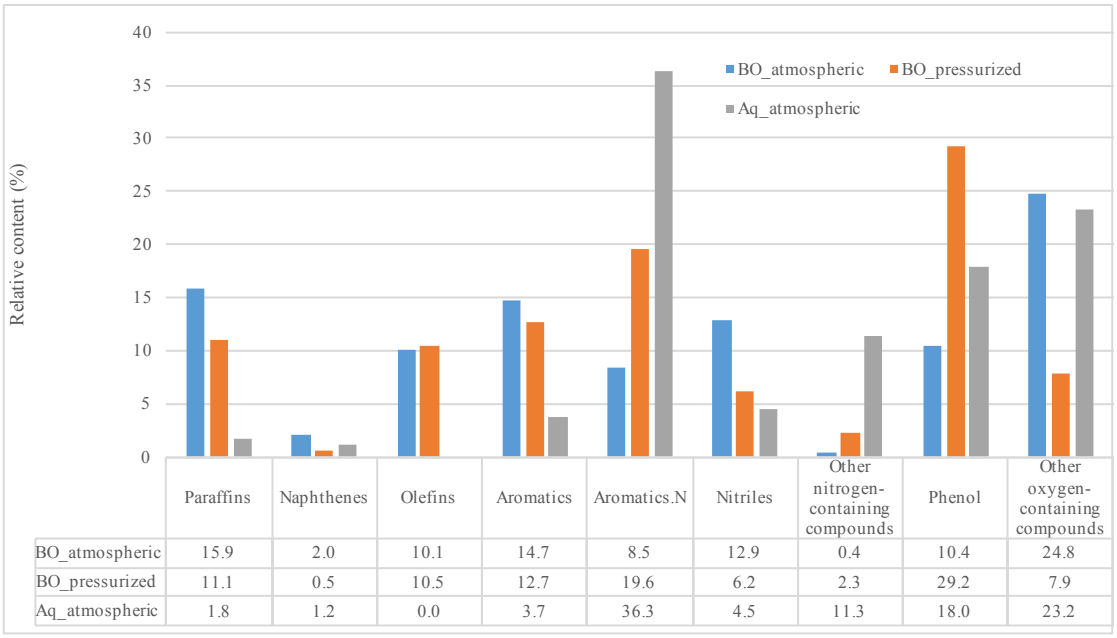

	Paraffins	Naphthenes	Olefins	Aromatics	Aromatics.N	Nitriles	Other nitrogen-containing compounds	Phenol	Other oxygen-containing compounds
BO_atmospheric	15.9	2.0	10.1	14.7	8.5	12.9	0.4	10.4	24.8
BO_pressurized	11.1	0.5	10.5	12.7	19.6	6.2	2.3	29.2	7.9
Aq_atmospheric	1.8	1.2	0.0	3.7	36.3	4.5	11.3	18.0	23.2

Figure 2.9. Functional groups present in liquid product from atmospheric pyrolysis and bio-oil from pressurized pyrolysis.

Table 2.2 and Table 2.3 shows the relative percentages of chemical compounds for the liquid product (i.e., bio-oil and aqueous) obtained from atmospheric pyrolysis. More than 100 chemical compounds were detected from the GC-MS. Paraffins and aromatics were the highest components found in bio-oil while the aqueous product contained mostly (N)-containing aromatics and (O)-containing compounds. Phenol was also one of the main components found in both bio-oil and aqueous phase with 2-methoxy phenol as the highest compound. It was reported that most lignocellulosic biomass produced phenol as a major composition [60,69]. The carbon ranges of aliphatic compounds found in bio-oil were C_7-C_{17}. These compounds made the bio-oil became more interesting source of energy. The results from the GC-MS was in agreement with the FTIR results.

Table 2.2. Chemical compositions of bio-oil from atmospheric pyrolysis.

Compounds	Relative content (%)	Compounds	Relative content (%)
Paraffin	**15.85**	**Napthene**	**2.04**
Hexadecane	4.23	Cyclopropane, 1-heptyl-2-methyl-	1.65
Octane	2.05	Cyclopropane, 1-ethyl-2-heptyl-	0.39
Nonane	1.85		
Decane	1.57	**Olefin**	**10.05**
Heptadecane	1.34	1-Octene	1.26
Undecane	1.30	3-Hexadecene, (Z)-	1.25
Tridecane	1.10	1-Undecene	1.18
Heptane	1.06	9-Octadecene, (E)-	1.06
Tetradecane	0.97	1-Heptene	0.91
Tetracosane	0.27	8-Heptadecene	0.87
Heptane, 3-ethyl-2-methyl-	0.11	1-Pentadecene	0.71
		1-Undecene, 10-methyl-	0.67
Aromatic	**14.67**	1-Dodecene	0.66
Toluene	8.33	1-Tridecene	0.42
Ethylbenzene	2.28	2-Octene, (E)-	0.27
Benzene, butyl-	0.90	2-Decene, (Z)-	0.22
Benzene, 1,3-dimethyl-	0.60	3-Nonene, (E)-	0.18
Benzene, propyl-	0.49	2-Octene	0.16
Benzene	0.47	1-Heptadecene	0.12
Benzene, pentyl-	0.43	7-Tetradecene, (E)-	0.11
Benzene, 1-ethenyl-2-methyl-	0.35		
Indane	0.23		
Benzene, 1,3,5-trimethyl-	0.21		
Benzene, (1,2-dimethylpropyl)-	0.20		
Benzene, 1-ethyl-3-methyl-	0.18		

Table 2.2. continued

Compounds	Relative content (%)	Compounds	Relative content (%)
(N)-containing Aromatic	**8.50**	**Phenol**	**10.44**
Pyrrole	2.66	Phenol, 2-methoxy-	3.29
Indole	1.54	Phenol	1.98
Aniline	1.28	Phenol, 4-methyl-	1.89
1H-Pyrrole, 2,5-dimethyl-	0.82	Phenol, 4-ethyl-2-methoxy-	0.93
1H-Pyrrole, 1-methyl-	0.76	Phenol, 2-methoxy-4-methyl-	0.56
1H-Pyrrole, 2-ethyl-4-methyl-	0.66	Phenol, 2-methyl-	0.50
Benzenepropanenitrile	0.30	Phenol, 3,5-dimethyl-	0.47
1H-Pyrrole, 3-methyl-	0.23	Phenol, 4-ethyl-	0.42
1H-Pyrrole, 2-ethyl-	0.14	Phenol, 2,6-dimethoxy-	0.40
Pyrrolidine, 1-(1-oxo-9-octadecenyl)-, (Z)-	0.11		
		Other (O)-containing	**24.79**
Nitrile	**12.91**	Oleic Acid	7.23
Hexadecanenitrile	5.73	9-Octadecenamide, (Z)-	3.73
Oleanitrile	4.71	9-Octadecenoic acid (Z)-, methyl ester	3.61
Pentanenitrile, 4-methyl-	0.99	Hexadecanamide	2.69
Butanenitrile, 3-methyl-	0.64	N-Methyldodecanamide	2.23
Octanenitrile	0.49	Hexadecanoic acid, methyl ester	1.81
Hexanenitrile	0.18	9,12-Octadecadienoic acid (Z,Z)-, methyl ester	1.16
Butanenitrile	0.17	Octadecanoic acid, methyl ester	0.91
		Octadecanamide	0.68
Other (N)-containing	**0.43**	Furan, 2,5-dimethyl-	0.44
Propane, 2-methyl-2-nitro-	0.43	2-Cyclopenten-1-one, 2,3-dimethyl-	0.30

Table 2.3. Chemical compositions of aqueous phase from atmospheric pyrolysis.

Compounds	Relative content (%)	Compounds	Relative content (%)
Paraffin	**1.77**	**(N)-containing Aromatic**	**36.26**
Decane, 2,9-dimethyl-	0.68	Pyrrole	15.53
Hexadecane	0.43	Pyrazine, methyl-	3.38
Nonane	0.42	Pyrazine, 2,6-dimethyl-	3.22
Octane	0.24	Pyridine	3.06
		1H-Pyrrole, 1-methyl-	2.06
Aromatic	**3.71**	Pyrazine, ethyl-	1.98
Ethylbenzene	1.86	Pyridine, 2-methyl-	1.97
Toluene	1.85	5,10-Diethoxy-2,3,7,8-tetrahydro-1H,6H-dipyrrolo[1,2-a	1.33
		Pyrazine, 2-ethyl-6-methyl-	1.27
napthene	**1.21**	Pyrrolidine, 1-acetyl-	1.01
Cyclobutane, 1,2,3,4-tetramethyl-	1.21	Pyrazine, 3-ethyl-2,5-dimethyl-	0.71
		Pyrrolo[1,2-a]pyrazine-1,4-dione, hexahydro-3-(2-methylpropyl)-	0.58
Nitrile	**4.53**	Pyridine, 2,6-dimethyl-	0.16
Butanenitrile, 3-methyl-	1.46		
Butanenitrile	1.07	**Other (N)-containing**	**11.32**
Pentanenitrile, 4-methyl-	0.95	2,5-Pyrrolidinedione, 1-methyl-	5.55
Isobutyronitrile	0.55	Silanediamine, 1,1-dimethyl-N,N'-diphenyl-	3.63
Butanenitrile, 2-methyl-	0.5	2-Furanmethanamine, tetrahydro-	2.14

Table 2.3. continued

Compounds	Relative content (%)	Compounds	Relative content (%)
Phenol	**17.96**	**Ketone**	**16**
Phenol, 2-methoxy-	10.4	2-Buta+A32:B39none2-Butanone	4.44
Phenol	3.2	2-Cyclopenten-1-one, 2-methyl-	2.03
Phenol, 2,6-dimethoxy-	1.67	Cyclopentanone	2.03
Phenol, 2-methoxy-4-methyl-	1.43	2-Cyclopenten-1-one, 3-methyl-	1.7
Phenol, 4-ethyl-2-methoxy-	0.65	Ethanone, 1-(2-furanyl)-	1.66
Phenol, 2-methyl-	0.61	2-Cyclopenten-1-one, 2,3-dimethyl-	1.43
		Ethanone, 1-(1H-pyrrol-2-yl)-	1.34
Other (O)-containing	**7.24**	2-Pentanone	0.66
9-Octadecenoic acid (Z)-, methyl ester	0.36	2-Butanone, 3-methyl-	0.46
9-Octadecenoic acid, methyl ester, (E)-	0.51	(R)-(+)-3-Methylcyclopentanone	0.25
Hexadecanoic acid, methyl ester	0.49		
2-Furanmethanol	4.29		
2-Furanmethanol, tetrahydro-	0.75		
Furan, tetrahydro-	0.84		

2.3.3.3. Gaseous product

During the heating process of pyrolysis run, the gaseous product was collected at different temperatures before it reached 500^{o}C. Then, the gas samples were analyzed for their composition using a GC. Figure 2.10 shows the concentration (%v/v) of each gas components at different temperatures. Different amounts of combustible gases such as hydrogen, carbon monoxide, and hydrocarbons (methane, ethylene, ethane, propene, and propane) were generated from the pyrolysis process over temperatures. It can be observed that CO_2 decreased while combustible gases increased with an increase of temperatures during the pyrolysis run. Many studies also observed the increase of hydrogen and hydrocarbons with the decrease of carbon dioxide as the pyrolysis temperatures increased [38,52,60]. The secondary thermal cracking of volatiles resulted in the release of hydrogen and hydrocarbon gases at a higher temperature [60]. The amount of carbon dioxide produced decreased with an increase of pyrolysis temperature because carbon dioxide was rather released at low temperature. In addition, the discharge of CO_x gases was a result of oxygenated compounds contained in biomass through decarboxylation [36,70].

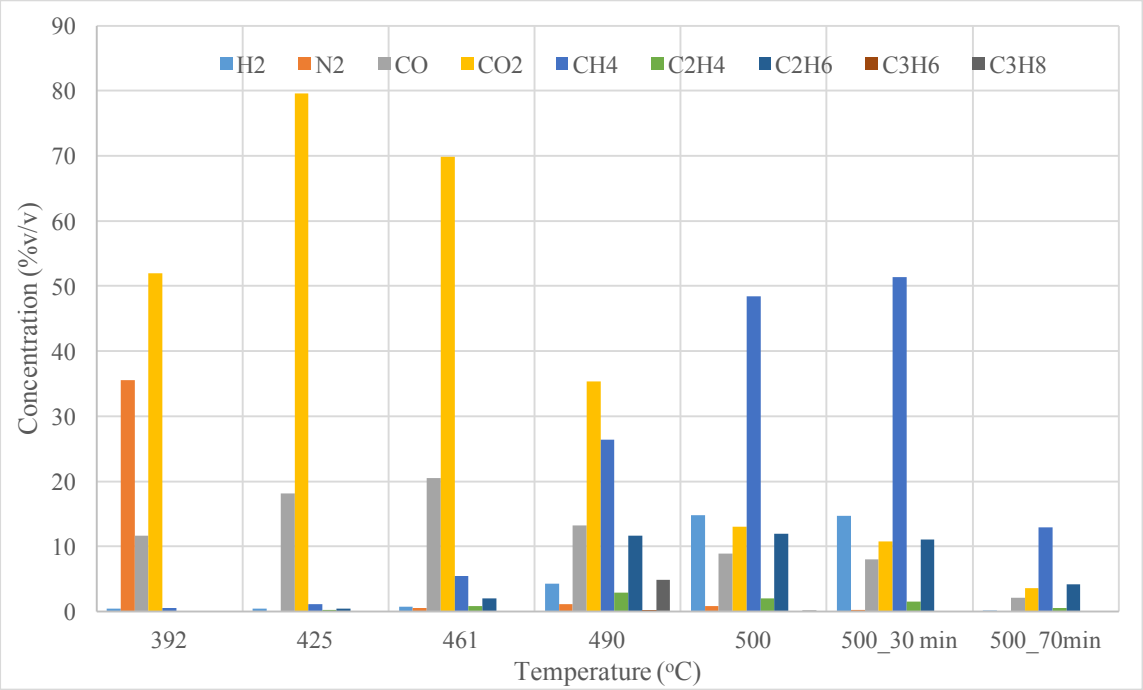

Figure 2.10. Gas compositions generated during the pyrolysis heating process.

The combustible gases were mostly generated at 490-500°C and were maximized after maintaining the temperature at 500°C for 30 min. This could be explained by more vapors cracking occurred at higher temperatures which formed the incondensable gaseous product [71]. Among all combustible gases, the highest amount of the gas produced came from methane. It was reported that methane was likely to generate at the temperatures between 480-520°C [72], which agreed with the results obtained from this experiment. However, only small amount of combustible gases were generated after maintaining the temperature at 500°C for 70 min. Figure 2.11 compared the gross heating values of each gas components of the gaseous product generated from atmospheric and pressurized pyrolysis. The pressurized pyrolysis yielded 2.1 MJ/kg

while the atmospheric pyrolysis yielded 1.2 MJ/kg of gaseous product. For both atmospheric and pressurized pyrolysis, the total energy of pyrolysis gas came mostly from methane, ethane and propane.

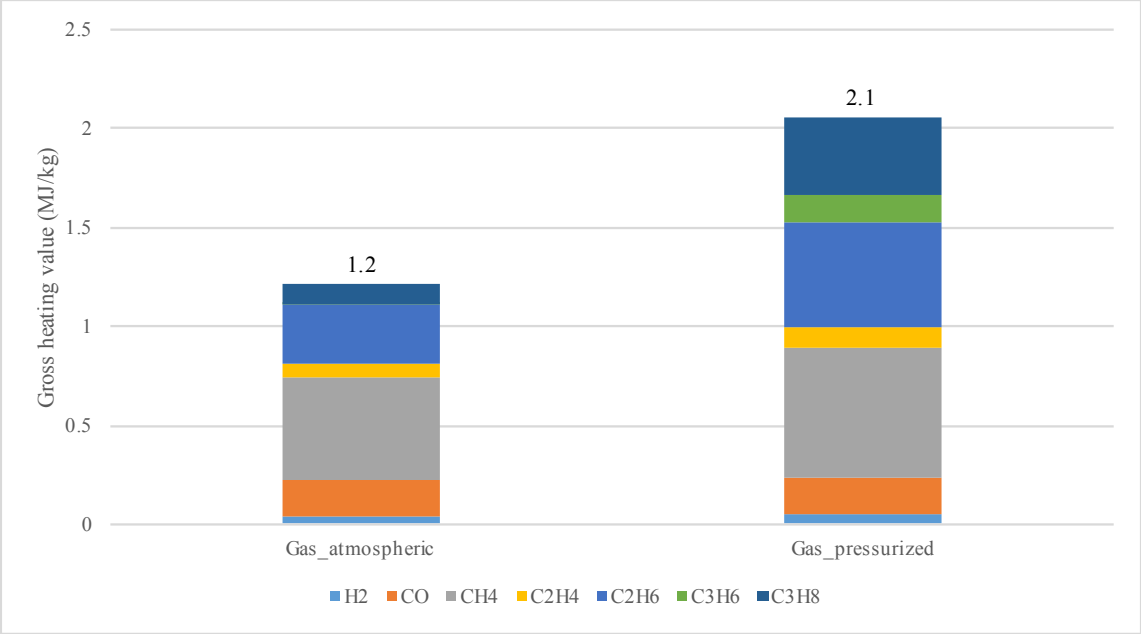

Figure 2.11. Gross heating value of gaseous product generated from atmospheric and pressurized pyrolysis.

2.3.4. Mass and energy distribution

Mass and energy distribution for pyrolysis processes at atmospheric condition were determined based on product yields and their product heating values and compared with that from pressurized pyrolysis as demonstrated in Figure 2.12. The mass conversion efficiencies were obtained at 89.7% for atmospheric pyrolysis and 89.2% for pressurized pyrolysis which were not significantly different. In addition, the total energy

recoveries were found to be 76.3% for both pyrolysis conditions. Biochar yielded the highest amount among all pyrolysis products for both mass and energy distributions at both atmospheric and pressurized pyrolysis. Atmospheric pyrolysis produced more liquid product than pressurized pyrolysis which resulted in more energy distribution. However, mass and energy distribution of gaseous product from pressurized pyrolysis was considerably higher than that from atmospheric pyrolysis. More combustible gases were generated under elevated pressure because of the secondary cracking of volatiles which were likely to occur under pressurized conditions. Additionally, more incondensable gaseous components were formed as the gases were retained inside the reactor to maintain the pressure.

High mass portion of aqueous fraction resulted in low energy distribution found in liquid product which led to the energy losses in pyrolysis process. The thermal degradation of lignin and hemicellulose could lead to a significant mass loss in the form of volatiles [73]. In addition, the formation of noncombustible substances such as water or carbon dioxide could lead to the losses in mass and energy distributions as well as some uncollectible products stuck in the reactor [52]. The bench-scale reactor used in the current study made some bio-oil and biochar adhered to the wall and some condensed bio-oil remained in the gas line leading to the percent loss. According to the previous studies, similar mass losses were observed using the same reactor [38,52,60].

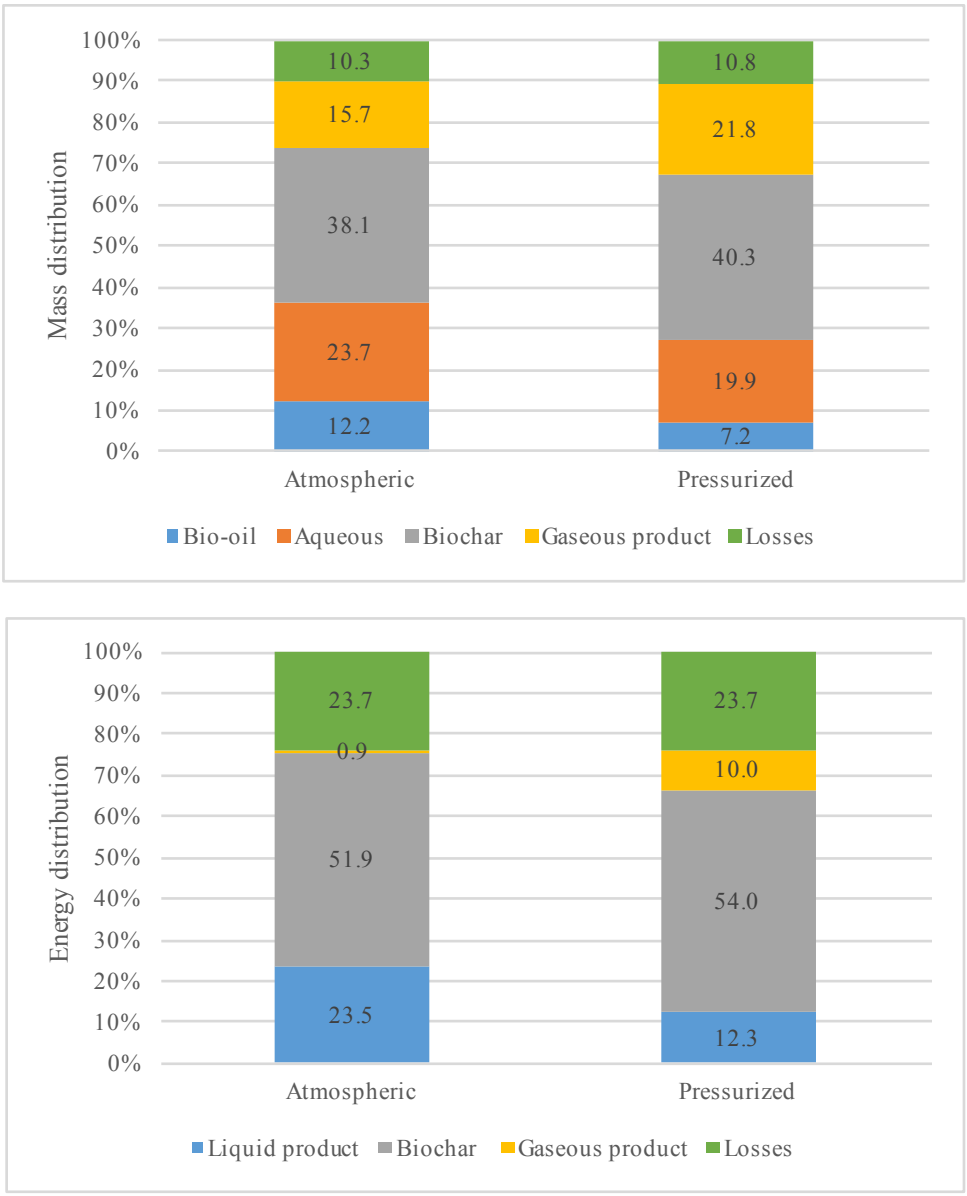

Figure 2.12. Mass and energy distributions of products from atmospheric and pressurized pyrolysis.

2.4. Conclusion

Pyrolysis of Jatropha de-oiled cake using batch reactor was performed under atmospheric conditions. The pyrolysis yields and product properties were compared with

those from pressurized pyrolysis. Jatropha residue was successfully turned into energy products via pyrolysis. The HHVs of biochar and bio-oil were improved from Jatropha residues. The highest energy distribution was obtained from biochar, followed by the bio-oil and gaseous products. In addition, the chemical compositions of pyrolysis products showed the possibility of using this as fuel replacement. High carbon content present in the biochar showed high potential applications for activated carbon or fuel substitute. Bio-oil also contained high hydrocarbon compounds and some nitrogen and oxygen containing compounds, which needed further upgrading process to make it acceptable to use as transportation fuel. As compared with the pressurized pyrolysis, the results indicated that the operating pressures affected the product yields and properties. The overall mass and energy distributions of both pyrolysis conditions were not significantly different. However, the atmospheric pyrolysis generated more bio-oil while the pressurized pyrolysis produced more bio-char and gaseous product.

3. INVESTIGATION OF ACTIVATED CARBON PREPARATION FROM PYROLYSIS BIOCHAR USING RESPONSE SURFACE METHODOLOGY

3.1. Introduction

Biochar is the black solid product obtained as a residual by-product from pyrolysis process. It contains high carbon up to 60 wt%. Typically, the biochar yield depends on pyrolysis temperature. The yield, which ranges between 15-40 wt% of input biomass [74], decreases with an increase in pyrolysis temperature. Currently, the biochar is used as a soil amendment, sold for carbon sequestration or abandoned.

The biochar structure is composed of the linkage aromatic carbon rings which are unsystematically stacked and randomly arranged [75]. Biochar has a high potential to be used as a catalyst support due to the abundant and low-cost renewable carbon source. The commercial activated carbons are mostly produced from petroleum and coal which are more expensive and not environmentally friendly. Therefore, the activated carbon from biochar seems to be a promising option which is cheaper, renewable and environmentally friendly [76].

Response surface methodology (RSM) is one of statistical tools that can be used to evaluate the relationships between several explanatory variables with one or more response [77]. Many studies on activated carbon studies use the RSM to investigate the effects of input variables (i.e., activation parameters) on performance measures of the system or characteristics of the product. The RSM will approximate the response functions based on the most critical factors that affect those responses [78-80].

This study aims to evaluate the effect of activating conditions such as impregnation ratio, activation temperature, and time on the activated carbon yield and properties. The statistical correlation between the activation parameters and process responses (yield, carbon content, and surface area) were examined using the response surface methodology. Additionally, the optimum condition for the highest surface area production was determined. The adsorption ability of the activated carbon at optimum surface area was investigated and compared with the original biochar.

3.2. Materials and Methods

3.2.1. Material and characterization

Jatropha biochar, a product obtained from the atmospheric pyrolysis at 500^{o}C in the previous chapter, was selected as a precursor for activated carbon preparation. The biochar was first analyzed for its physical and chemical properties. Physical properties such as particle density, surface area, and ash content were analyzed. The chemical properties included compositional analysis, proximate analysis, elemental composition, and functional groups.

3.2.2. Activated biochar preparation

There were two processes for activated carbon preparation, including chemical and physical activation. First, the biochar was crushed and sieved to obtain a uniform size using sieve set No.20 (850 μm) and No.80 (180 μm) stackable sieves. The sample remained on No.80 sieve proceeded the further steps. The chemical activation was first performed by mixing the sieved sample with 8 M KOH solution with ratios of

biochar:KOH equal to 0.6, 1.2, and 1.8. The KOH ratio in this study referred to the weight of biochar used per the weight of KOH in solution. The mixed solution was agitated continuously for four hours. After the reaction was completed, the activated biochar was filtered using a glass filter crucible and dried in 105^{o}C oven for 24 h. The dried impregnated sample was then activated at different temperatures including 600, 725, and 850^{o}C under the nitrogen flow of 0.4 L/min. The activation time varied from 60 to 120 min. After that, the activated carbon was soaked in 0.5 M HCl solution and stirred for 2 h in order to remove the impurities and reduce the ash content. Then, the sample was washed several times with distilled water until the pH of the washing solution became neutral. Finally, the activated carbon was dried in 105^{o}C for 24 h before further analysis. The yield of activated carbon was calculated using the equation below.

$$\text{Yield (wt\%)} = (\text{Weight of activated carbon/Weight of biochar}) \times 100\% \qquad (3.1)$$

3.2.3. Analysis of activated carbon

The activated biochar was analyzed for its chemical and physical properties. Surface area of the activated carbon were examined using a Nova Surface area and Pore Size Analyzer (Quantachrome Instruments). The activated biochar samples were degassed at 300^{o}C under nitrogen gas for a minimum of 4 h. The specific surface areas of the activated carbon were estimated by the Brunauer-Emmett-Teller (BET) method. Particle density was also determined using a pycnometer (Accupyc 1330, Micromeritics). Proximate analysis was performed in accordance to ASTM D 3172 and E 1755. Elemental composition was done using the Vario MICRO Elemental Analyzer (Elementar Analysemsysteme GmbH, Germany) by following ASTM D 3176 and the

empirical formulas were then calculated. The functional groups present in the activated carbon and the commercial activated carbon from Sigma Aldrich were identified using a Shimadzu IRAffinity-1 FTIR (Fourier Transform Infrared) Spectrophotometer (Shimadzu, Inc.). The PARR isoperibol bomb calorimeter was used to determine the gross calorific values of activated biochar in reference to ASTM D 2015.

3.2.4. Experimental design and statistical analysis

The response surface methodology was selected to determine the effect of the explanatory variables and obtain the optimal responses. Three factors that had effects on the characteristics of activated carbon including impregnation ratio, activation temperature and time were used in this study. The Box-Behnken design for three factors was selected as an experimental design. This design had treatment combinations which were at the midpoints of the edges of the selected experimental ranges as illustrated in Figure 3.1.

A total of 16 experimental runs were generated by Design Expert program version 9 as shown in Table 3.1. The fitness of the regression models between the responses and study variables were estimated using the analysis of variance (ANOVA). The product yield and energy recovery as shown in the equations below were used for the data analysis in this study.

Product yield (%wt) = (mass of activated carbon/mass of initial biochar) x 100% (3.2)

$$\text{Energy recovery (\%)} = \text{Product yield} \times (HV_{\text{activated carbon}}/HV_{\text{biochar}}) \quad (3.3)$$

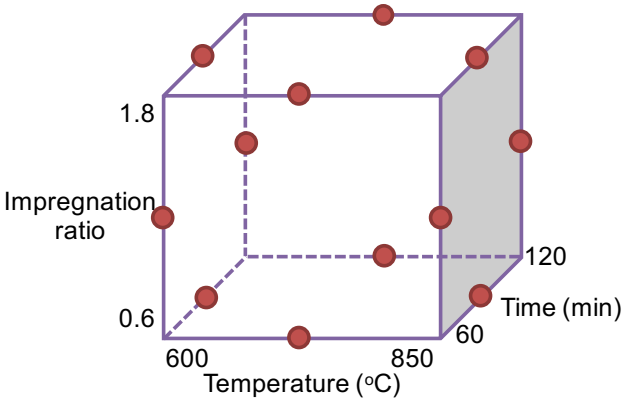

Figure 3.1. Box-Behnken design for activation parameters.

Table 3.1. Summary of experimental runs for biochar activated carbon.

Std	Run	KOH ratio	Temp	Time	Coded variable level		
					KOH ratio	Temp	Time
9	1	1.2	600	60	0	-1	-1
5	8	0.6	725	60	-1	0	-1
6	3	1.8	725	60	+1	0	-1
10	15	1.2	850	60	0	+1	-1
1	14	0.6	600	90	-1	-1	0
2	10	1.8	600	90	+1	-1	0
13	5	1.2	725	90	0	0	0
16	7	1.2	725	90	0	0	0
15	12	1.2	725	90	0	0	0
14	16	1.2	725	90	0	0	0
3	11	0.6	850	90	-1	+1	0
4	13	1.8	850	90	+1	+1	0
11	9	1.2	600	120	0	-1	+1
7	6	0.6	725	120	-1	0	+1
8	4	1.8	725	120	+1	0	+1
12	2	1.2	850	120	0	+1	+1

3.2.5. Adsorption analysis

The adsorption abilities of activated biochar at the optimum condition and the initial biochar obtained from pyrolysis were analyzed and compared. The acetaminophen

and ibuprofen solutions were prepared using deionized water with the initial concentration of 10 mg/L. Sulfuric acid (1M) was used for the pH adjustment. For each run, approximately 100 mg of biochar sample was mixed with 100 ml of adsorbate solution. The flasks containing the mixture solution were then placed in the incubator shaker at 30^{o}C with the speed of 150 rpm for 24 h. The same condition was used for both acetaminophen and ibuprofen solutions. After completed reaction time, the mixture was filtered using a vacuum pump. The filtered solution was then analyzed via the UV-Vis spectrophotometer (VWR, PA) in order to determine the final absorbance. The concentrations of the final solution were calculated using the equations below.

Acetaminophen (at 243 nm): C_a (mg/L) = 15.165 x A_a (3.4)

Ibuprofen (at 222 nm): C_i (mg/L) = 21.304 x A_i (3.5)

Where

C_a, C_i = final concentration of acetaminophen and ibuprofen solutions.

A_a, A_i = the absorbance values obtained from the UV-Vis spectrophotometer

The percent removal was then calculated using the equation below.

$$\%\text{Removal} = \frac{(\text{Initial adsorbate conc.} - \text{Final adsorbate conc.})}{\text{Initial adsorbate conc.}} \times 100\% \quad (3.6)$$

3.3. Results and Discussion

3.3.1. Characterization of biochar

Jatropha biochar obtained from pyrolysis at 500^{o}C was used as a precursor for activated carbon preparation. The physical and chemical properties of Jatropha biochar were presented in Table 3.2. The proximate analysis indicated that biochar contained

high fixed carbon and low ash content. Moreover, the result from the ultimate analysis showed the absence of sulfur in biochar. As mentioned by Stavropoulos and Zabaniotou [81], the biochar that contained no sulfur and had low ash content was a good precursor for activated carbon production. The surface area of biochar was found to be 1.51 m^2/g, which was quite low compared to biochar produced from safflower seed press cake (14.14) [82]. However, Acikalin et al. [83] conducted the pyrolysis of pistachio shells at 500^oC and obtained the biochar with relatively low surface area (2.69 m^2/g). They suggested that the conventional pyrolysis without catalyst produced the biochar with very low surface area, but the physical or chemical activation could improve the surface area and porosity of pistachio shell biochar.

The compositional analysis of biochar was also analyzed. As comparted to the Jatropha raw seed and Jatropha de-oiled cake (section 2.3.1.), the extractives (water and ethanol) of biochar (5.24%) were substantially reduced from the Jatropha raw seed (44.6%) and de-oiled cake (20.4%). The highest composition found in biochar was the lignin component (63.7%), which was significantly increased from raw seed (26.1%) and de-oiled cake (39.2%). The sugar content was obtained by difference, so the losses were also included here. Cagnon et al. [84] studied the contributions of hemicellulose, cellulose, and lignin to the properties of chars. They also observed that lignin was the major component found in biochar as well as in an activated carbon. Additionally, lignin showed the highest carbon and lowest oxygen content compared to the cellulose and hemicellulose.

Table 3.2. Jatropha biochar characteristics.

Biochar characteristics		Biochar characteristics	
Particle density (g/cm^3)	0.76	*Proximate analysis (wt%)*	
Surface area (m^2/g)	1.51	*VCM*	30.3
Heating value (MJ/kg)	27.9	*FC*	56.6
Compositional analysis (wt%)		*Ash*	13.1
Extractives	5.2		
Water extractives	4.0	*Ultimate analysis (wt%)*	
Ethanol extractives	1.2	*C*	66.1
Lignin	63.7	*H*	3.0
Acid solubles	5.1	*N*	4.9
Acid insolubles	58.6	*O**	13.0
Protein	28.6		
Sugars	2.5	*Empirical formula*	$CH_{0.55}N_{0.06}O_{0.15}$

3.3.2. Effects of KOH ratio, activation temperature and time on activated carbon yield

The effects of the activation parameters including the KOH ratio (0.6,1.2, and 1.8), activation temperature (600, 725, and 850^{o}C) and time (60, 90, and 120 min) on activated carbon yield were investigated. A second-order polynomial equation was used to determine the parameter effects on product yield in terms of linear, quadratic, and interactive terms as shown in Equation 3.7. A polynomial of higher degree, such as the second-order model, must be used if the system has a curvature [77].

$$Y = \beta_0 + \sum_{i=1}^{k} \beta_i x_i + \sum_{i=1}^{k} \beta_{ii} x_i^2 + \sum_{i<j} \sum \beta_i x_i x_j + \epsilon \quad (3.7)$$

Where

Y = yield (%wt);

β_0 = model intercept;

β_i, β_{ii} = regression coefficients;

x_i = Studied parameters where i refers to a number of studied variables.

The Analysis of Variance (ANOVA) in the Design Expert software was used to analyze the p-value of each component in the equation. The p-values (α=0.05) were used to identify significant terms, so that they were then included in the model. Table 3.3 shows the significant terms that will be evolved in the regression model for the activated carbon yield prediction. According to the results, only KOH ratio and activation temperature significantly affected the activated carbon yield. The effects of these parameters on the activated carbon yield were also observed to be significant, according to Angin's work [78].

Table 3.3. Analysis of Variance for the regression model of activated carbon yield.

Source	Sum of squares	df	Mean square	F value	p-value
Model	108.82	3	36.27	20.17	< 0.0001
A-KOH ratio	*16.97*	*1*	*16.97*	*9.43*	*0.0097*
B-Temp	*79.06*	*1*	*79.06*	*43.95*	*< 0.0001*
AB	*12.8*	*1*	*12.8*	*7.12*	*0.0205*
Residual	21.58	12	1.8		
Lack of Fit	*14.42*	*9*	*1.6*	*0.67*	*0.7176*
Pure Error	*7.16*	*3*	*2.39*		
Cor Total	130.41	15			
R-squared	0.8345				

The linear terms (A and B) and interactive term (AB) were found to be significant based on p-values, so a two-factor interaction (2FI) model was used to fit the regression model. Equations 3.8 and 3.9 represent regression models for predicting the

activated carbon yield using the actual parameters and coded parameters (Table 3.1), respectively.

$$Yield_{actual}\ (\%wt) = 57.94 + 19.72*KOH\ ratio + 3.47\times10^{-3}*Temp - 0.024*KOH\ ratio*Temp \quad (3.8)$$

$$Yield_{coded}\ (\%wt) = 63.37 + 1.46A - 3.14B - 1.79AB \quad (3.9)$$

It must be taken into account that the prediction equations above are only accurate for the feedstock and the specific reactor configuration used in this study. Moreover, the equations might be useful only for the interpolation ranges conducted in this study (i.e., KOH ratio: 0.6-1.8, temperature: 600-850^{o}C, and activation time: 60-120 min). However, the significant parameters present in the model are still helpful to identify what factors affect the activated carbon yield for different biomass and activation conditions.

Figure 3.2 shows a contour plot of activated carbon yield based on the significant factors (impregnation ratio and activation temperature). The product yields varied from 59.4 to 69.8%. According to the contour plot, an increase in KOH ratio along with a decrease in temperature tended to increase the activated carbon yield. Therefore, the optimum activated carbon yield was obtained with biochar:KOH equal to 1.8 and activation temperature of 600^{o}C. Other studies on the activated carbon production from biochar also showed that the product yield decreased as the amount of KOH/g of biochar and activation temperature increased. Moreover, their product yields with similar operating conditions, such as olive-seed waste residue (32-76%) [81], safflower seed

press cake (29.06-78.78%) [82], and pine nut shell (23.16-56.21%) [85] were comparable to this study.

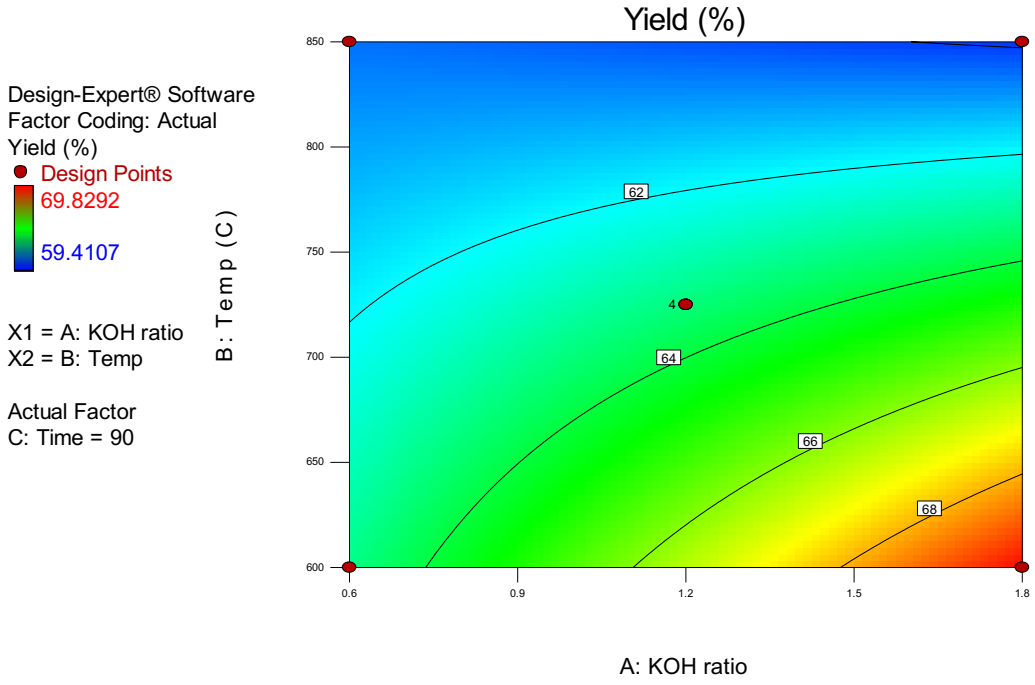

Figure 3.2. Contour plot for activated carbon yield.

3.3.3. Effects of KOH ratio, activation temperature and time on activated carbon properties

3.3.3.1. Proximate and ultimate analysis

The proximate and ultimate analysis results of activated biochar obtained from different combinations of impregnation ratio, activation temperature, and time are demonstrated in Table 3.4. Fixed carbon (FC) of activated carbon (70.4-83.6%) was

significantly improved from the original biochar (56.6%) and appeared to increase with a rise in activation temperatures and times for all impregnation ratio. On the other hand, VCM and ash tended to decrease with an increase of activation temperatures and times. The ash contents of activated carbon for all conditions were considerably lower than the original biochar (13.1%), which were found to be less than 5%. According to the effect of the impregnation ratio, the increase of impregnation ratio led to the increase of FC and the decrease of VCM. Similar trends were observed from many studies such as safflower seed press cake [82], pine nut shell [85], pistachio-nut shells [86], and sugar cane bagasse [87].

The carbon content of the activated carbon also showed an improvement from the initial biochar. This could be explained by the carbonization process, which was involved in the release of volatiles and elimination of non-carbon species resulting in a rich carbonaceous material [88]. The trend of carbon content found in the activated carbon at different condition was in agreement with the fixed carbon. Table 3.5 demonstrates the significant terms of the cubic regression model for the carbon content of activated biochar. The results from ANOVA showed that all parameters (KOH ratio, temperature, and time) and their interactive terms were found to significantly affect the carbon content of activated biochar at 90% confidence level. Other components such as hydrogen and oxygen were found to decrease with an increase in activation temperature from 600 to 850^{o}C.

Table 3.4. Effect of impregnation ratio, activation temperature, and time on proximate and ultimate analysis.

Impregnation ratio: 0.6		Proximate analysis (wt%)			Ultimate analysis (wt%)				
Temperature (^{o}C)	Time (min)	VCM	FC	Ash	C	H	N	S	O
600	90	25.0	70.4	4.6	65.1	2.1	6.0	0.06	22.1
725	60	19.9	75.6	4.5	70.0	1.9	5.4	0.07	18.1
725	120	17.3	78.1	4.6	73.7	1.8	5.0	0.05	14.9
850	90	11.4	83.6	5.0	74.3	1.3	4.6	0.06	14.7

Impregnation ratio: 1.2		Proximate analysis (wt%)			Ultimate analysis (wt%)				
Temperature (^{o}C)	Time (min)	VCM	FC	Ash	C	H	N	S	O
600	60	23.9	71.1	5.1	71.6	2.2	5.2	0.05	15.9
600	120	21.3	73.8	4.9	69.1	2.1	5.8	0.06	18.0
725	90	17.6	77.6	4.9	71.8	1.8	5.1	0.1	16.4
850	60	18.6	76.6	4.8	72.4	1.7	3.9	0.03	17.1
850	120	13.9	83.2	3.0	72.1	1.6	3.5	0.04	19.7

Impregnation ratio: 1.8		Proximate analysis (wt%)			Ultimate analysis (wt%)				
Temperature (^{o}C)	Time (min)	VCM	FC	Ash	C	H	N	S	O
600	90	21.0	74.4	4.6	65.9	2.2	5.8	0.04	21.4
725	60	14.8	80.3	5.0	68.5	1.7	5.2	0.06	19.6
725	120	12.6	82.7	4.7	72.0	1.7	5.2	0.05	16.3
850	90	14.6	80.5	4.9	74.4	1.3	4.0	0.06	15.2

Table 3.5. Analysis of Variance for the regression model of carbon content contained in activated carbon.

Source	Sum of squares	df	Mean square	F value	p-value
Model	104.71	12	8.73	214.17	0.0005
A-KOH ratio	*0.35*	*1*	*0.35*	*8.51*	*0.0616*
B-Temp	*3.69*	*1*	*3.69*	*90.48*	*0.0025*
C-Time	*1.89*	*1*	*1.89*	*46.47*	*0.0065*
AB	*1.31*	*1*	*1.31*	*32.04*	*0.0109*
AC	*1.11*	*1*	*1.11*	*27.16*	*0.0137*
BC	*1.09*	*1*	*1.09*	*26.8*	*0.0140*
A^2	*11.56*	*1*	*11.56*	*283.77*	*0.0005*
B^2	*3.58*	*1*	*3.58*	*87.98*	*0.0026*
C^2	*0.75*	*1*	*0.75*	*18.29*	*0.0235*
A^2B	*14.83*	*1*	*14.83*	*364.04*	*0.0003*
A^2C	*17.81*	*1*	*17.81*	*437.24*	*0.0002*
AB^2	*3.37*	*1*	*3.37*	*82.74*	*0.0028*
Cor Total	104.84	15			
R-squared	0.9988				

3.3.3.2. FTIR

The qualitative characterization of functional groups present in activated carbon was analyzed using the FTIR. The knowledge of surface functional groups could provide the understanding of the adsorption capability of the produced activated carbon [82]. Figure 3.3 demonstrates the FTIR spectra of the initial biochar and some selected activated carbons at different activating conditions. The FTIR spectra of activated carbon showed some difference from the initial biochar. However, the spectra of the activated carbon obtained from different conditions appeared to be the same, which indicated the similar functional group of activated carbon from different conditions. In comparison with the commercial activated carbon, the FTIR spectra of activated carbon

obtained from this study appeared to be similar to that commercial one from Sigma Aldrich. The peak observed at 2100 cm^{-1} for -C≡C- stretching in the commercial activated carbon suggested the presence of alkynes.

According to the FTIR spectrum of biochar, small peak bands observed at 1500-1400 cm^{-1} for C-C stretching (in ring) indicated the presence of aromatics. Another peak absorbance at 1000-950 cm^{-1} for =C-H bending suggested the presence of alkenes. However, the peak 1000-950 cm^{-1} appeared in biochar was absent from the activated carbon. A peak detected at 1600-1450 cm^{-1} in activated biochar was attributed to C-C=C symmetric and asymmetric stretching as an indicator for aromatics.

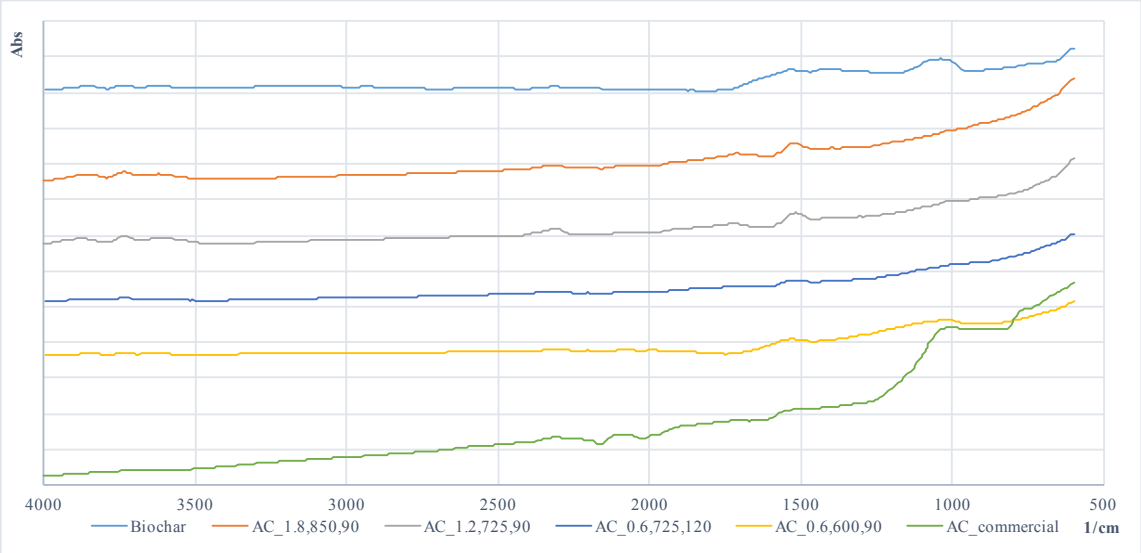

Figure 3.3. FTIR spectra of raw biochar, activated carbon at different activating condition, and commercial activated carbon from Sigma Aldrich.

3.3.3.3. Surface area

The activated carbon produced from different activating conditions was analyzed for the BET surface area. The surface areas obtained from activated carbon varied from 140 to 285 m^2/g depending on activating conditions. Like the activated carbon yield (section 3.3.2.), the second-order polynomial regression model was used to identify the parameter effects on surface area in terms of linear, quadratic, and interactive components. Table 3.6 shows the p-value of each significant parameter present in the model. The ANOVA results indicated that all linear parameters (A, B, and C) significantly affected the surface area of activated carbon. The impregnation ratio, activation temperature, and time were reported in many studies as the significant factors that affected the surface area of activated biochar during the physical and chemical activation [78,82,89]. The regression models used to predict the surface area of the produced activated carbon are represented in Equation 3.10 for the actual parameters and in Equation 3.11 for the coded parameters.

$$\text{Surface area}_{actual}\ (m^2/g) = 121.05 - 38.07*\text{KOH ratio} + 0.27*\text{Temp} - 0.73*\text{Time} \quad (3.10)$$

$$\text{Surface area}_{coded}\ (m^2/g) = 205.96 - 22.84A + 33.92B - 22.04C \quad (3.11)$$

Note that these regression models will be accurate only for predicting the surface area of activated biochar with the KOH ratio ranging between 0.6-1.8, the activation temperature from 600-850^{o}C, and the activation time between 60-120 min.

Figure 3.4 shows contour plots of activated carbon yield based on the significant factors (impregnation ratio and activation temperature). Figure 3.4a demonstrates the effects of impregnation ratio and activation temperature when the activation time is 60

min, while Figure 3.4b is for the activation time of 90 min. The contour plots for the activation time of 90 min revealed that low surface area was observed at low activation temperatures and high amounts of biochar:KOH (i.e., low KOH concentration). On the other hand, when the activation time was reduced to 60 min, the increases in activation temperature and KOH concentration resulted in a higher surface area. Therefore, the optimum surface area of 285 m^2/g was obtained when the biochar:KOH was equal to 0.6 with the activation temperature and time of 850^oC and 60 min, respectively.

Table 3.6. Analysis of Variance for the regression model of activated carbon surface area.

Source	Sum of squares	df	Mean square	F value	p-value
Model	17263.76	3	5754.59	8.37	0.0028
A-KOH ratio	*4173.87*	*1*	*4173.87*	*6.07*	*0.0298*
B-Temp	*9203.17*	*1*	*9203.17*	*13.39*	*0.0033*
C-Time	*3886.71*	*1*	*3886.71*	*5.65*	*0.0349*
Residual	8250.51	12	687.54		
Lack of Fit	*7365.04*	*9*	*818.34*	*2.77*	*0.217*
Pure Error	*885.47*	*3*	*295.16*		
Cor Total	25514.27	15			
R-squared	0.8766				

Although the highest surface area obtained from this study was substantially improved from the original biochar (1.51 m^2/g), it was quite low compared to other studies of activated carbon production from agricultural wastes material such as sugar cane bagasse (320 m^2/g) [60], cocoa pod husk (490 m^2/g) [62], and safflower seed press cake (249-772 m^2/g) [82], which used almost the same activation method as in this study. This could be explained by the condensed aromatic structures present in biochar, which might be resistant to a thermal degradation. This resulted in the inhibition of surface area and porous structure development during the activation process [91]. This was consistent with the FTIR results from section 3.3.3.2, which indicated the presence of aromatics in Jatropha biochar as a precursor for activated carbon production in this study.

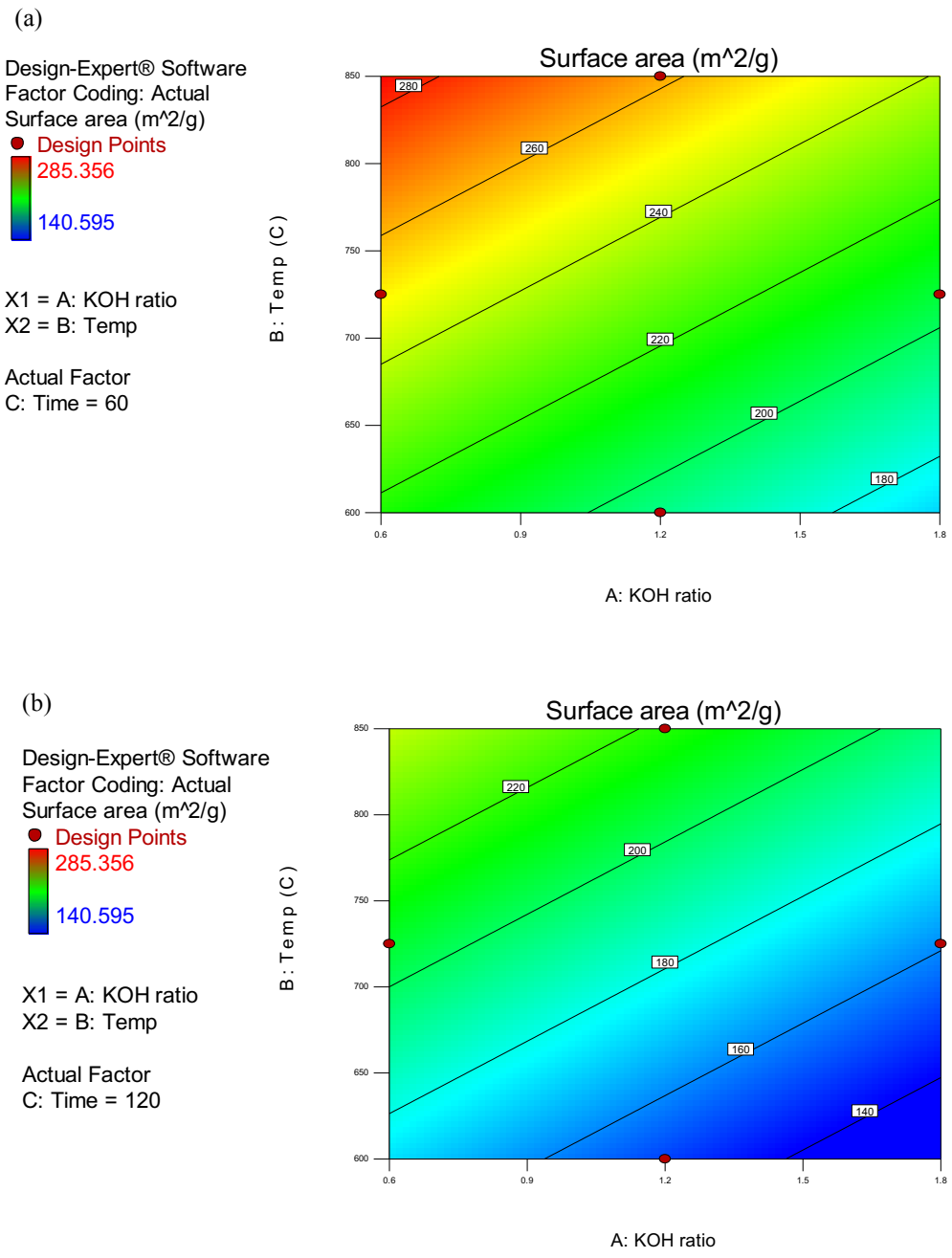

Figure 3.4. Contour plot for surface area of activated carbon at activation time of (a) 60 min (b) 120 min

3.3.4. Adsorption characteristic

The original biochar and activated carbon with the highest surface area (285 m^2/g) was analyzed for the adsorption ability of Acetaminophen and Ibuprofen as shown in Table 3.7. The results showed that the original biochar obtained from pyrolysis had a poor adsorption ability for Acetaminophen and Ibuprofen. However, the activated carbon produced from this biochar showed a major improvement in adsorption ability. The optimum contaminant removal efficiency was obtained at 90.3% for Acetaminophen, where the pH solution was set to 4.0. This indicated the effectiveness of the biochar activation process, which significantly enhanced the sorption ability of contaminants. The commercial activated carbons are mostly produced from petroleum and coal, which are more expensive and not environmentally friendly. Therefore, the activated carbon from biochar seems to be a promising option that is cheaper, renewable and environmentally friendly.

Table 3.7. Adsorption of Acetaminophen and Ibuprofen for biochar and activated carbon.

pH = 2.0			
Adsorbent	**Adsorbate compound**	**Final adsorbate concentration (mg/L)**	**%Removal**
Raw biochar	Acetaminophen	ND	ND
	Ibuprofen	9.08	9.24
Activated carbon	Acetaminophen	5.97	40.3
	Ibuprofen	6.01	39.9
pH = 4.0			
Adsorbent	**Adsorbate compound**	**Final adsorbate concentration (mg/L)**	**%Removal**
Raw biochar	Acetaminophen	ND	ND
	Ibuprofen	ND	ND
Activated carbon	Acetaminophen	0.97	90.3
	Ibuprofen	6.77	32.3

3.4. Conclusion

The biochar as a solid product from pyrolysis was used as a precursor for activated carbon production via physical and chemical treatments. The activation parameters including impregnation ratio, activation temperature, and time were varied in order to study the effects on product yield and properties. The response surface method with the Box-Behnken design was used in this study. The results showed that only impregnation ratio and activation temperature affected the activated carbon yield. The properties of activated carbon such as carbon content, ash content, and surface area were significantly improved from the original biochar. However, the optimum surface area of activated carbon obtained from this study was quite low. This was due to a condensed carbon structure found in the biochar precursor, which might be inappropriate for the production of activated carbon with a high surface area. Nonetheless, the activated

carbon revealed a major improvement in adsorption ability for Acetaminophen and Ibuprofen from the biochar.

4. UPGRADING OF LIQUID PRODUCT VIA FRACTIONAL DISTILLATION AND CATALYTIC UPGRADING

4.1. Introduction

During the pyrolysis process, the produced heavy volatiles are condensed and formed into the liquid product. In general, the bio-oil is a black viscous smoky oil with a very strong irritable smell. The pyrolysis of oilseed by-product has been investigated by many researchers with the pyrolysis temperature ranging from 450-550^{o}C. The liquid product yield was found to be 40-60 wt% [11,34-36]. The pyrolytic oil contains a variety of functional groups with different molecular weights of chemical compounds such as hydrocarbons, acids, alcohols, esters and ketone. Some of these compounds lead to some undesirable properties of bio-oil such as low heating value, high viscosity, high acidity and instability. These properties prevent bio-oil from being used directly as a transportation fuel [92].

The properties of bio-oil can be improved by physical or chemical methods. Physical methods include filtration, solvent addition, emulsion, and distillation. Fractional distillation is the most common way to refine the bio-oil by using the different boiling points of components contained in bio-oil. Examples of chemical methods include catalytic hydrogenation, fluidized catalyzed cracking, catalytic esterification, and steam reforming. The catalytic hydrogenation method has been used widely for the bio-oil upgrading. It is appropriate for the bio-oil that has high oxygenate compounds. According to the catalytic hydrogenation method, the bio-oil is operated at high pressure

with the use of hydrogen and catalyst to remove oxygen in the form of water or carbon dioxide from the bio-oil [93].

The aim of this study was to improve the qualities of bio-oil using the physical (fractional distillation) and chemical (catalytic hydrotreatment) methods. The specific objectives for the fractional distillation part are:

(a) to investigate the product yields and properties of the distillates from the pyrolysis liquid product (bio-oil and aqueous);

(b) to determine the mass and energy distributions of the distillates; and

(c) to evaluate the potential of the distillates to serve as biofuels.

One of the distillate fractions obtained from the fractional distillation was selected to perform the catalytic hydrotreatment. The specific objective for this part are:

(d) to study the effects of operating temperature on product yield and properties;

(e) to investigate the catalyst efficiency based on the degree of deoxygenation, product yield, hydrogen consumption, and turnover frequency; and

(f) to evaluate the applications for the upgraded product and compare with the original bio-oil and distillates from fractional distillation.

4.2. Materials and Methods

4.2.1. Liquid product

The liquid product used in this study was produced from pyrolysis of Jatropha de-oiled cake using a batch reactor at 500^{o}C and atmospheric pressure. This liquid product comprised of two separated layers i.e., aqueous phase and organic phase (bio-

oil). The experimental set-up of pyrolysis was described in Chapter 2. Both aqueous and organic phases were then subjected to the fractional distillation under atmospheric pressure.

4.2.2. Fractional distillation set-up

The experimental set-up for fractional distillation used in this study is illustrated in Figure 4.1. The distillation system consisted of a 250-ml distillation flask, a distillation head with a condenser attached to a Vigreux fractionating column, a 4-way distribution adapter, and 15-ml receiving flasks. For each distillation run, approximately 50 g of the sample was transferred into the pre-weighed round-bottom distillation flask with boiling stones to prevent superheating. The fractionating column was wrapped with an aluminum foil sheet to minimize the temperature fluctuation. The thermocouple was connected at the top of the fractionating column to monitor the temperature inside the column. The distillation head was connected to the distribution adapter with four pre-weighted receiving flasks attached at the end of the adapter. A small amount of grease was applied to all connection joints for a complete seal and to prevent glassware from becoming stuck.

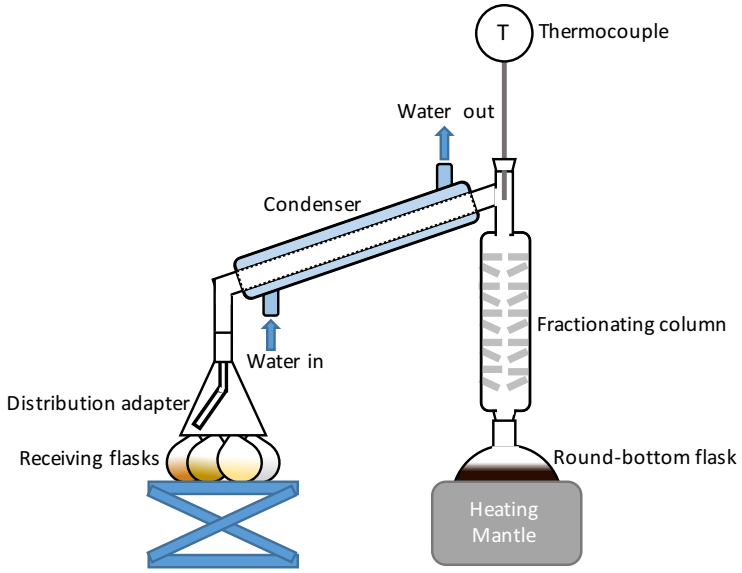

Figure 4.1. Distillation set-up for liquid product.

The sample inside the distillation flask was heated using the heating mantle controller while the cooling water flowed through the condenser. The boiling point ranges for each fraction of bio-oil and aqueous phases were selected as shown in Table 4.1. When the vapor reached a specified temperature, the heating rate was slightly reduced to maintain the temperature at that condensation line. The condensate was collected at the end of distribution adapter which connected to the pre-weighed receiving flask. A sudden rise in temperature was observed after the distillate with the lower boiling point had been collected, which meant the new fraction with higher boiling point would boil and be collected. The distribution adapter was turned as a new fraction was collected. The distillate yields of each fraction were calculated using Equation 4.1. The distillation runs for both bio-oil and aqueous phases were done in triplicates and the

average along with the standard deviation values were reported as the indication of experimental errors.

$$\text{Distillate yield (\%)} = \frac{\text{Weight of distillate fraction}}{\text{Weight of (bio-oil/aqueous)}} \times 100\% \quad (4.1)$$

Table 4.1. Temperature ranges for fractional distillation.

Sample	Distillate	Vapor Temperature (^{o}C)
Bio-oil	Fraction 1 (BD1)	< 100
	Fraction 2 (BD2)	100 - 230
	Fraction 3 (BD3)	230 - 275
	Residue	> 275
Aqueous	Fraction 1 (AD1)	< 100
	Fraction 2 (AD2)	100 - 150
	Fraction 3 (AD3)	150 - 170
	Residue	> 175

4.2.3. Catalytic upgrading of bio-oil distillate

The bio-oil distillate fraction was selected to perform the catalytic upgrading process based on its properties. The process diagram for the fractional distillation and upgrading system is demonstrated in Figure 4.2. The upgrading system consisted of a 50-ml Micro Robinson-Mahoney catalytic reactor (Autoclave Engineers), internal stirrer, heater jacket, and controller boxes (Autoclave Engineers) which were used to control the temperature and stirring speed. System lines were made of stainless steel tubing with back pressure regulator and relief valve (Swagelock). The reactor could handle up to 5000 psi at 343^{o}C. Thermocouples were used to measure the inside reactor and heater

jacket temperatures. The inside reactor pressure was also measured by the gauge pressure with a maximum reading of 5000 psi.

The experiments were designed to study the effect of operating temperatures on the yields and characteristics of upgraded products. The operating temperatures were selected at 150, 200, and 250^{o}C. Each temperature was done in triplicates. The commercial catalyst used for the bio-oil upgrading was Pd/C with 10 %wt loading from Sigma Aldrich. For each experimental run, around 7 g of bio-oil distillate was loaded to the reactor along with approximately 0.35 g of catalyst (5%wt of bio-oil). The reactor was closed tightly and the leak test was performed at 1300 psi to ensure that no leak would occur during the run.

At the beginning of each run, hydrogen gas was purged to the system at room temperature and 200 psi for 10 min in order to remove the air inside the reactor. After purging, the initial pressure was adjusted to 600 psi. The stirrer speed was selected around 400-430 rpm to create the homogeneity of the temperature inside reactor. Then, the heater jacket was turned on. Typically, the heater jacket temperature would be set at twice the inside temperature. The operating time was chosen at 5 h which began counting when the heater was started. The heater and stirrer were stopped after 5 h and the reactor was allowed to cool down to room temperature. The pressure and temperature after cooling down were recorded before the gas samples were collected. The upgraded distillate was collected by pouring it into a glass filter which connected to the vacuum pump. The reactor was washed with acetone in order to collect the liquid product adhered to the reactor wall (high viscosity). The residue left on the glass filter

was a combination of used catalyst and coke. Therefore, the amount of coke was calculated by subtracting the mass of the initial catalyst from the mass of the final residue that remained on the glass filter. The acetone was then removed from the acetone-soluble filtrate by evaporation. The product after the removal of the acetone was defined as tar.

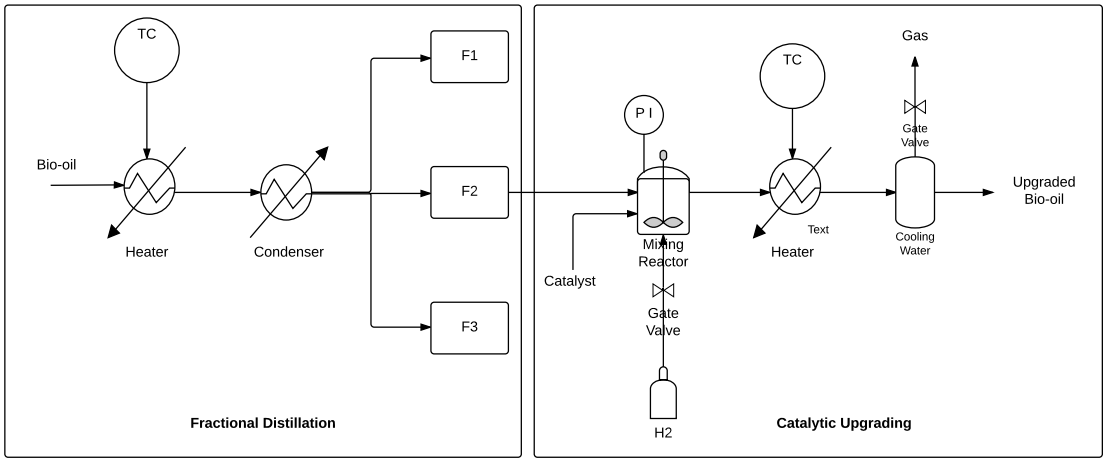

Figure 4.2. Process diagram for fractional distillation and catalytic upgrading.

4.2.4. Characterization of distillate fractions and upgraded products

Each distillate fraction and upgraded bio-oil were analyzed for its physical and chemical properties. The higher heating value (HHV) was determined in accordance with ASTM D2015 using PARR isoperibol bomb calorimeter (Model 6200, Parr Instrument Company, Moline, IL). The moisture content was analyzed following the ASTM E203 by the Karl-Fisher Titration method using KF Titrino 701 (Metrohm, USA Inc.). The total acid number (TAN) was also determined by following ASTM D974. The

elemental composition was investigated using Vario MICRO Elemental Analyzer (Elementar Analysemsysteme GmbH, Germany). The functional groups present in the distillates were examined using Shimadzu IRAffinity-1 FTIR Spectrophotometer (Shimadzu, Inc.). The chemical composition was analyzed by GC-MS analysis using Shimadzu QP2010Plus. The GC column used was ZB5MS (30 m length × 0.25 mm i.d., 0.25 μm film thickness). The column oven was programmed to hold at 40^{o}C for 5 min, then ramped at a rate of 5^{o}C/min to 300^{o}C and held for 5 min. The injection temperature was 295^{o}C and helium was used as a carrier gas with a flow rate of 0.83 ml/min. The injector split ratio was set to 50:1. The MS ion source temperature was 295^{o}C and the interface temperature was 320^{o}C. The kinematic viscosity of the bio-oil distillates and upgraded bio-oil were measured by following ASTM D445 using Cannon-Fenske Reverse-flow viscometer.

The gas product collected from the catalytic upgrading was analyzed for its composition using the SRI Multiple Gas Analyzer #1 (MG#1) gas chromatograph (SRI GC, Torrance, CA). The solid product remained on the glass filter (used catalyst + coke) was investigated for the surface area by a Nova Surface area and Pore Size Analyzer (Quantachrome Instruments).

4.2.5. Data analysis

The degree of deoxygenation (DOD) was used to determine the effectiveness of the catalytic upgrading process as shown in the equation below.

$$\%DOD = (O_{distillate} - O_{upgraded})/ O_{distillate} \times 100\% \quad (4.2)$$

Where

$O_{distillate}$ = %wt of oxygen contained in the distillate bio-oil

$O_{upgraded}$ = %wt of oxygen contained in the upgraded bio-oil

The %wt of oxygen was obtained from the ultimate analysis by calculating the difference.

The hydrogen consumption was also determined using the following equation.

$$H_2 \text{ consumption} = (n_{H2,initial} - n_{H2,final}) \times (22.4 \text{ Nl/mol})/m_{distillate}$$

Where

$$n_{H2,initial} = (V_{reactor} \times P_i)/(R \times T_i)$$

$$n_{H2,final} = X_{H2,f} \times (V_{gas\ space} \times P_f)/(R \times T_f)$$

$m_{distillate}$ = weight of the bio-oil distillate used for the upgrading process

$n_{H2,initial}$, $n_{H2,final}$ = amount of hydrogen (in moles) in the reactor before and after reaction

$V_{gas\ space}$ = volume of gas space inside the reactor (no occupied by liquid)

P_i, P_f = initial and final pressure in the reactor

T_i, T_f = initial and final temperature in the reactor

$X_{H2,f}$ = mole fraction of hydrogen in the reactor after reaction

R = gas constant (8.314 L kPa K^{-1} mol^{-1})

In addition, the moles of hydrogen consumption per gram of catalyst used per time or the turnover frequency (TOF) was determined using Equation 4.3.

$$\text{TOF (moles/g catalyst-h)} = (n_{H2,initial} - n_{H2,final})/(m_{catalyst} \times \text{reaction time}) \quad (4.3)$$

Where

$m_{catalyst}$ = weight of catalyst used in the upgrading process

The statistical data analyses including Analysis of Variance (ANOVA) and Fisher's Least Significant Difference (LSD) were performed at 95% confidence level. The average values and standard deviations were reported.

4.3. Results and Discussion

4.3.1. Fractional distillation of bio-oil

4.3.1.1. Distillate yields

Fractional distillation of liquid product obtained from pyrolysis of Jatropha de-oiled cake were conducted using various boiling point ranges. The distillation experiments yielded three fractions from bio-oil (BD1, BD2, and BD3) and three fractions from aqueous product (AD1, AD2, and AD3) as demonstrated in Figure 4.3 and Figure 4.4. The color of the distillates obtained from both bio-oil and aqueous product appeared to be darker as the boiling point range increased. The first fraction from bio-oil (BD1) was composed of two immiscible layers i.e., organic and aqueous phases. The organic layer in BD1 was light yellow with a strong smell, while the aqueous layer was colorless, which may be owed to the water content contained in bio-oil. BD2, BD3, and heavy fraction (residue) had a single layer with dark yellow, dark brown, and black color, respectively. The residue was very sticky and did not have a strong odor compared to other fractions. However, both distillate fractions obtained from the aqueous product showed no layer separation with less odor compared to BD1 (organic), BD2, and BD3. AD1 and AD2 were transparent solutions with light yellow and brown color, respectively.

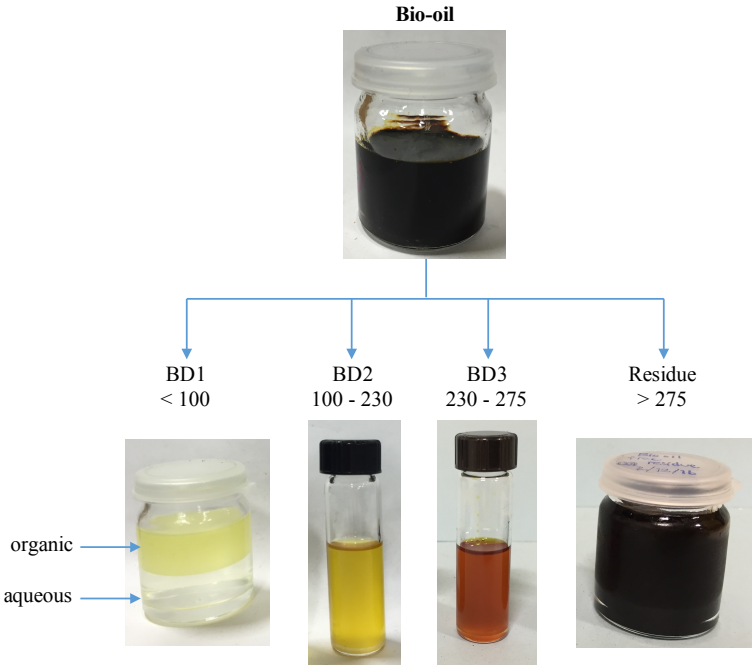

Figure 4.3. Distillate fractions obtained from bio-oil.

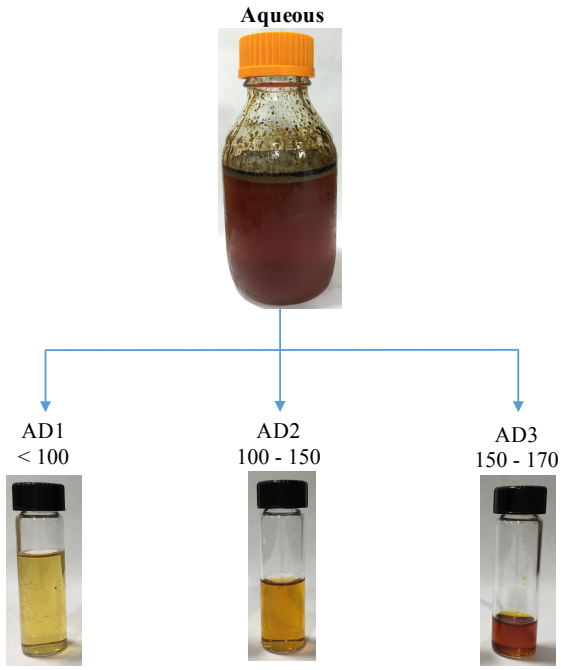

Figure 4.4. Distillate fractions obtained from aqueous product.

Mass distribution of the distillate fractions from bio-oil and aqueous product were demonstrated in Figure 4.5. The fractional distillation yielded the overall mass recovery of 97% for bio-oil and 96% for aqueous product. The first fraction (BD1) from bio-oil yielded 19%, which composed of 10% organic and 9% aqueous phases. Heavy fraction (> 275^{o}C) yielded the highest amount (37%) for distillation of bio-oil, which can be explained by high portion of C16-C19 hydrocarbons and heterocompounds contained in raw bio-oil, which had a boiling point greater than 271^{o}C [94] (as previously discussed in chapter 2). According to the fractional distillation of aqueous product, AD1 (< 100^{o}C) yielded the highest mass recovery (65%), followed by AD2 (28%) while only 2% was recovered from AD3 (150-170^{o}C). This may be attributed to high moisture content (67%) present in aqueous product. However, the distillate fractions may contain some water-soluble organic compounds as suggested by the GCMS and FTIR results from aqueous product shown in Table 2.3. The chemical compositions of the distillates will be discussed later in this section.

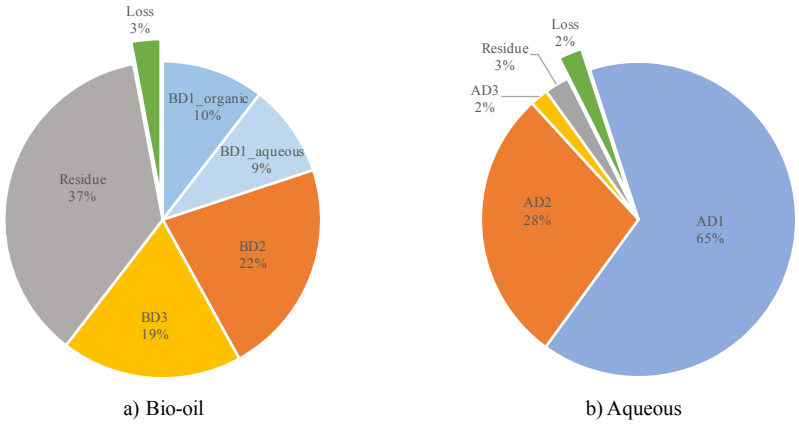

Figure 4.5. Mass distribution of distillate fractions from bio-oil and aqueous product.

4.3.1.2. Characteristics of distillate fractions

The quality and components of bio-oil can be improved by physical and chemical methods. Fractional distillation is one of the physical methods that has been used widely in petroleum refineries. This section demonstrates the change of bio-oil and aqueous product distillate properties from their original substances. These properties included both physical and chemical characteristics such as moisture content, heating value, total acid number, viscosity, elemental compositions, and chemical compounds.

Figure 4.6 compares the moisture content of bio-oil, aqueous product, and their distillates. Moisture content of bio-oil distillates (1.6-2.3%) significantly decreased from the original bio-oil (8.2%) except the aqueous layer from BD1 (75.7%). Figure 4.3 shows a separated layer of organic and aqueous fractions. The highest moisture content found in the aqueous layer revealed the effectiveness of fractional distillation for water

removal, which improved the quality of bio-oil. High moisture content in bio-oil led to a low energy value which affected its combustion performance.

The moisture contents of aqueous distillates were also analyzed as demonstrated in Figure 4.6. The results revealed that water was the main component present in aqueous product. The aqueous phase obtained from pyrolysis had 67.2% of moisture content. This could be due to the possibility that there could be some water-soluble organic compounds contained in the aqueous product. After fractional distillation, the first distillate fraction (AD1: <100^{o}C) contained 73% of moisture content which was considerably higher than the aqueous product. The moisture content of the distillates significantly reduced as the boiling point increased as shown in Figure 4.6. This indicated that most of the water present in aqueous product was removed near the water boiling point. The lowest moisture content was found in AD3 (13.7%), suggesting that most of the water-soluble organic compounds might condense at 150-170^{o}C.

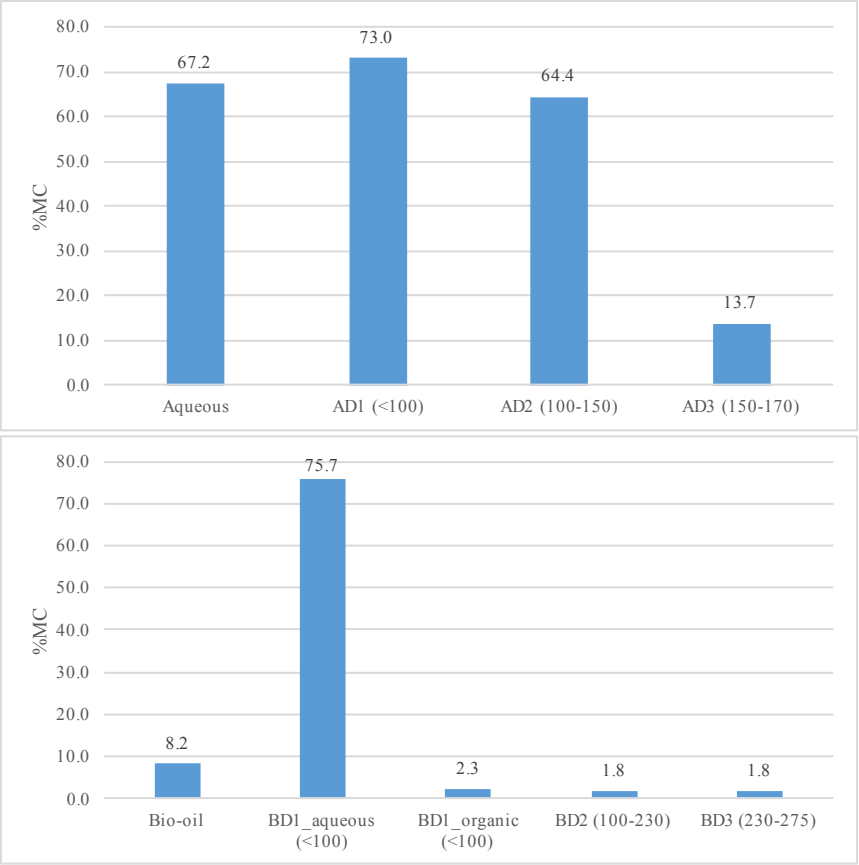

Figure 4.6. Moisture content of aqueous and bio-oil distillate fractions.

Total acid number (TAN) referred to the amount of KOH in mg needed to neutralize a gram of oil which was used to determine the acidity of the oil product. TAN has been used widely as a quality indicator for petroleum oil stability and possibility of corrosion problem. The degradation of lignocellulosic biomass from pyrolysis could lead to the existence of acids in a liquid product. The aqueous and bio-oil distillates were analyzed for TAN as shown in Figure 4.7. The lowest TAN was obtained from the first fraction of aqueous distillate (AD1) and appeared to increase as the boiling point increased. The distillation of bio-oil showed the major reduction in TAN for the distillate

fractions. Similarly, the lowest TAN was found in the organic phase of BD1 (0.2 mg KOH/g) which was even lower than the standard requirement for pure biodiesel (0.5 mg KOH/g) [95] However, TAN of BD2 and BD3 were obtained at 13.8 and 28.1 mg KOH/g which needed a further upgrading process to bring down the acidity. High concentrations of acidic compounds were obtained in the fractions with higher boiling points for both aqueous and bio-oil distillates.

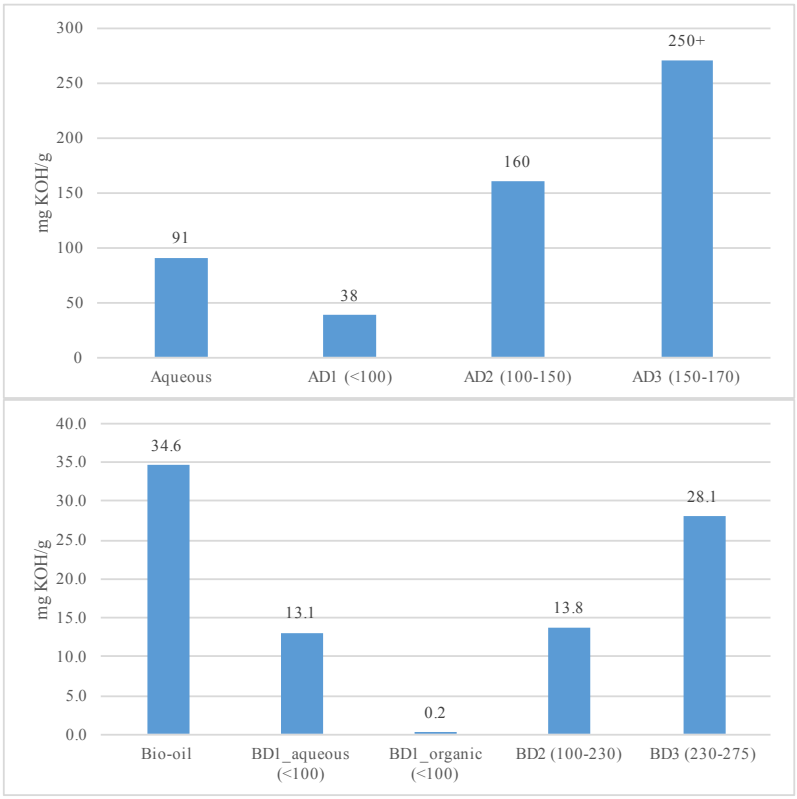

Figure 4.7. Total acid number of aqueous and bio-oil distillate fractions.

The gross heating values of the distillates were also compared to the original product (i.e., raw bio-oil and aqueous) as shown in Figure 4.8. The heating values of the distillates improved from the original bio-oil and aqueous phase except the AD1 and the aqueous layer of BD1. However, the AD2 still had low energy content compared to the AD3. This might be due to high water content contained in the distillate products, which lowered their energy values. All bio-oil distillate fractions showed significant improvement of heating values from bio-oil after fractional distillation. The highest energy content was found in the organic phase of BD1 (40.4 MJ/kg). This was close to the heating value of pure biodiesel (40.5 MJ/kg) as specified by the US department of Energy [96]. However, the heating value of the aqueous phase of BD1 was undetectable by the bomb calorimeter. This could be due to a very low energy content in the BD1_aqueous since it contained extremely high water content. Moreover, this suggested that most of the water was removed in the first fraction ($< 100^{o}C$) and formed a separate layer in BD1.

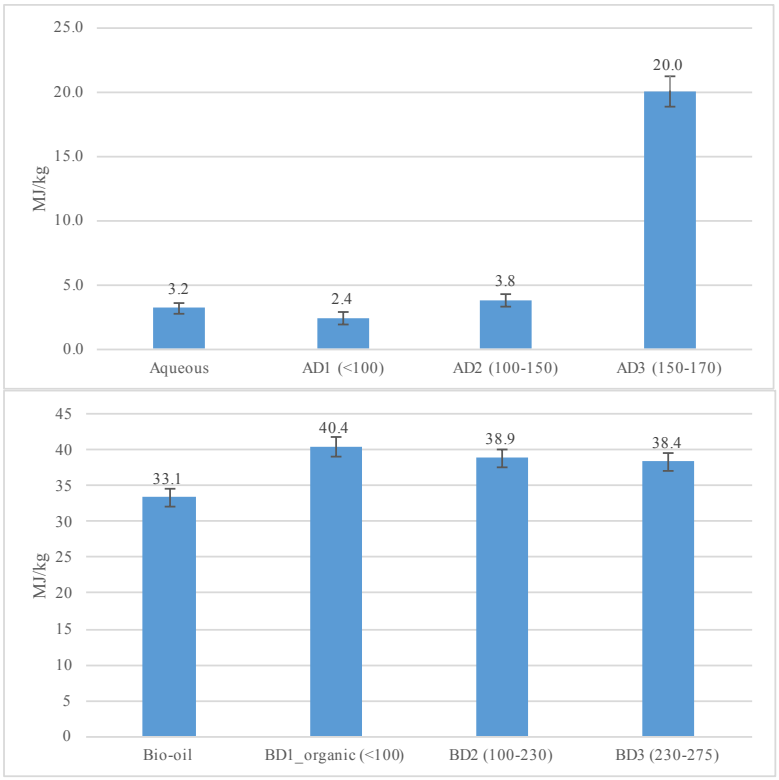

Figure 4.8. Gross heating value of aqueous and bio-oil distillate fractions.

4.3.1.3. Chemical composition of distillate fractions

The ultimate analysis provided the information of elemental composition (C, H, N, S) in weight percent, which had been used to identify the possibility of either using the distillates energy product or improving them further. The elemental compositions of aqueous and bio-oil distillates were analyzed as demonstrated in Figure 4.9. The original aqueous product contained around 73% oxygen and 9% carbon. After distillation, the highest oxygen content was obtained in the first fraction (86%) then decreased as the boiling point increased. In the last fraction (AD3), the oxygen content reduced to 44% with carbon content increased to 35%. Moreover, the nitrogen contents of the distillates

were found to be increased as the boiling points increased. Nitrogen content was concentrated in AD3 which was around 14%. Laredo et al. also performed the distillation of oil that was used as a feedstock for diesel production and obtained the same trend of nitrogen compounds, which concentrated in the fractions with higher boiling points [97].

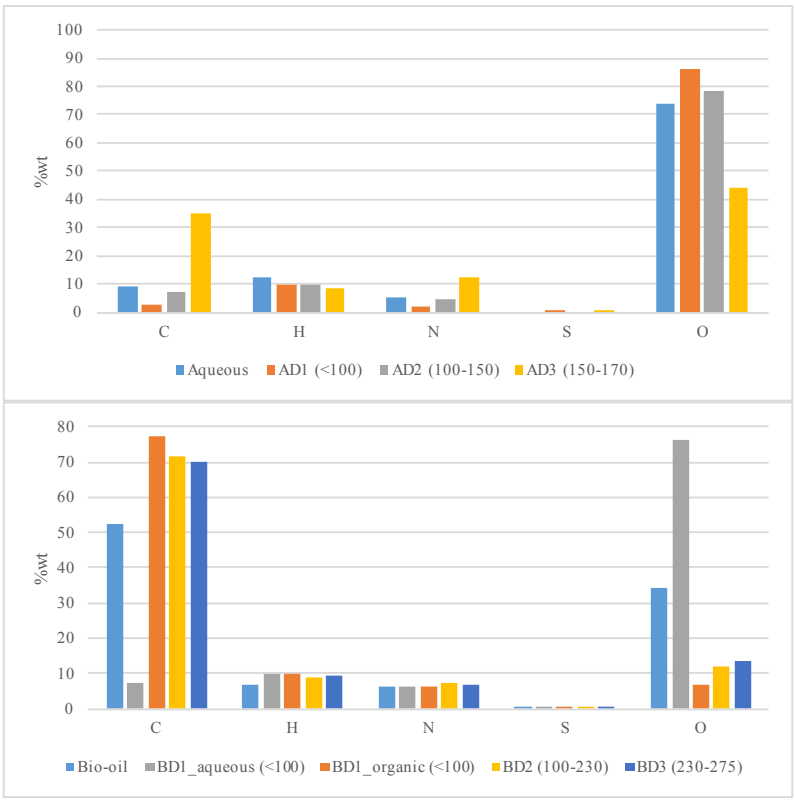

Figure 4.9. Ultimate analysis of aqueous and bio-oil distillate fractions.

On the other hand, the raw bio-oil contained 52% of carbon and 34% of oxygen contents. The results from the ultimate analysis showed an improvement of the

distillates' quality. The highest oxygen content (76%) with lowest carbon content (9%) were obtained in the aqueous layer of BD1. The carbon contents of the remaining distillates (BD1_organic, BD2, and BD3) considerably increased from the raw bio-oil with major reductions in oxygen contents. The results from ultimate analysis could support the energy contents of the distillates, as high carbon and low oxygen content would lead to higher energy values. Therefore, the trends for heating values of distillate were in agreement with the result from the ultimate analysis.

The Van Krevelen diagram was constructed to understand how the bio-oil distillate fractions were located and compared with the commercial fuels (gasoline and diesel from Shell station) as shown in Figure 4.10. It can be seen that the raw bio-oil point is far away from the commercial gasoline and diesel area. However, the bio-oil distillates as a product from fractional distillation were closer to the commercial transport fuel points on the diagram. BD3 had the highest H/C ratio but with the highest O/C ratio as well, which made it far from the gasoline area. However, BD1_organic had the lowest O/C ratio and, with a reasonable H/C value, it became closest to the gasoline point.

The functional groups present in the distillates were also analyzed using the FTIR. The FTIR spectra of each distillate fractions of aqueous and bio-oil are demonstrated in Figure 4.11. The functional groups which related to the observed peaks of each fractions are summarized as shown in Table 4.2.

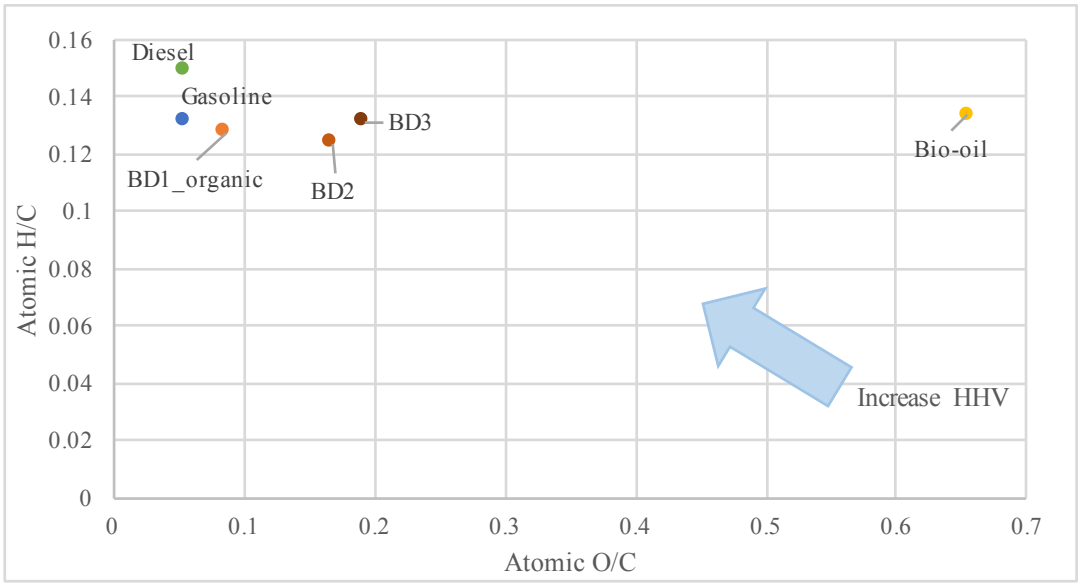

Figure 4.10. Van Krevelen diagram of raw bio-oil, bio-oil distillate fractions, and commercial transport fuels.

As mentioned in section 2.3.3.2, the dominant peak found in the aqueous product at 3640-3200 cm^{-1} indicated the presence of water, phenols, and alcohols. This peak still appeared prominently in the aqueous distillates (AD1 and AD2) but significantly reduced in AD3. The minimal peak of AD3 between 3640-3200 cm^{-1} suggested that it might contain mostly organic compounds such as ketones, carboxylic acids, esters, amides, and nitriles with small amount of water. Other components found in the original aqueous such as alkanes, aldehydes, amines, amides, and nitro compounds were distributed in the aqueous distillate fractions.

The raw bio-oil and its distillate spectra appeared to be the same but they differed from the aqueous layer of BD1. The BD1_aqueous spectrum looked similar to the spectrum of the first fraction of aqueous distillates. The dominant peak of BD1_aqueous

at 3640-3200 cm^{-1} was not observed in the other distillate fractions. These peak positions detected in BD1_aqueous indicated that it might consist mainly of water, which agreed with the moisture content results from section 4.3.1.2. Another prominent peak observed in BD1_aqueous was at 1650-1550 cm^{-1} which corresponded to N-H bending vibrations, suggesting the presence of amines and amides. The higher intensity of the peaks at 730 cm^{-1} and 700 cm^{-1} might indicate the higher concentration of aromatics and alkanes in BD1.

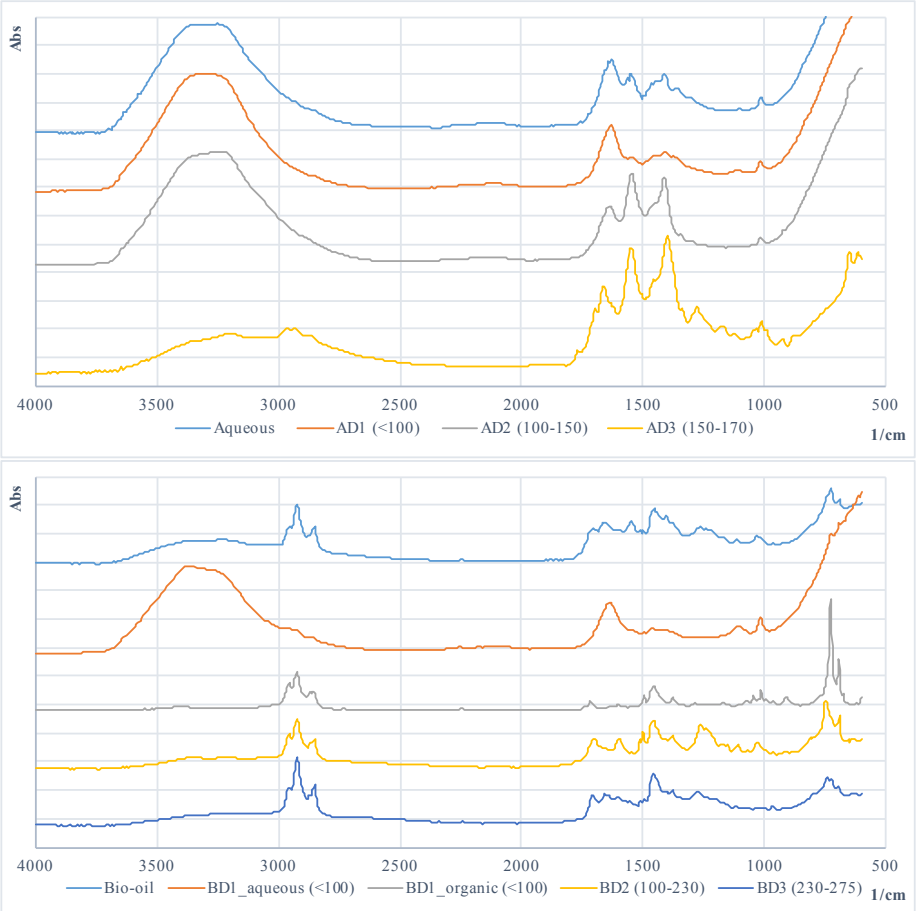

Figure 4.11. FTIR spectra of aqueous and bio-oil distillate fractions.

Table 4.2. FTIR functional group composition present in distillate fractions.

Frequency range (cm^{-1})	Bond	Functional group	Distillate fraction containing compounds	
			Aqueous	Bio-oil
3640-3610	O-H stretch, free hydroxyl	Alcohols, Phenols	AD1, AD2, AD3	BD1_aqueous
3500-3200	O-H stretch, H-bonded	Alcohols, Phenols, Water	AD1, AD2, AD3	BD1_aqueous
3100-3000	C-H stretch	Aromatics	-	BD1_organic, BD2, BD3
3100-3000	=C-H stretch	Alkenes	-	BD1_organic, BD2, BD3
3000-2850	C-H stretch	Alkanes	-	BD1_organic, BD2, BD3
1750-1650	C=O stretch	Ketones, Aldehydes	AD1, AD2, AD3	-
1680-1640	-C=C- stretch	Alkenes	-	BD1_organic, BD2, BD3
1650-1550	N-H bend	Amines, Amides	AD1, AD2, AD3	BD1_aqueous
1600-1585	C-C stretch (in-ring)	Aromatics	-	BD2, BD3
1550-1475	N-O asymmetric stretch	Nitro compounds	AD2, AD3	BD1_organic, BD2, BD3
1500-1400	C-C stretch (in-ring)	Aromatics	AD2, AD3	BD1_organic, BD2, BD3
1470-1450	C-H bend	Alkanes	AD1, AD2, AD3	BD1_organic, BD2, BD3
1370-1350	C-H rock	Alkanes	-	BD1_organic, BD2, BD3
1360-1290	N-O symmetric stretch	Nitro compounds	AD2, AD3	BD2, BD3
1335-1250	C-N stretch	Aromatics amines	AD3	BD2, BD3
1320-1000	C-O stretch	Alcohols, Carboxylic acids, Esters	AD1	BD1_aqueous, BD1_organic, BD2, BD3
1000-650	=C-H bend	Alkenes	-	BD1_organic, BD2, BD3
900-675	C-H	Aromatics	-	BD1_organic, BD2, BD3
725-720	C-H rock	Alkanes	-	BD1_organic, BD2, BD3

According to the properties of the distillates mentioned above, bio-oil distillate fractions except the aqueous layer from BD1 had a potential to be used as a fuel substitute. Therefore, to understand the characteristics of the bio-oil distillates in more details, GC-MS was selected to determine the chemical compositions present in each bio-oil distillate fractions. This could help to identify the applications of the distillates as well as whether they needed the further upgrading process or not.

Figure 4.12 demonstrates the total percent relative content of chemical compounds contained in original bio-oil and bio-oil distillates by functional groups. The highest compound found in raw bio-oil was oxygenates (24.8%) followed by paraffins (15.9%) and aromatics (14.7%). The raw bio-oil also contained a high amount of nitrogen-containing compounds due to the amount of protein contained in Jatropha de-oiled cake (Table 2.1). Both oxygenated and nitrogenated compounds were undesirable since they deteriorated the quality of bio-oil. The presence of oxygenates made bio-oil acidic. The nitrogenated compounds led to the NOx emission if bio-oil was used as combustion fuel. In addition, the nitrogen could immobilize the downstream catalyst if the bio-oil was co-processed with crude oil in petroleum refineries [71].

The results show an improvement of bio-oil distillates' quality. The original bio-oil with small portions of hydrocarbons (42.8%) was successfully upgraded into higher-concentrated fractions via fractional distillation. The percent relative contents of hydrocarbons (paraffins, napthenes, olefins, cyclo.olefins, and aromatics) in all distillate fractions were improved and the highest percentage was achieved in the first fraction (84%). The (O)-containing compounds of the distillates were significantly reduced from

the original bio-oil. Additionally, the nitriles of BD1_organic were lower than the original bio-oil but notably increased in BD2 and BD3.

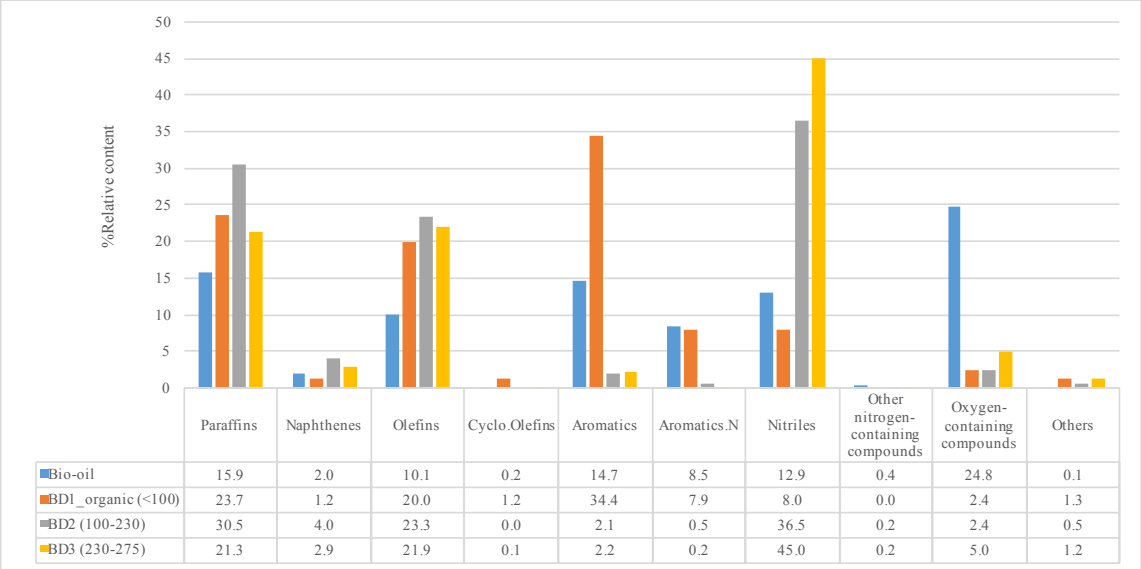

	Paraffins	Naphthenes	Olefins	Cyclo.Olefins	Aromatics	Aromatics.N	Nitriles	Other nitrogen-containing compounds	Oxygen-containing compounds	Others
Bio-oil	15.9	2.0	10.1	0.2	14.7	8.5	12.9	0.4	24.8	0.1
BD1_organic (<100)	23.7	1.2	20.0	1.2	34.4	7.9	8.0	0.0	2.4	1.3
BD2 (100-230)	30.5	4.0	23.3	0.0	2.1	0.5	36.5	0.2	2.4	0.5
BD3 (230-275)	21.3	2.9	21.9	0.1	2.2	0.2	45.0	0.2	5.0	1.2

Figure 4.12. Functional group present in raw bio-oil and its distillate fraction.

To understand the characteristics of separation in the micro-level model, the degree of separation was used as an indicator to evaluate the bio-oil separation properties, which was calculated in terms of separation factor β. The degree of separation was first defined by Guo et al. [98] where they separated bio-oil into two fractions (distilled and residual fractions) using molecular distillation. The equation below was formulated to compute β using the quantities of components contained in the distilled and residual fractions.

$$\beta = \frac{M_{DF}}{M_{DF}+M_{RF}} \tag{4.4}$$

Where

M_{DF}, M_{RF} = Quantity of the component in the distilled and residual fractions.

However, this equation was modified in order to be used with n distillate fractions. The modified equation is shown below.

$$\beta = \frac{M_i}{\sum_{i=1}^{n} M_{BF_i}} \quad (4.5)$$

Where

$M_i = Y_i \times X_i$

Mi = quantity of component in fraction i

n = number of distillate fractions

M_{BFi} = quantity of component in each distillate fraction i where i ranges from 1 to n

Y_i = yield of fraction i

X_i = proportion of component in fraction i (%relative content from GC-MS)

Therefore, the value of β equal to one indicated the completed separation of that component as defined by Guo et al. [98]. Since this study had three distillate fractions, the value of $\beta > 0.33$ indicated the greater proportion of that compound than other fractions. The value of β close to zero indicated the compound was not effectively separated. Table 4.3 shows the chemical compounds contained in BD1_organic, BD2 and BD3 along with their quantities and the degree of separation.

According to the table, around 140 chemical compounds were observed in bio-oil distillates. The majority of compounds found in the distillate fractions were paraffins, naphthenes, olefins, and aromatics. The highest chemical compounds found in the first distillate fraction was toluene, which also had a separation factor close to 1. Nitriles

were mostly found in BD2 and BD3, especially hexadecanennitrile and oleanitrile, which appeared to be difficult to separate according to the amounts found in both fractions. However, all components showed the value of separation factor (β) greater than 0.33. In addition, more than 80 compounds were completely separated (β=1). This suggested the powerful separation of bio-oil components for this distillation process.

Table 4.3. Chemical compounds and separation factor of bio-oil distillate fractions.

Compound	%Mass in each fraction			Beta
	BD1_organic	BD2	BD3	
Paraffins				
Nonane	0.65	0.11	0.21	0.67
Decane	0.48	0.33	0.25	0.45
Octane	0.47	0.07	0.27	0.58
Undecane	0.26	0.00	0.00	1.00
Heptane	0.22	0.04	0.20	0.48
Tridecane	0.12	0.00	0.17	0.59
Dodecane	0.10	0.25	0.12	0.53
Hexadecane	0.03	4.51	2.60	0.63
Heptane, 3-ethyl-2-methyl-	0.03	0.00	0.02	0.65
Nonane, 2-methyl-	0.01	0.00	0.00	1.00
Nonadecane	0.00	0.11	0.00	0.97
Pentadecane	0.00	0.76	0.00	1.00
Tetratriacontane	0.00	0.25	0.00	1.00
Octacosane	0.00	0.15	0.00	1.00
Heneicosane	0.00	0.11	0.00	1.00
Butane, 2-methyl-	0.00	0.03	0.00	1.00
Octadecane	0.00	0.00	0.20	1.00
Pentane, 3-ethyl-2-methyl-	0.00	0.00	0.01	1.00
Naphthenes				
Cyclohexane, (1-methylethyl)-	0.04	0.00	0.00	1.00
Cyclopentane, butyl-	0.03	0.00	0.00	1.00
Cyclopentane, pentyl-	0.03	0.00	0.00	1.00

Table 4.3. Continued

Compound	%Mass in each fraction			Beta
	BD1_organic	BD2	BD3	
Naphthenes				
Cyclopentane, propyl-	0.01	0.00	0.00	1.00
n-Nonylcyclohexane	0.00	0.14	0.11	0.56
Cyclohexane, undecyl-	0.00	0.14	0.10	0.58
n-Tridecylcyclohexane	0.00	0.13	0.00	1.00
Cyclopentane, 1-pentyl-2-propyl-	0.00	0.10	0.06	0.64
Cyclododecane	0.00	0.10	0.00	1.00
Cyclopentane, nonyl-	0.00	0.08	0.00	1.00
Cyclopentane, decyl-	0.00	0.06	0.05	0.55
Cyclotetradecane	0.00	0.04	0.06	0.59
1,3-Dimethyl-(3,7-dimethyloctyl)cyclohexane	0.00	0.04	0.00	1.00
Cyclopropane, 1-heptyl-2-methyl-	0.00	0.02	0.00	1.00
Dodecane, 1-cyclopentyl-4-(3-cyclopentylpropyl)-	0.00	0.01	0.00	1.00
Cyclohexane, 1,1'-(1-methyl-1,3-propanediyl)bis-	0.00	0.00	0.17	1.00
Olefins				
1-Decene	0.43	0.05	0.05	0.81
2-Octene	0.34	0.00	0.00	1.00
1-Tetradecene	0.24	0.00	0.29	0.55
1-Heptene	0.21	0.01	0.09	0.67
1-Undecene	0.18	0.31	0.08	0.54
3-Decene	0.13	0.00	0.00	1.00
cis-2-Nonene	0.11	0.00	0.02	0.81
3-Nonene, (E)-	0.10	0.00	0.00	1.00
2-Undecene, (Z)-	0.08	0.08	0.13	0.46
2-Octene, (E)-	0.07	0.00	0.00	1.00
1-Dodecene	0.07	0.00	0.06	0.53
3-Tetradecene, (Z)-	0.06	0.35	0.05	0.76
3-Tetradecene, (E)-	0.05	0.00	0.00	1.00
2-Decene, (Z)-	0.05	0.06	0.02	0.47
trans-3-Decene	0.05	0.00	0.00	1.00
1,3-Nonadiene, (E)-	0.04	0.00	0.00	1.00
3-Undecene, (E)-	0.03	0.00	0.03	0.50
4-Dodecene, (Z)-	0.02	0.00	0.04	0.69

Table 4.3. continued

Compound	%Mass in each fraction			Beta
	BD1_organic	BD2	BD3	
Olefins				
Cyclohexene	0.02	0.00	0.00	1.00
3-Dodecene, (E)-	0.01	0.00	0.00	1.00
3-Dodecene, (Z)-	0.01	0.00	0.00	1.00
2-Dodecene, (E)-	0.01	0.00	0.00	1.00
5-Tetradecene, (E)-	0.01	0.00	0.00	1.00
1-Octene	0.01	0.09	0.00	0.95
9-Octadecene, (E)-	0.00	2.20	0.00	1.00
3-Hexadecene, (Z)-	0.00	0.62	0.17	0.78
3-Eicosene, (E)-	0.00	0.29	0.00	1.00
5-Eicosene, (E)-	0.00	0.28	0.00	1.00
9-Nonadecene	0.00	0.11	0.00	1.00
2-Dodecene, (Z)-	0.00	0.07	0.02	0.73
9-Eicosene, (E)-	0.00	0.05	0.00	1.00
8-Heptadecene	0.00	0.00	2.08	1.00
1-Hexadecene	0.00	0.00	0.32	1.00
7-Tetradecene	0.00	0.00	0.12	1.00
E-7-Octadecene	0.00	0.00	0.12	1.00
1-Nonene	0.00	0.00	0.08	1.00
4-Tetradecene, (Z)-	0.00	0.00	0.08	1.00
1-Tridecene	0.00	0.00	0.07	1.00
6-Tetradecene, (Z)-	0.00	0.00	0.04	1.00
2-Decene, (E)-	0.00	0.00	0.04	1.00
1-Pentadecene	0.00	0.00	0.03	1.00
2-Octene, (Z)-	0.00	0.00	0.02	1.00
Cyclo.Olefins				
Cyclopentene, 3-methyl-	0.04	0.00	0.00	1.00
Cyclopentene, 1-pentyl-	0.03	0.00	0.00	1.00
Cyclohexene,1-propyl-	0.03	0.00	0.00	1.00
Cyclohexene, 1-butyl-	0.02	0.00	0.00	1.00
Cyclohexene	0.00	0.00	0.02	1.00
Aromatics				
Toluene	1.73	0.09	0.35	0.80
Ethylbenzene	0.76	0.06	0.04	0.88
Benzene, 1,3-dimethyl-	0.21	0.00	0.00	1.00

Table 4.3. continued

Compound	%Mass in each fraction			Beta
	BD1_organic	BD2	BD3	
Aromatics				
Benzene, 1-ethyl-2-methyl-	0.15	0.02	0.00	0.87
Benzene, propyl-	0.15	0.03	0.00	0.84
Benzene, butyl-	0.11	0.07	0.00	0.59
Benzene	0.08	0.00	0.00	1.00
Benzene, 1,2,3-trimethyl-	0.08	0.00	0.00	1.00
Benzene, 1-propenyl-	0.05	0.00	0.00	1.00
Benzene, pentyl-	0.05	0.07	0.00	0.60
Benzene, 1-ethyl-3-methyl-	0.04	0.00	0.00	1.00
Pyridine, 2,6-dimethyl-	0.03	0.00	0.00	1.00
Benzene, 1-methyl-4-(2-methylpropyl)-	0.02	0.00	0.00	1.00
Benzene, hexyl-	0.02	0.00	0.00	1.00
Benzene, dodecyl-	0.01	0.00	0.00	1.00
Benzene, 1-methyl-4-(2-methylpropyl)-	0.00	0.04	0.02	0.63
1-Methyl-2-n-hexylbenzene	0.00	0.01	0.00	1.00
Nitriles				
Pentanenitrile, 4-methyl-	0.20	0.06	0.00	0.78
4,4-Dimethyl-3-oxopentanenitrile	0.15	0.00	0.00	1.00
Butanenitrile, 3-methyl-	0.15	0.00	0.00	1.00
Isobutyronitrile	0.07	0.00	0.00	1.00
Pentanenitrile	0.07	0.00	0.00	1.00
Butanenitrile	0.06	0.00	0.00	1.00
Hexanenitrile	0.04	0.02	0.00	0.65
Heptanonitrile	0.03	0.05	0.00	0.61
Octanenitrile	0.02	0.00	0.03	0.54
Hexadecanenitrile	0.00	3.32	3.58	0.52
Oleanitrile	0.00	2.33	3.46	0.60
Nonadecanenitrile	0.00	1.87	0.01	0.99
Dodecanenitrile	0.00	0.14	0.00	1.00
Nonanenitrile	0.00	0.07	0.01	0.84
Octanenitrile	0.00	0.05	1.42	0.97
2-Pentenenitrile, 5-hydroxy-, (E)-	0.00	0.03	0.00	1.00
Pentadecanenitrile	0.00	0.02	0.01	0.57
Decanenitrile	0.00	0.00	0.03	1.00

Table 4.3. continued

Compound	%Mass in each fraction			Beta
	BD1_organic	BD2	BD3	
Aromatics.N				
Pyrrole	0.61	0.00	0.01	0.98
Pyridine, 2-methyl-	0.15	0.00	0.00	1.00
Pyrazine, ethyl-	0.03	0.00	0.00	1.00
3-Methylpyridazine	0.00	0.12	0.00	1.00
Benzenepropanenitrile	0.00	0.07	0.00	1.00
Indole	0.00	0.00	0.02	1.00
Other (N)-containing				
Propane, 2-methyl-2-nitro-	0.00	0.04	0.00	1.00
N-Methyldodecanamide	0.00	0.03	0.13	0.82
1H-Indole, 3-methyl-	0.00	0.00	0.04	1.00
(O)-containing				
2-Pentanone, 3-methyl-	0.13	0.00	0.00	1.00
Ethanone, 1-(2-furanyl)-	0.05	0.00	0.00	1.00
n-Hexadecanoic acid	0.03	0.00	0.00	1.00
2,4-Hexadien-1-ol	0.02	0.00	0.00	1.00
2-Cyclopenten-1-one, 2-methyl-	0.02	0.00	0.00	1.00
3-Hexanone	0.01	0.00	0.00	1.00
E-14-Hexadecenal	0.00	0.34	0.22	0.60
Hexadecanoic acid, methyl ester	0.00	0.09	0.16	0.63
2,5-Pyrrolidinedione, 1-methyl-	0.00	0.03	0.00	1.00
Octadecanoic acid, methyl ester	0.00	0.03	0.06	0.68
n-Tridecan-1-ol	0.00	0.02	0.12	0.89
Z-10-Pentadecen-1-ol	0.00	0.00	0.18	1.00
E-15-Heptadecenal	0.00	0.00	0.01	1.00
Others				
7-Heptadecene, 1-chloro-	0.00	0.11	0.07	0.61
Silanediamine, 1,1-dimethyl-N,N'-diphenyl-	0.00	0.00	0.10	1.00
Sulfurous acid, octadecyl 2-propyl ester	0.00	0.00	0.05	1.00
Trichloroacetic acid, pentadecyl ester	0.00	0.00	0.01	1.00

4.3.2. Catalytic upgrading of bio-oil distillate

Based on the distillate yields and properties discussed in the previous sections, BD2 (100-230^{o}C) was selected as a precursor for the hydrotreatment process. Pd/C with 10 wt% loading was used as a catalyst with different operating temperatures (150, 200, and 250^{o}C)

4.3.2.1. Product yields

The effects of temperatures on product yields from the hydrotreatment of Jatropha bio-oil distillate were investigated. The product from hydrotreatment consisted of liquid product (upgraded oil and tar), solid product (coke), and gases. The preferable product from the hydrotreatment was the upgraded bio-oil. Figure 4.13 compares the upgraded product with the starting materials (original bio-oil and its distillate). The original bio-oil was a dark viscous liquid. After the distillation, it became a smoky dark brown solution with less viscosity. Finally, the hydrotreatment of the distillate resulted in a more transparent light brown solution. Moreover, the hydrotreated bio-oil distillate appeared to be more free-flowing than the distillate and bio-oil.

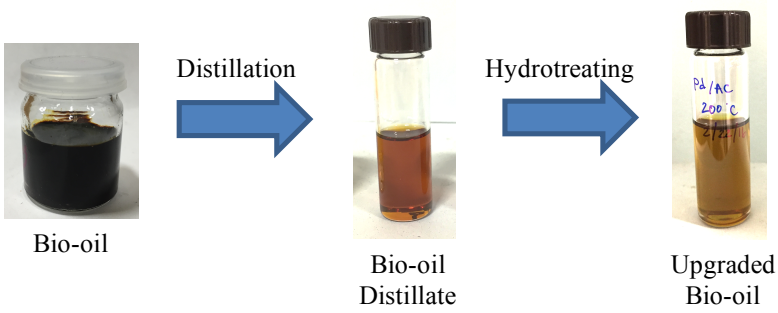

Figure 4.13. Raw bio-oil, bio-oil distillate fraction, and upgraded distillate.

Figure 4.14 shows the product yields from the hydrotreatment process at different operating temperatures. The upgraded oil yields varied from 36.5-64.9 wt% and the optimum was observed at 200^{o}C. Higher operating temperatures (250-450^{o}C) resulted in higher degrees of deoxygenation because of a better catalytic activity. Nevertheless, this could reduce the oil yield with an increase in gas yield because the cracking reaction occurred instead of deoxygenation [99]. In this study, the upgraded oil yields were higher than many studies using the same catalyst for the hydrotreatment of raw bio-oil such as pine sawdust [100], mallee woody [101], and beech wood [102]. By using the raw bio-oil as a starting material for the hydrotreatment, the upgraded liquid product usually consisted of two phases (i.e., organic and aqueous phases) while the upgraded liquid product in this study contained only the organic phase. The upgraded liquid product with two layers was also observed in many studies on the catalytic upgrading of raw bio-oil [102-104].

The catalytic upgrading of raw bio-oil could improve its quality. However, this made the upgrading process inefficient due to the complicated bio-oil composition. This resulted in a loss of some organics compound to the aqueous phase, which was observed as a water layer in the upgraded liquid product. Moreover, it led to a reduction of the upgraded oil yield. Therefore, the fractionation of bio-oil before the hydrotreatment process might be a more efficient way to produce good quality liquid fuel than treating the whole bio-oil [105-107]. The characterization of upgraded bio-oil will be discussed in deeper detail in subsequent sections.

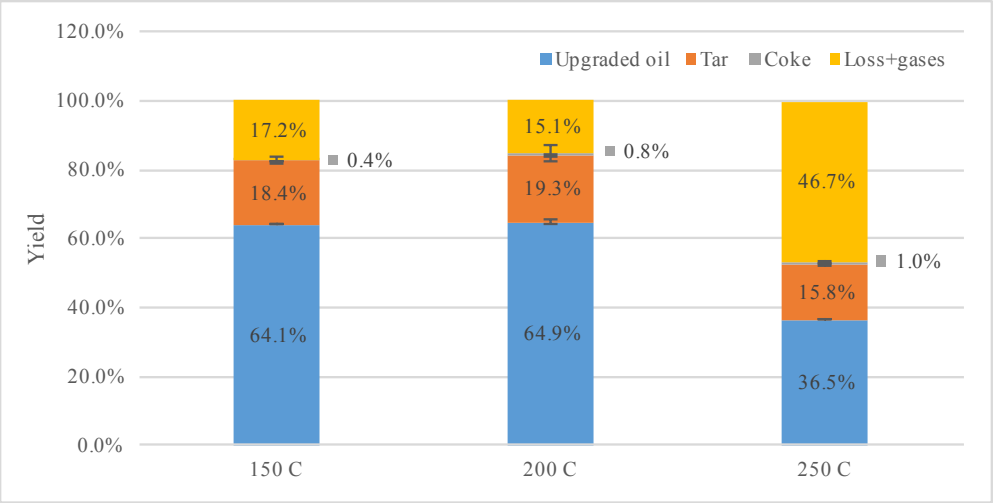

Figure 4.14. Product yields from catalytic upgrading at different temperatures.

4.3.2.2. Upgraded oil properties

The physical and chemical properties of upgraded bio-oil at different operating temperatures including moisture content, heating value, total acid number, and elemental composition were summarized and compared with the distillate fraction (BD2) as shown in Table 4.4.

Table 4.4. Characteristics of bio-oil distillate and its upgraded product at different temperatures.

	BD2	Upgraded oil 150°C	Upgraded oil 200°C	Upgraded oil 250°C
M.C. (%wt)	4.06	1.83	0.87	0.73
HHV (MJ/kg)	38.9	40.3	41.3	40.2
TAN (mg KOH/g)	13.8	4.30	4.16	1.59
Ultimate analysis (wt%)				
C	71.4	73.4	75.3	74.7
N	7.6	7.3	7.2	8.0
H	8.9	8.8	9.6	9.7
S	0.1	0.3	0.1	0.1
*O**	12.0	10.2	7.8	7.5
%DOD	-	15.0	35.0	37.7

The moisture content of upgraded bio-oil distillate was significantly reduced from the starting material (BD2) and appeared to decrease with an increase of operating temperatures. The moisture content of the upgraded liquid product at 200°C was not significantly different from 250°C. According to Bu et al. [108], the reduction of water in upgraded product was due to the decarboxylation and dehydration reactions during the catalytic hydrotreatment process. Thus, the water contained in the starting material was transferred to the aqueous layer as observed as a water separation in upgraded liquid product. However, no water layer was detected in the upgraded bio-oil in this study. The hydrotreating temperatures used in this experiment ranged from 150-250°C, which was considered as a mild hydrotreating as proposed by Venderbosch et al. [107]. Therefore, the insufficient water production during the hydrogenation step could result in the absence of water phase.

The heating value of the upgraded liquid product was also analyzed. The HHV of all upgraded bio-oils was significantly improved from the initial distillate feed (BD2). This indicated the effectualness of hydrotreating process, which enhanced the energy content of upgraded product. The highest HHV was found at 200^{o}C while the others from 150 and 250^{o}C were not significantly different.

The knowledge elemental composition can be used to support the heating value of the product as explained in section 2.3.3.1. The results from the ultimate analysis revealed the effective hydrotreating process of bio-oil distillate by increasing the carbon content while reducing the oxygen content of upgraded product, which led to the increase in energy content. The highest carbon content along with the lowest oxygen content were obtained at 200^{o}C. The degree of deoxygenation was then calculated based on the initial oxygen content in distillate and final oxygen content in upgraded product as shown in Table 4.4. The highest %DOD was observed at 250^{o}C (37.7%). The percent deoxygenation increased with an increase of operating temperatures which indicated a better catalytic activity at higher temperatures. Hydrogen content was observed to be slightly increased with an increase of operating temperatures. Remon et al. [109] studied the effects of operating temperature on a catalytic upgrading of pinewood bio-oil and obtained the same trend for the elemental composition results.

Van Krevelen diagram was constructed to compare the upgraded bio-oil distillates with the starting material (BD2), raw bio-oil, and commercial transport fuels (from Shell station) as demonstrated in Figure 4.15. Low O/C and high H/C ratios were preferable since they increase the energy content of the fuel products. The energy

contained in C-O bond is lower than that in C-H and C-C bonds, hence leads to lower energy content. According to the previous section, the quality of bio-oil distillates from fractional distillation was significantly improved from the raw bio-oil and tended to approach the gasoline region. Likewise, the quality of upgraded liquid product from catalytic upgrading of bio-oil distillates was enhanced and getting closer to the gasoline region.

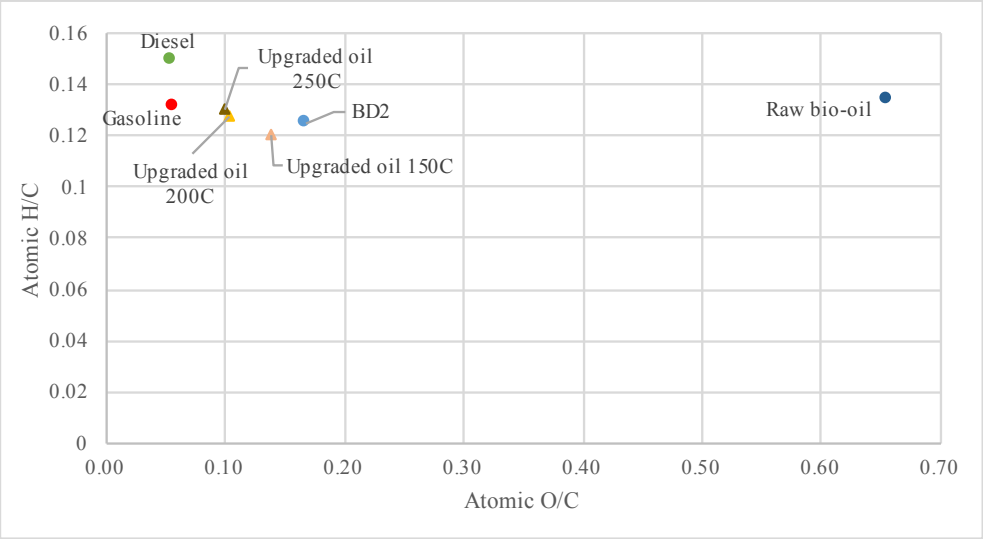

Figure 4.15. Van Krevelen diagram of raw bio-oil, bio-oil distillate, catalytic upgraded oil, and commercial transport fuels.

The acidity of bio-oil product is also an important factor for fuel quality control since it could lead to the corrosion problems when used as transport fuel. Total acid number was used to indicate the acidity level of fuel product. Oxygenated compound was one of the main components that effected the acidity of bio-oil. Therefore, the

reduction of oxygen content related to the acid number present in the upgraded liquid product. According to Table 4.4, TAN of upgraded oil (1.59-4.3) was considerably lower than the initial bio-oil distillate (13.8), which was also supported by the reduction of oxygen content with regard to the ultimate analysis results.

4.3.2.3. Chemical composition of upgraded oil

The upgraded bio-oil at different operating temperatures was analyzed for the chemical compounds by GC-MS. Figure 4.16 compares the functional groups of compounds present in the bio-oil distillate (BD2) and upgraded products. Bio-oil distillate contained high amount of hydrocarbon especially paraffins and olefins. However, due to high amount of nitrogen-containing compounds contained in the distillate, a further upgrading process was needed in order to remove these unwanted compounds.

According to Figure 4.16, significant changes in the chemical compositions from the distillate to the upgraded products were observed. Hydrocarbons such as paraffins, naphthenes, and aromatics contained in the upgraded products were significantly increased from the starting material (BD2). The nitrogen-containing and other oxygen-containing compounds were notably reduced from the BD2 after catalytic upgrading. However, the phenolic compounds were formed in the upgraded products even the starting material did not contain any phenolic compounds. This will be explained later in deeper detail in the subsequent sections.

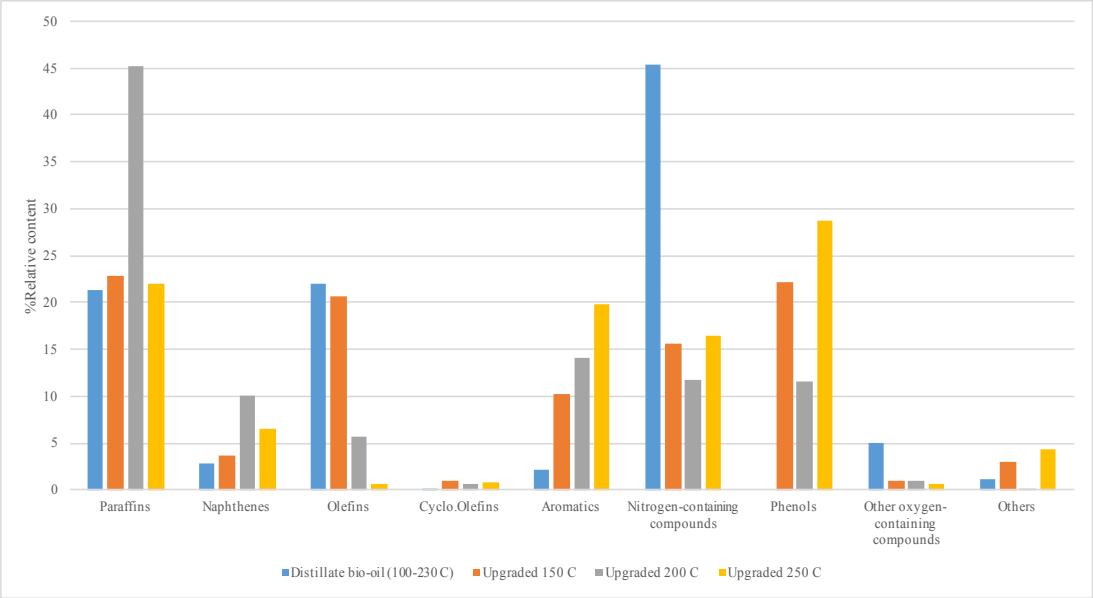

Figure 4.16. Functional group present in bio-oil distillate and its upgraded product at different temperatures.

The operating temperatures also showed some effects on the chemical compositions of the upgraded products. By increasing the operating temperatures, the aromatic contents were considerably increased while the olefins were significantly decreased. However, by considering the desirable compounds consisted in the fuel products (i.e., high amounts of hydrocarbon with low amounts of nitrogenates and oxygenates), the upgraded product from 200^{o}C appeared to be the optimum condition. Figure 4.17 summarizes the main compounds contained in bio-oil distillate and its upgraded product by functional groups. The highest hydrocarbons and lowest unwanted compounds (nitrogenates and oxygenates) were achieved in the upgraded product at 200^{o}C. At the optimum condition, hydrocarbon content was increased from 48.4% in BD2 to 75.7% in the upgraded product. In addition, a major reduction in nitrogen-

containing compounds of BD2 was also observed, which was substantially decreased from 45.4% to 11.7% in upgraded product. This suggested the effectiveness of the catalyst for the hydrotreatment process.

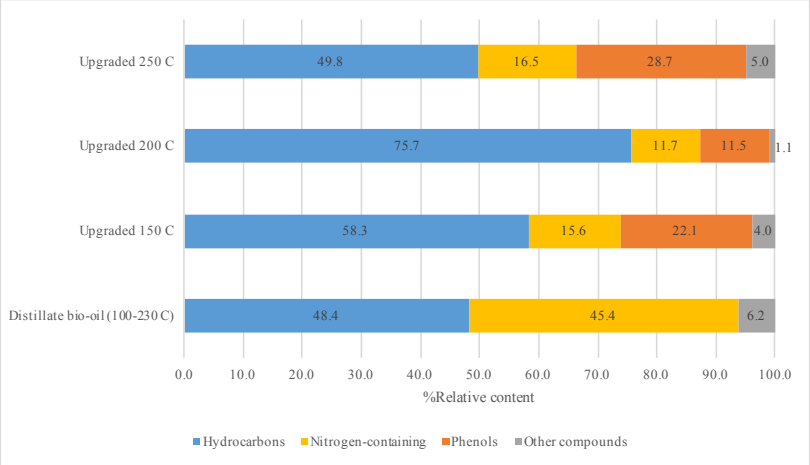

Figure 4.17. Functional group of distillate and its hydrotreated products.

For a better understanding in the chemical compounds contained in the upgraded product. The hydrocarbon compounds found in the distillate were compared with those in the upgraded bio-oil at optimum condition as summarized in Table 4.5. Obviously, more paraffins, naphthenes, and aromatics were formed in the upgraded product. Many studies also observed the increase of aromatic compounds in the upgraded bio-oil, which could be explained by the depolymerization of lignin-derived oligomers during the upgrading process [110-112]. Table 4.6 also summarizes the major oxygenated compounds present in bio-oil distillate and upgraded product. The absence of ketones and aldehydes suggested their conversion to alcohols during the hydrotreatment, which

was also observed by Venderbosch et al. [107]. The hydrogenation of the aldehydes and ketones to alcohols was detected as they performed a mild hydrotreatment of pyrolysis oil at 225^{o}C using Ru catalyst. Moreover, some oxygenated compounds such as hexadecanoic acid methyl ester and octadecanoic acid, methyl ester were converted to long chain hydrocarbon. However, a formation of phenolic compounds was observed to be higher in the upgraded product than the starting material. This phenomenon was also reported in many studies [110,113]. This indicated the alkylation of aromatic compounds occurred during the hydrotreatment process. Huang et al. [114] also reported the formation of methylated and ethylated phenols when the depolymerization of lignin was conducted in a supercritical ethanol using CuMgAlOx as catalyst.

Another crucial improvement in the hydrotreated product was a major reduction in nitrogen-containing compounds. Table 4.7 compares the nitrogen-containing compounds in bio-oil distillate and hydrotreated product. The reduction of nitrogen-containing compounds along with the rise in hydrocarbons could be a result of a denitrogenation of aliphatic nitrogen compounds, which converted nitriles to paraffins, for example, hexadecanenitrile to hexadecane and octadecanenitrile to octadecane [115].

The selectivity of Pd/C catalyst based on the carbon number was also summarized as shown in Table 4.8. The carbon ranges were selected based on the refinery products [116]. Paraffins in the upgraded product with C5 to C12 (gasoline) and C12 to C16 (kerosene) were significantly increased after hydrotreatment process. More concentration of paraffins in the hydrotreated product was a consequence to the hydrogenation of olefins or cracking of other higher paraffins. This could be supported

by the reduction of paraffins with high carbon number (diesel and lubricating oil ranges) as well as the olefins in the upgraded product as shown in Table 4.8. Furthermore, a major increase in aliphatic paraffins (C12-C16) in the hydrotreated bio-oil could be a result of the hydrodenitrogenation of alkanenitriles. The results showed no alkanenitriles with C12-C16 was found in the upgraded product, which indicated the alkanenitriles were completely denitrogenated [115].

Table 4.5. Major hydrocarbons in bio-oil distillate and its hydrotreated product.

Compounds	%relative content		Compounds	%relative content	
	BD2	Upgraded oil 200C		BD2	Upgraded oil 200C
Paraffins			***Napthenes***		
Butane, 2-methyl-	0.12	-	Cyclohexane	-	0.74
Heptane	0.16	1.18	Cyclobutane, (1-methylethylidene)-	-	0.2
Octane	0.32	1.41	Isopropylcyclobutane	-	0.25
Nonane	0.48	1.59	Cyclohexane, ethenyl-	-	0.17
Decane	1.48	2.82	Cyclohexane, ethyl-	-	0.48
Undecane	-	3.99	Cyclopentane, 1-ethyl-2-methyl-	-	0.1
Dodecane	1.14	-	Cyclopentane, 1-ethyl-2-methyl-, cis-	-	0.39
Tridecane	-	10.09	Cyclopentane, propyl-	-	0.27
Pentadecane	3.47	-	Cyclohexane, propyl-	-	0.43
Hexadecane	20.49	23.49	Cyclopentane, butyl-	-	0.21
Octadecane	-	0.11	Cyclopentane, pentyl-	-	0.34
Nonadecane	0.49	0.39	Cyclopropane, 1-heptyl-2-methyl-	0.11	-
Eicosane, 2-methyl-	-	0.12	Cyclododecane	0.45	-
Heneicosane	0.51	-	Cyclooctane, 1,2-diethyl-	-	0.41
Octacosane	0.69	-	Cyclopentane, 1-pentyl-2-propyl-	0.47	0.33
Tetratriacontane	1.15	-	Cyclotridecane	-	0.83
			Cyclopentane, nonyl-	0.38	-
Olefins			Cyclotetradecane	0.20	0.79
1-Heptene	0.06	-	Cyclopentane, decyl-	0.29	2.21
1,4-Pentadiene, 2,3,3-trimethyl-	-	0.33	n-Nonylcyclohexane	0.65	1.06
1-Octene	0.05	-	Cyclohexane, undecyl-	0.62	0.54
1-Decene	0.23	-	1,3-Dimethyl-(3,7-dimethyloctyl)cyclohexane	0.19	-

Table 4.5. continued

Compounds	%relative content		Compounds	%relative content	
	BD2	Upgraded oil 200C		BD2	Upgraded oil 200C
Olefins			***Napthenes***		
2-Decene, (Z)-	0.27	-	n-Tridecylcyclohexane	0.58	-
1-Undecene	1.39	-	Dodecane, 1-cyclopentyl-4-(3-cyclopentylpropyl)-	0.06	-
2-Undecene, (Z)-	0.37	0.54	Cyclohexane, eicosyl-	-	0.32
2-Dodecene, (Z)-	0.31	-			
6-Tridecene, (Z)-	-	0.6	***Aromatics***		
1-Tetradecene	2.43	-	Toluene	0.39	2.87
3-Tetradecene, (E)-	0.53	-	Benzene, methoxy-	-	0.16
3-Tetradecene, (Z)-	1.58	-	Benzene, 1,3-dimethyl-	-	0.23
5-Tetradecene, (E)-	-	0.79	Ethylbenzene	0.29	2.03
3-Hexadecene, (Z)-	2.80	-	o-Xylene	-	0.97
8-Heptadecene	-	1.43	Benzene, 1-ethenyl-2-methyl-	0.10	-
3-Octadecene, (E)-	-	0.47	Indane	-	1.08
9-Octadecene, (E)-	9.99	-	Benzene, 1-ethyl-2-methyl-	-	0.38
9-Nonadecene	0.49	0.55	Benzene, 1,2,3-trimethyl-	-	0.19
9-Nonadecene	-	-	Benzene, 1,3,5-trimethyl-	-	0.47
3-Eicosene, (E)-	1.33	0.49	Benzene, propyl-	0.13	1.4
5-Eicosene, (E)-	1.27	-	Benzene, butyl-	0.34	-
9-Eicosene, (E)-	0.24	-	Benzene, 1-methyl-4-(2-methylpropyl)-	0.16	-
1-Docosene	-	0.49	Benzene, pentyl-	0.32	1.51
			Benzene, hexyl-	0.19	1.71
Cyclo.Olefins			1-Methyl-2-n-hexylbenzene	0.06	0.48
Cyclohexene	-	0.57	Benzene, octyl-	-	0.76
Cyclopentene, 4-methyl-	-	0.11	Benzene, dodecyl-	0.08	-

Table 4.6. Major oxygenates in bio-oil distillate and its hydrotreated product.

Compounds	%relative content		Compounds	%relative content	
	BD2	Upgraded oil 200C		BD2	Upgraded oil 200C
Alcohols			***Ketones***		
n-Tridecan-1-ol	0.07		2,5-Pyrrolidinedione, 1-methyl-	0.14	-
1-Hexadecanol	-	0.89			
			Aldehydes		
Phenols	-		E-14-Hexadecenal	1.54	-
Phenol	-	5.07			
Phenol, 3-methyl-	-	3.86	***Esters***		
Phenol, 2,5-dimethyl-	-	1.66	Hexadecanoic acid, methyl ester	0.43	-
Phenol, 4-(1-methylethyl)-	-	0.94	Octadecanoic acid, methyl ester	0.13	-

Table 4.7. Major nitrogenates in bio-oil distillate and its hydrotreated product.

Compounds	%relative content		Compounds	%relative content	
	BD2	Upgraded oil 200C		BD2	Upgraded oil 200C
Aromatics.N			***Nitriles***		
Pyrrole	-	0.34	2-Pentenenitrile, 5-hydroxy-, (E)-	0.14	-
3-Methylpyridazine	0.54	-	Butanenitrile, 3-methyl-	-	0.95
Pyridine, 2,3,4,5-tetrahydro-	-	0.66	Pentanenitrile	-	0.06
1H-Pyrrole, 2,5-dimethyl-	-	1.1	Hexanenitrile	0.09	-
2,3,4-Trimethylpyrrole	-	1.74	Pentanenitrile, 4-methyl-	0.25	1.54
2,3-Diazabicyclo[2.2.1]hept-2-ene, 1,4-dimethyl-	-	0.15	4,4-Dimethyl-3-oxopentanenitrile	-	1.07
Aniline, N-methyl-	-	0.78	Heptanonitrile	0.24	
Pyridine, 2,4-dimethyl-	-	0.26	Octanenitrile	0.22	-
1H-Pyrrole, 3-ethyl-2,4-dimethyl-	-	0.63	Nonanenitrile	0.32	-
			Benzenepropanenitrile	0.32	-
Amides			Dodecanenitrile	0.64	-
N-Methyldodecanamide	0.13	-	Pentadecanenitrile	0.08	-
			Hexadecanenitrile	15.10	-
Others			Oleanitrile	10.58	-
Propane, 2-methyl-2-nitro-	0.16	-	Octadecanenitrile	-	0.67
7-Heptadecene, 1-chloro-	0.48	-	Nonadecanenitrile	8.49	1.75

Table 4.8. Selectivity of Pd/C catalyst based on carbon number.

	%Relative content							
	Gasoline (C5-C12)		Kerosene (C12-C16)		Diesel (C14-C19)		Lubricating oil (C20-C40)	
	BD2	Upgraded oil	BD2	Upgraded oil	BD2	Upgraded oil	BD2	Upgraded oil
Paraffins	3.7	11.0	25.1	33.6	24.4	24.0	2.4	0.1
Olefins	2.7	0.9	7.7	1.4	17.8	3.2	2.8	1.0
Napthenes	0.6	4.0	2.4	5.6	2.9	4.6	0.1	0.3
Cyclo.Olefins	-	0.7	-	-	-	-	-	-
Aromatics	1.9	13.0	0.1	1.2	0.1	0.8	-	-
Nitriles	2.2	3.6	15.8	0.0	34.3	2.4	-	-

4.3.2.4. Hydrogen consumption and turnover frequency

The hydrogen consumptions from the hydrotreatment process were calculated in unit of Normal liters per kg bio-oil distillate. The initial and final operating conditions as well as the hydrogen composition from gas analysis were used to obtain the hydrogen consumption. The hydrogen consumption values for the upgraded bio-oil at 150, 200, and 250^{o}C were found at 29.5, 85.6, and 89.4 Nl/kg bio-oil distillate, respectively. This indicated that during the hydrotreatment process, the catalyst became more active at higher operating temperatures because more hydrogen was consumed.

Additionally, the turnover frequency (TOF) was calculated to investigate the catalytic activity for catalysts in terms of hydrogen consumption per gram of catalyst per operating time (mmol H_2/g-hr). More precisely, TOF is the amount in moles of substrate that can be utilized by a catalyst before it became inactivated. As expected, the TOF increased with an increase in operating temperatures, so better catalytic activity occurred at higher temperatures. The TOF values for the hydrotreated product using Pd/C as a catalyst at 150, 200, and 250^{o}C were obtained at 5.3, 15.3, and 16.0 mmol H_2/g-hr, respectively.

4.3.2.5. Gas and solid product analysis

The gas product from catalytic upgrading process was collected after the reactor cooled down to room temperature, then analyzed for the gas composition. Hydrocarbon gases with C1 to C3, hydrogen, carbon monoxide, and carbon dioxide were obtained from the hydrotreatment process at all operating temperatures as demonstrated in Figure 4.18. The decarbonylation of carbonyl compounds (aldehydes and ketones) could lead to

the production of CO. The formation of CO_2 might be due to the decarboxylation of acids and ester derivatives through cracking, which also produced the hydrocarbon gases as obtained in the gas product. High amounts of hydrocarbon gases produced could be a result of a cracking of higher alkanes present in the starting material [117]. The increases of all gas components, occurring in accordance with the increases of operating temperatures, could be supported by better catalytic activity occurred at higher temperatures as mentioned in section 4.3.2.4.

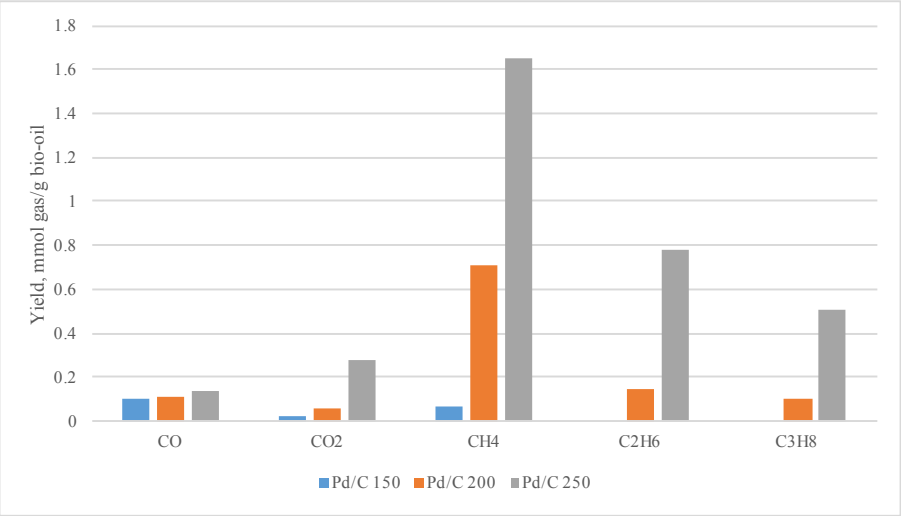

Figure 4.18. Gas composition for different hydrotreating temperatures.

The solid product as a residue from the catalytic upgrading at different operating temperatures was analyzed for the surface area as shown in Figure 4.19. According to the graph, the catalyst used for this study had the surface area of 829 m^2/g. However, the surface area of the solid residue (used catalyst) substantially decreased from the initial

catalyst. In addition, the surface area of the solid residue was observed to be decreased with the increase of operating temperatures. This could be explained by the coke formation during the hydrotreatment process resulting in a pore blocking, so it reduced the surface area of the catalyst. Duan and Savage [117] explained that the thermocatalytic reactions such as deoxygenation, cracking, aromatization, isomerization, and polymerization led to the production of coke, tar, gas, water, and the upgraded oil fraction.

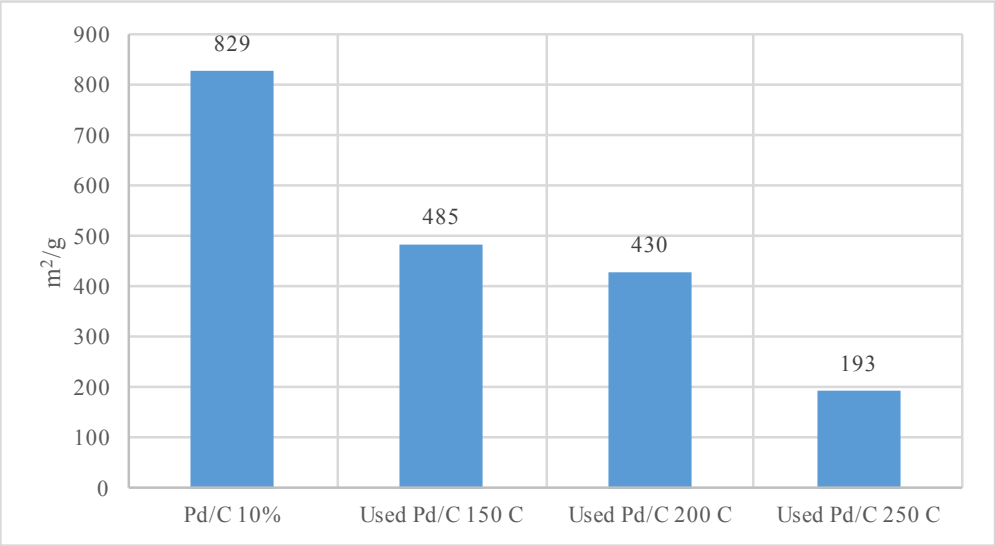

Figure 4.19. BET surface area of Pd/C catalyst before and after hydrotreating process.

The formation of coke was also supported by the ultimate analysis results as demonstrated in Figure 4.20. The carbon content of the used catalyst increased from the original catalyst as a result of a coke formation on the catalyst. Appleby et al. studied the

coke formation in the catalytic cracking and found that aromatics and olefins involved in the starting oil had the strongest tendency in coke formation during the catalytic cracking process [118]. Therefore, more carbon content was observed in the solid residue.

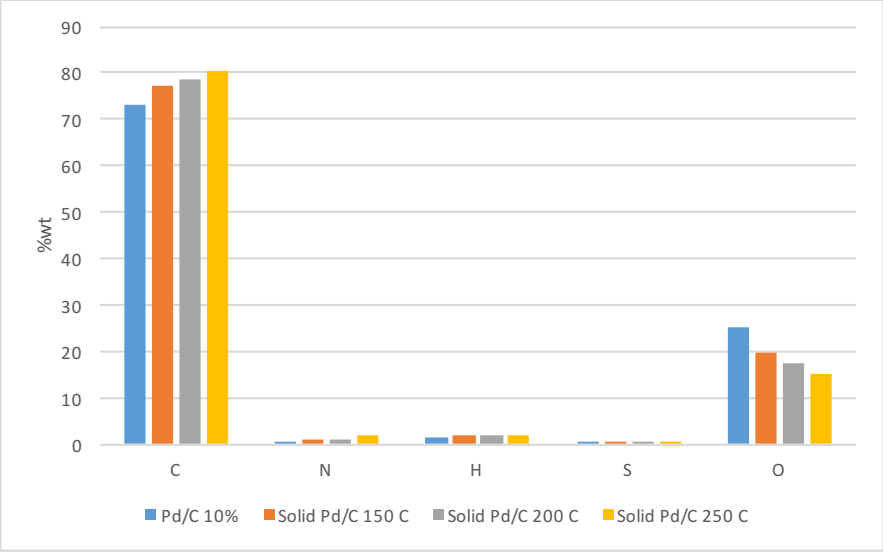

Figure 4.20. Ultimate analysis of Pd/C and solid residue from hydrotreating process.

4.3.3. Comparison of bio-oil distillate, upgraded bio-oil distillate, and commercial fuel products

The physical and chemical properties of the product obtained from fractional distillation and catalytic upgrading were compared to the original bio-oil and commercial fuels as shown in Table 4.9. Obviously, the qualities of pyrolysis oil were significantly improved after conducting the physical (fractional distillation) and chemical (catalytic hydrotreatment) upgrading. According to Figure 4.21, Van Krevelen

diagram shows that the raw bio-oil was located far from the transport fuel region. After the upgrading processes were accomplished, the upgraded products got closer to the commercial fuel region. The improvement of upgraded product quality made it become more useful than the original bio-oil.

Table 4.9. Characteristics of raw bio-oil, bio-oil distillates, hydrotreated distillate, and commercial fuels.

	Raw bio-oil	BD1 (organic)	BD2	Upgraded BD2 (200C)	Commercial		Biodiesel (FAME)
					Gasoline	Diesel	
Viscosity (cSt)	25	0.7	4.3	3.8	0.6	2.7	4-5
Density (kg/m^3)	986	722	920	885	717	823	880
MC (%)	8.2	2.3	1.8	0.9	< 0.1	0.5	0.05 (max)
TAN (mg KOH/g)	34.6	0.2	13.8	4.16	< 0.01	0.01	0.5 (max)
HHV (MJ/kg)	33.1	40.4	38.9	41.3	45.4	43.8	39
Ultimate analysis (wt%)							
C	52.4	77	71.4	75.3	83.4	82.4	76.2
H	7	9.8	7.6	7.2	11.1	12.3	12.6
N	6.2	6.4	8.9	9.6	0.8	0.7	N/A
S	0.1	0.1	0.1	0.1	0.1	0.1	N/A
*O**	34.3	6.6	12	7.8	4.7	4.5	11.2

According to the fractional distillation, the distillate from the first fraction appeared to have the best qualities among all fractions, which was comparable to the biodiesel (FAME). The properties of BD1_organic were also close to the gasoline. However, it may need the further upgrading process to improve its qualities so that it meets the specifications of the gasoline. The removal of oxygen and nitrogen contents is taken into account, which can reduce the moisture and acid number, hence a better heating value.

The second fraction (BD2) from fractional distillation was then selected to conduct the hydrotreating process using Pd/C as a catalyst. The quality of upgraded distillate was improved and getting closer to the diesel. However, the moisture content and acid number still exceeded the specification of diesel. The possible applications of the upgraded products from this study were to blend with a low-acid crude oil to lower the acidity or to use as a feedstock for co-processing with crude oil in the petroleum refineries.

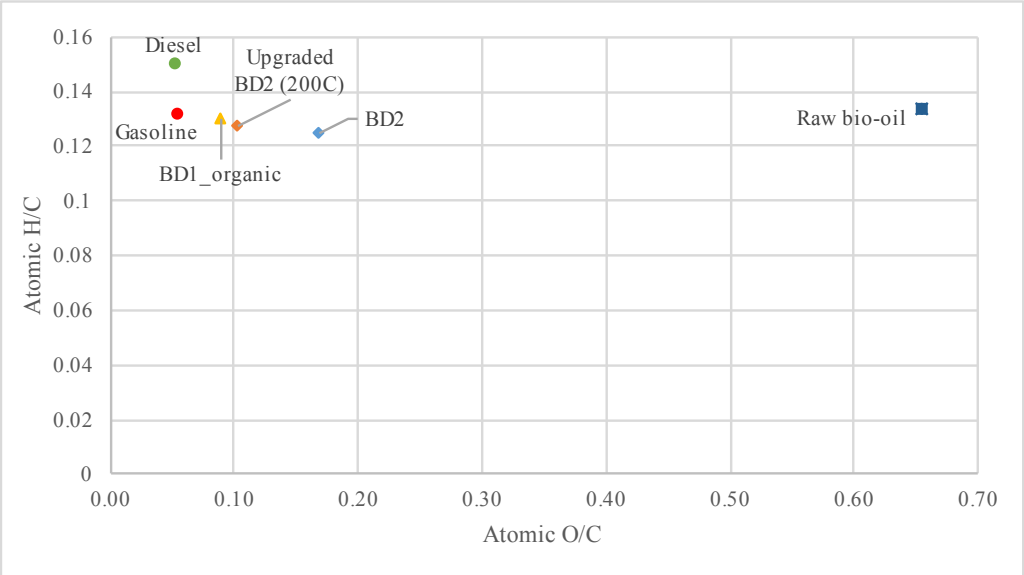

Figure 4.21. Van Krevelen diagram of raw bio-oil, distillate fractions, hydrotreated distillate, and commercial fuel.

4.4. Conclusion

The physical and chemical upgrading processes for the Jatropha bio-oil were conducted. First, fractional distillation of bio-oil and aqueous phase were performed; three distillate fractions of each bio-oil and aqueous product were obtained. The bio-oil distillate properties such as low moisture content, low acid number, and high energy content, were improved. In terms of chemical composition, more hydrocarbons were observed in the distillate fractions and most of the water was removed, which was obtained as a separated layer. This made the bio-oil distillates become an interesting option to be used as fuel substitute. On the other hand, the separation of aqueous phase showed that the aqueous product contained mostly water, oxygenated, and nitrogenated compounds.

Next, the bio-oil distillate (BD2) was chosen for the catalytic upgrading using Pd/C as a catalyst. The effects of operating temperature were investigated. Results showed that the operating temperatures affected the upgraded product yield and quality. The quality of upgraded products at all operating temperatures were improved from the bio-oil distillate. The optimum condition in terms of product yield and quality was obtained at 200^{o}C. The hydrocarbon content increased from 48% in the bio-oil distillate to 76% in the upgraded product with a major reduction in nitrogen and oxygen containing compounds. This indicated the effectiveness of using Pd/C catalyst for Jatropha bio-oil distillate upgrading.

By comparing the upgraded products with the commercial transport fuels. The first fraction of bio-oil distillate (BD1) was comparable to the biodiesel and gasoline.

The hydrotreated product was also improved and close to the diesel properties. However, there were some factors, such as moisture content and acid number, that made the upgraded product not qualified to use as commercial fuels. Therefore, some potential applications of the upgraded product are blending it with the low-acid crude oil to bring down the acidity or using it in the petroleum refineries as co-processing feedstock with crude oil.

5. OVERALL ANALYSIS OF ENERGY PRODUCTION FROM JATROPHA SEED

5.1. Introduction

In the previous chapters, concepts and experimental results on different energy conversion of Jatropha waste into energy products were discussed. Jatropha waste as a residue from the oil extraction process was considered as a potential feedstock for an alternative energy source. Therefore, many energy conversion processes including mechanical, physico-chemical, and thermo-chemical methods were used to turn Jatropha waste into energy products as well as to upgrade it into more valuable energy products. The energy conversions of Jatropha de-oiled cake could reduce the waste product, so it could be advantageous to the environment. It also increased the economic profit and appropriated for the development of bio-based economies.

This chapter combines all energy conversion processes of Jatropha waste in this study. The mass and energy distributions for the overall energy production were investigated. The overall conversion efficiencies were examined in order to determine whether these conversion processes could recover more than 50% of mass/energy contained in Jatropha waste. The CO_2 emission as an indicator of the environmental impact was evaluated. In addition, the net energy ratio and the net energy balance were calculated in order to determine if the energy conversion process was sustainable or not.

5.2. Methodology

5.2.1. Mass and energy distribution for the overall process

Figure 5.1 summarized all energy conversion processes including mechanical, physico-chemical, and thermo-chemical, which were used for the energy conversions of Jatropha seed in the previous and current studies. In the previous studies [28], the Jatropha seed was a starting material for the energy conversion process. The oil extraction of Jatropha seed was conducted using a screw press machine. The extracted oil was then refined and converted into biodiesel via a transesterification process. In this study, the Jatropha de-oiled cake obtained as a residue from the oil extraction was considered a starting material for the energy conversion process. Pyrolysis was selected as the first step to convert the Jatropha residue into three energy products (i.e., liquid product, biochar, and gaseous product). The liquid product was then upgraded via physical (fractional distillation) and chemical (catalytic hydrotreatment) methods. The biochar was also used as a precursor for activated carbon production.

In each conversion step, the amount of input material and output product were recorded as well as their energy contents. The mass and energy distributions for each conversion process were calculated using the equations below. Then the overall process yields, mass and energy distribution could be identified.

$$\text{Product yield (\%wt)} = \frac{\text{Product weight}}{\text{Initial biomass weight}} \times 100 \quad (5.1)$$

$$\text{\%Energy recovery} = \text{Product yield (\%wt)} \times \frac{\text{HHV of product}}{\text{HHV of input material}} \quad (5.2)$$

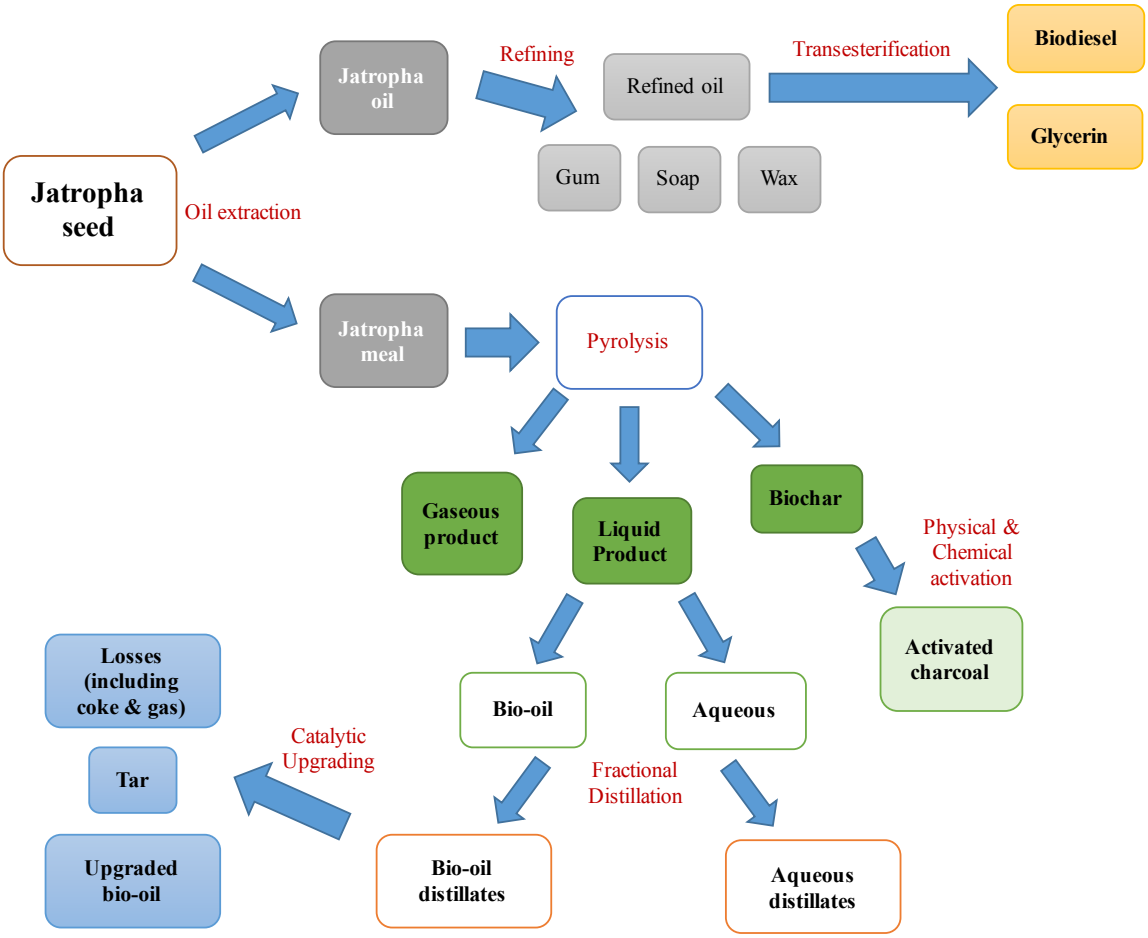

Figure 5.1. Summary of energy conversion processes of Jatropha seed.

5.2.2. Life cycle analysis

A Life Cycle Assessment (LCA) is commonly used to investigate the environmental impacts for any production system by including the overall product life cycle [119]. In this study, a simple LCA was conducted to identify the global warming potential (GWP), which was expressed in kg of CO_2 equivalents (g CO_2 de-oiled cake.). The greenhouse gas (GHG) emissions that generated from the conversions of Jatropha de-oiled cake to produce the energy products were evaluated. The emission allocation

procedure was taken into account. The allocation should be defined between the bio-energy product and its co-products in proportion to their energy content. The allocation occurred when the co-products generated during the process were not recycled to provide heat or power. The LCA constructed in this study was based on the Greenhouse Gases Regulated Emissions and Energy use in Transportation (GREET) platform.

Net energy ratio (NER) and net energy balance (NEB) were commonly used as the indicators to summarize the net energy produced from a specific system. NER was the output energy over the input energy while NEB was to subtract the input energy from the output energy [120]. Based on the results from the previous chapters on different conversion processes, the life cycle energy assessment was conducted for some energy products such as bio-oil distillate from the first fraction (BD1_organic), the upgraded distillate from catalytic hydrotreatment, and the activated biochar. The process diagrams in Figure 5.2 demonstrate the energy conversions of Jatropha de-oiled cake into different energy products. The energy and mass balance shown in Figure 5.2 were used to determine the NER and the NEB.

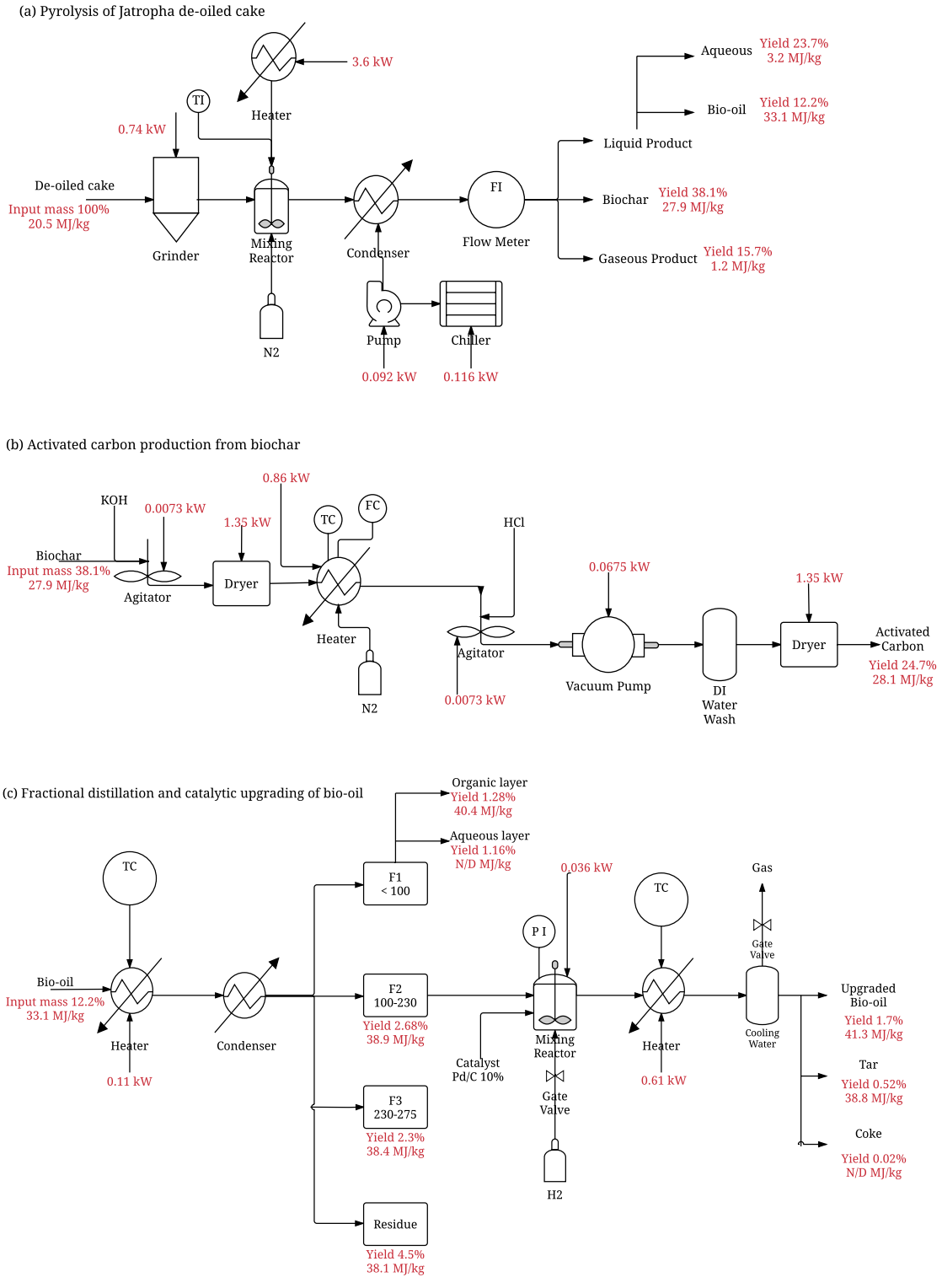

Figure 5.2. Process diagrams of energy conversions of Jatropha de-oiled cake

The equations used to calculate NER and NEB were adapted from the study of Rocha et al. [121]. Therefore, NER and NEB of the energy conversion processes were determined based on the following equations.

$$NER = \frac{HV_{energy\ product} + \sum HV_{co\text{-}products}}{\text{Energy required to produce energy product}} \quad (5.3)$$

$$NEB = HV_{energy\ product} + \sum HV_{co\text{-}products} - \text{Energy to produce energy product} \quad (5.4)$$

5.3. Results and Discussion

5.3.1. Mass and energy distribution for the overall energy conversion process

5.3.1.1. Jatropha whole seed

The mass and energy values of all products obtained from a mechanical, physico-chemical, and thermo-chemical conversion processes were used to determine the overall energy conversion process of the Jatropha seed into energy products

Figure 5.3 demonstrates mass and energy distribution of final energy products obtained from energy conversions of raw Jatropha seed. Based on overall energy conversion processes, 82% of mass recovery and 81.5% of energy recovery were achieved. Most of the mass and energy distributions were obtained from biodiesel product followed by activated biochar. Mass and energy recoveries of energy products based on Jatropha de-oiled cake are shown in Figure 5.4. More than 50% of mass and energy recoveries could be acquired from Jatropha meal (74.3% for mass and 54.5% for energy). The highest mass and energy distributions were found in activated biochar. The aqueous product from pyrolysis process could be a reason for high amounts of energy loss due to high moisture content found in aqueous products. Moreover, the physical and

chemical treatment of biochar into activated carbon also led to significant amount of losses, 65% of mass recovery was obtained from activated carbon preparation.

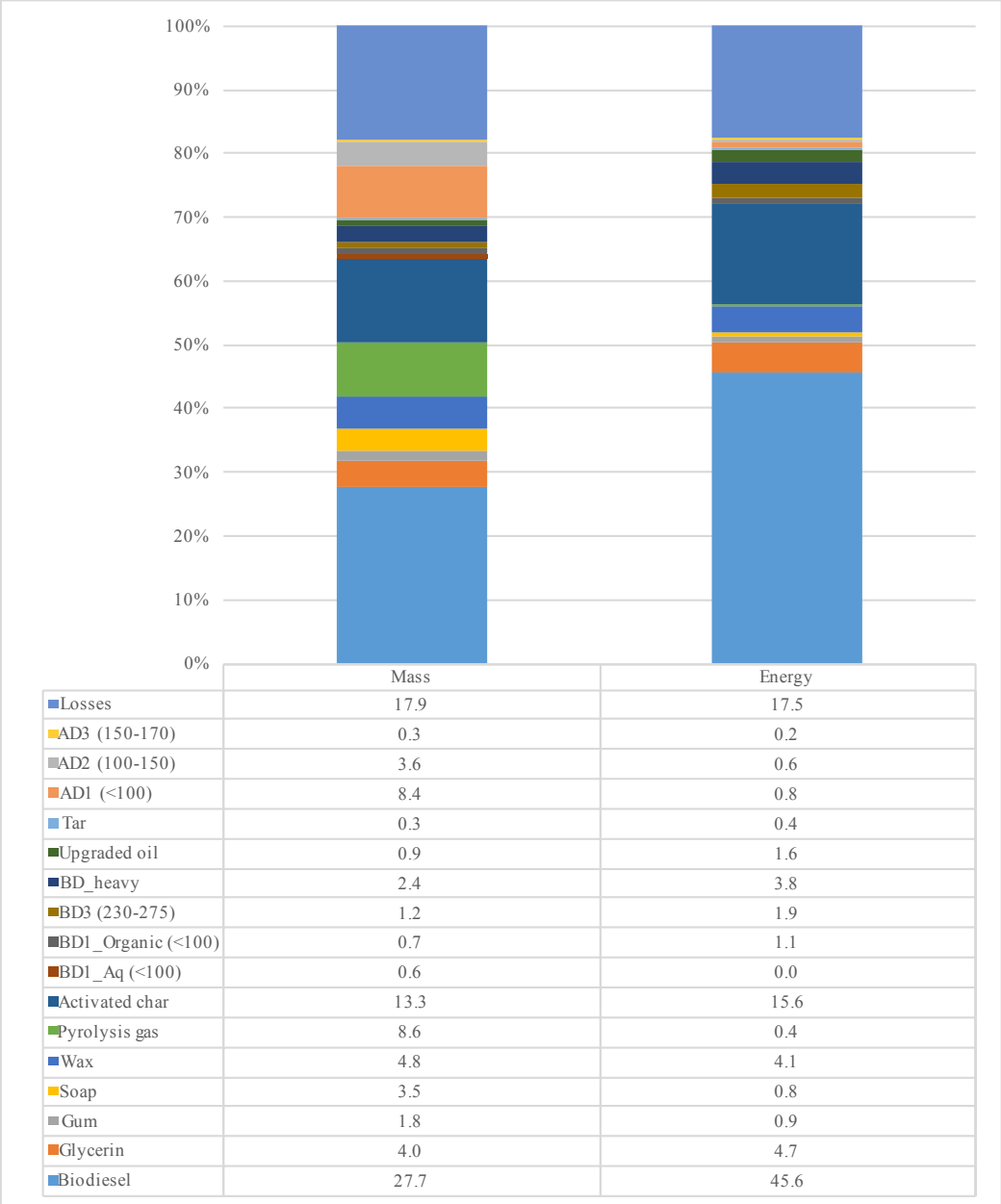

	Mass	Energy
Losses	17.9	17.5
AD3 (150-170)	0.3	0.2
AD2 (100-150)	3.6	0.6
AD1 (<100)	8.4	0.8
Tar	0.3	0.4
Upgraded oil	0.9	1.6
BD_heavy	2.4	3.8
BD3 (230-275)	1.2	1.9
BD1_Organic (<100)	0.7	1.1
BD1_Aq (<100)	0.6	0.0
Activated char	13.3	15.6
Pyrolysis gas	8.6	0.4
Wax	4.8	4.1
Soap	3.5	0.8
Gum	1.8	0.9
Glycerin	4.0	4.7
Biodiesel	27.7	45.6

Figure 5.3. Mass and energy distribution of the overall energy conversions of Jatropha seed.

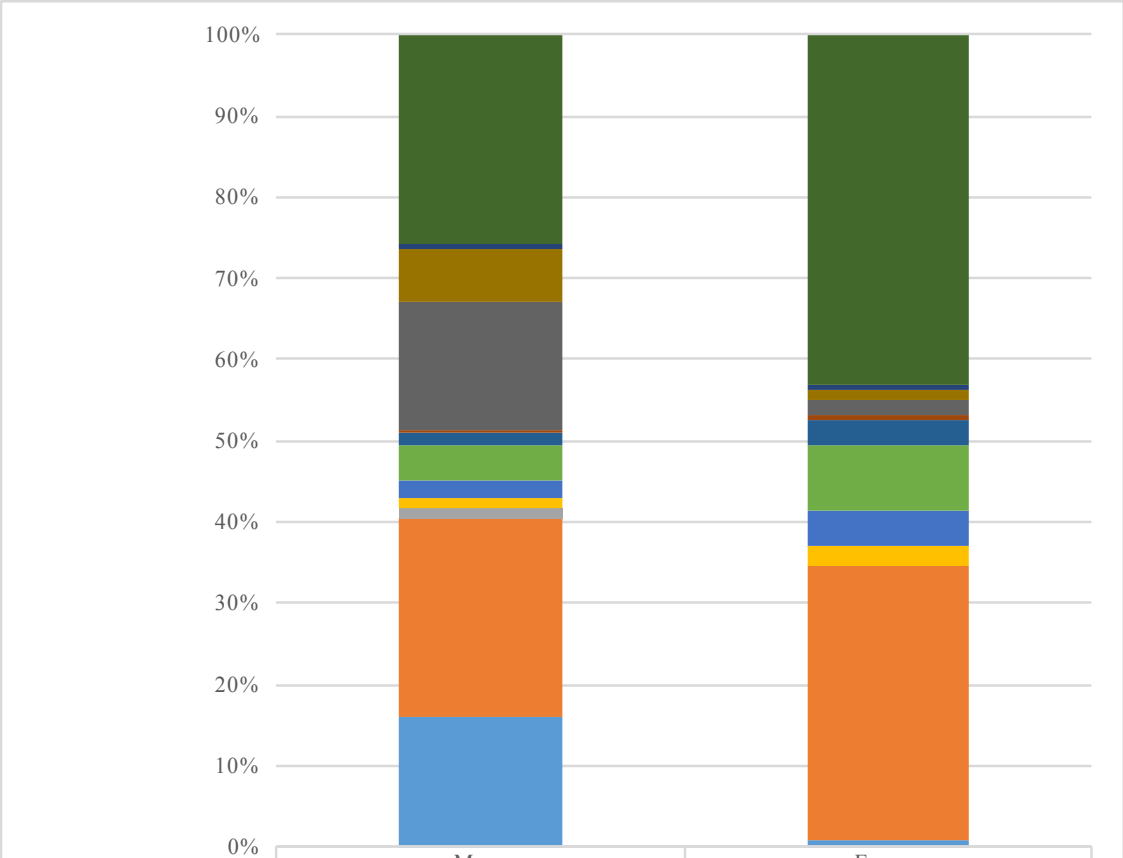

	Mass	Energy
Losses	25.7	43.2
AD3 (150-170)	0.5	0.5
AD2 (100-150)	6.7	1.2
AD1 (<100)	15.6	1.8
Tar	0.4	0.8
Upgraded oil	1.4	2.9
BD_heavy	4.4	8.1
BD3 (230-275)	2.2	4.2
BD1_Organic (<100)	1.3	2.5
BD1_Aq (<100)	1.1	0.0
Activated char	24.6	33.8
Pyrolysis gas	16.0	0.9

Figure 5.4. Mass and energy distribution of the overall energy conversions of Jatropha de-oiled cake.

5.3.1.2. Jatropha whole fruit

Jatropha is a multipurpose plant. Especially, the oil contained in its seed is one of the best candidates for biodiesel production. The annual seed production was reported to range between 400 to 1200 kg/ha depending upon growing conditions. However, Jatropha fruit is composed of approximately 30-37.5% shell and 62.5-70% seed [122-124]. Therefore, if optimal conditions of Jatropha seed yields were achieved (1200 kg/ha), approximately 2000-2800 kg/ha of shell remained as a waste after the seed was removed. Previous study [125] reported the success of biogas production from Jatropha fruit hull and its combination with cow manure. The biogas yield from Jatropha fruit hull was obtained at 162.5 L/kg of dry matter with 57% methane content while the optimum biogas production was achieved using the mixture of Jatropha fruit hull and cow manure (1:2). The optimal biogas production yielded 403.8 L/kg of dry matter with 58% methane content.

The annual mass and energy distributions from energy conversion processes of Jatropha seed and its de-oiled cake are demonstrated in Figure 5.5. If the annual seed production was achieved at 1200 kg/ha, approximately 333 kg of biodiesel and 159 kg of activated biochar could be obtained. This led to the energy content of $13x10^3$ MJ from biodiesel and 4.2x103 MJ from activated char. However, if the whole Jatropha fruit was used for the energy conversion process, up to 455 m^3 of biogas could be acquired per ha per year. Moreover, if only the energy value of methane contained in biogas production was taken into account, approximately $9.4x10^3$ MJ/ha/yr could be obtained from Jatropha fruit hull.

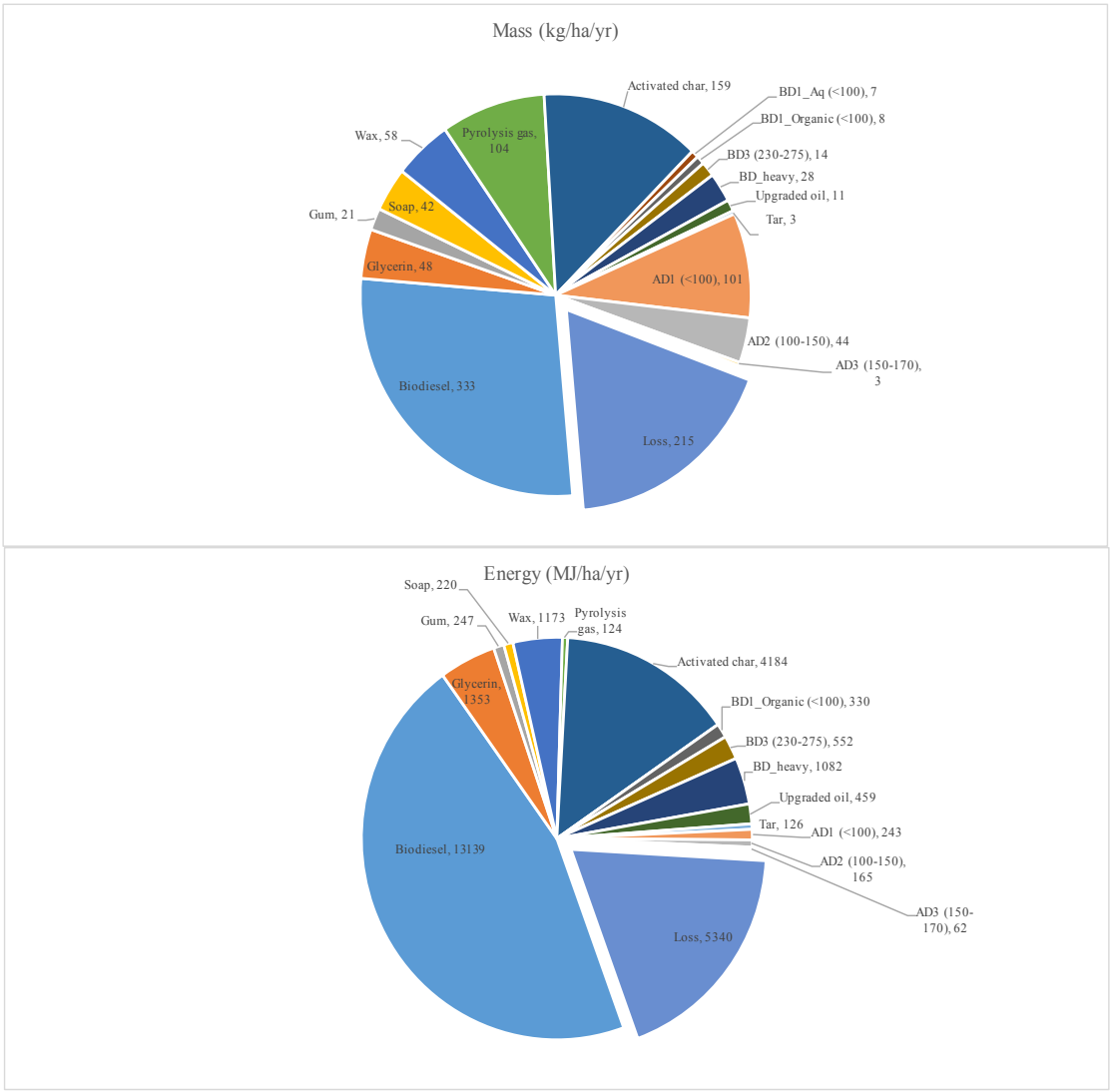

Figure 5.5. Mass and energy distribution of energy products from Jatropha seed based on 1200 kg of seed yield per ha per year.

5.3.2. Life cycle analysis

A common functional unit, namely 1 kg of Jatropha de-oiled cake, was engaged in the LCA for this study. The energy conversion processes of Jatropha de-oiled cake to

produce energy products via pyrolysis, physical and chemical activation for activated carbon, and fractional distillation and catalytic upgrading of bio-oil were taken into account to evaluate the GHG emission, NER, and NEB. In order to determine the GHG emissions for each conversion step, a carbon balance was needed for an evaluation in the allocation procedure. The carbon balance diagram of the input material and output products for all conversion processes is summarized in Figure 5.6. The unit of the carbon shown in the diagram is %Carbon per kg de-oiled cake. According to the diagram, the input feedstock contained 43.3% of carbon. After combining all energy conversion processes, the final energy products contained a total of 31.1% carbon based on the initial carbon input (43.3%), so approximately 12% of carbon was lost during the conversion processes. More than half of the total carbon recovered from all energy products was found in the activated carbon.

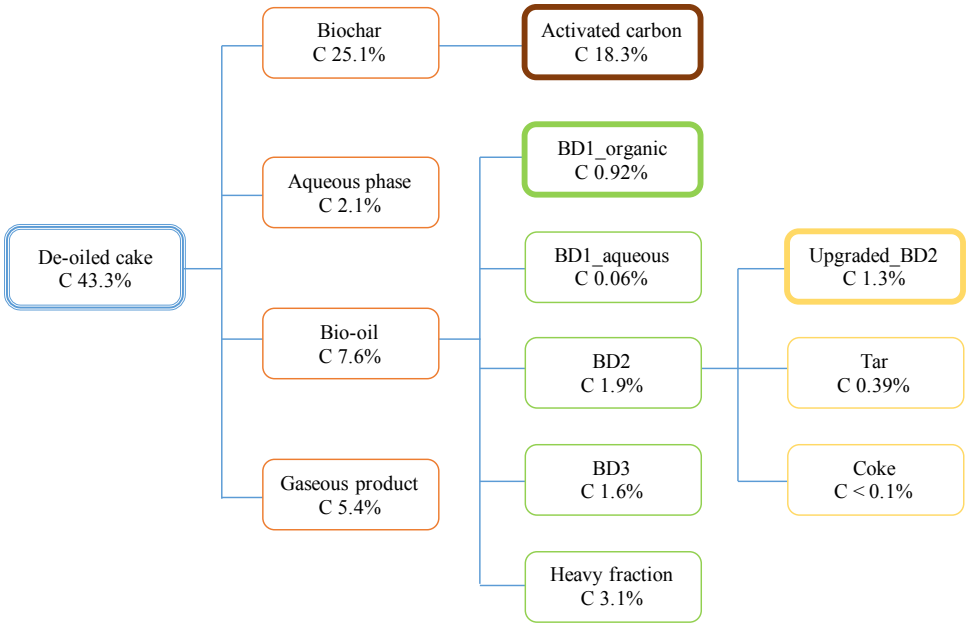

Figure 5.6. Carbon distribution in products from energy conversion of de-oiled cake (%Carbon per kg de-oiled cake).

The GHG emission from the electricity used with respect to the energy conversion processes of the activated carbon, the bio-oil distillate (BD1_organic), and the upgraded distillate are demonstrated in Figure 5.7. The electricity consumption was calculated based on the electric power of the equipment and time used. The highest CO_2 emission was found in the activated carbon production process, while the fractional distillation of bio-oil to get the first distillate fraction released the lowest amount of CO_2. According to the catalytic upgraded product, the GHG emission was significantly increased during the hydrotreatment process.

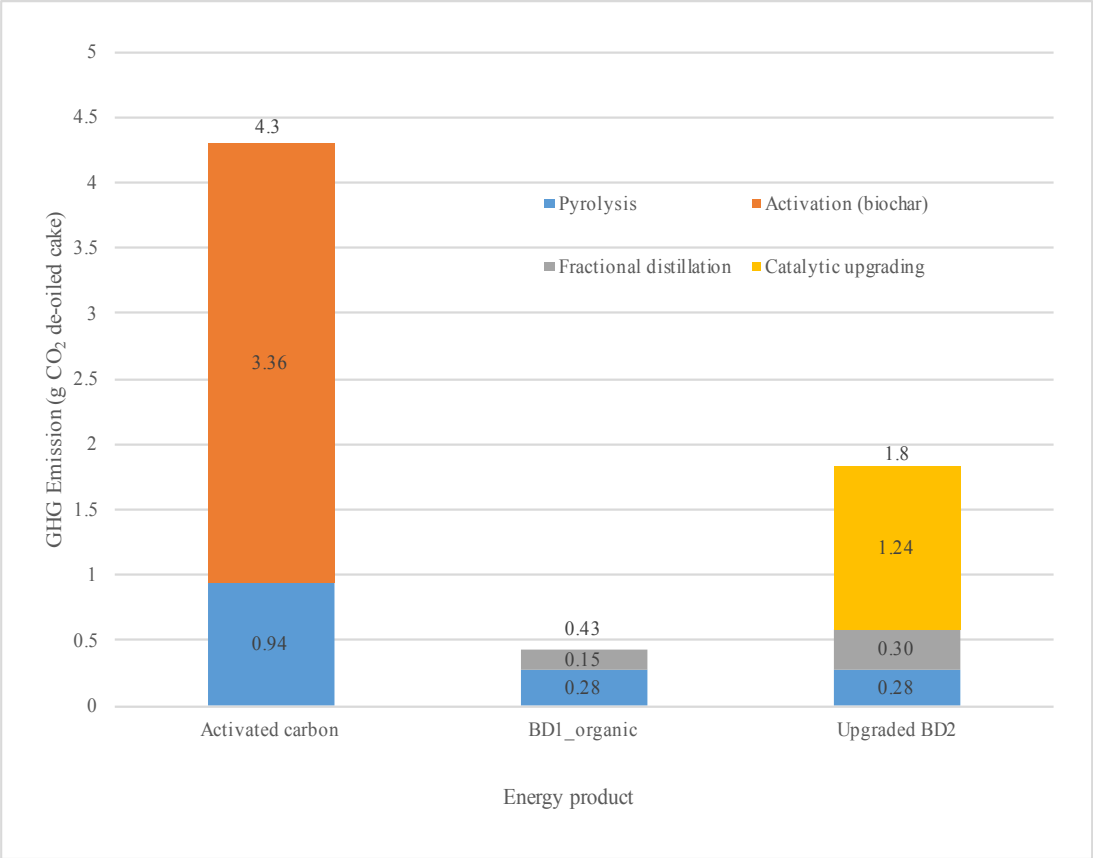

Figure 5.7. Carbon dioxide emission from electricity consumed during production process.

The NER and NEB of the energy products were also determined as shown in Table 5.1. The energy products obtained from the conversions of Jatropha de-oiled cake showed a positive value of NEB and NER values were greater than 1. This indicated a sustainable process for the Jatropha de-oiled cake conversions. The lowest NER and NEB values were found in the activated carbon due to a small increase in energy content of the activated carbon from the biochar. However, the energy content of the activated carbon was not an important factor for the applications of activate carbon.

Table 5.1. NER and NEB of products from energy conversion of de-oiled cake.

	NER	NEB
Bio-oil	1.6	12.6
Biochar	1.4	7.4
Activated carbon	1.0	0.2
BD1_organic	1.2	7.3
Upgraded BD2	1.2	8.2

5.4. Conclusion

Jatropha press cake, which was obtained as a residue after the oil extraction process, was used as a feedstock for energy conversion processes including mechanical, physico-chemical, and thermo-chemical methods. Jatropha waste was successfully turned into different energy products such as activated carbon and liquid biofuels that had a quality comparable to the commercial fuels. The analysis of mass and energy balance revealed that more than 50% of mass and energy recoveries could be acquired from the Jatropha meal (74.3% for mass and 54.5% for energy). However, this study only focused on Jatropha seed, which was around 62.5-70% of Jatropha fruit. The use of Jatropha hull (30-37.5%) was reported as a co-biomass with cow manure for the biogas production. The LCA of energy conversions for Jatropha waste was also conducted. The CO_2 emissions due to the electricity used in the productions of activated carbon, bio-oil distillate (BD1), and upgraded distillate were found at 4.3, 0.43, and 1.8 g CO_2 de-oiled cake, respectively. NER and NEB of the energy products generated from Jatropha press cake showed the positive values, which indicated the sustainable energy conversion process.

6. OVERALL CONCLUSIONS AND RECOMMENDATIONS

This research aimed at investigating the potential of utilizing the Jatropha waste meal as an alternative energy source via different conversion methods. In the previous chapters, concepts and experimental work on each energy conversion pathway were explained. Pyrolysis was selected as a first step to convert Jatropha waste into 3 energy products (i.e., liquid product, solid biochar, and gaseous product). The physical and chemical treatment were applied to the liquid product in order to make it suitable for fossil fuel replacement. On the other hand, biochar, a carbon-rich material, was used as a precursor for the activated carbon production. To achieve the research objectives, four studies were conducted and the major findings were summarized as presented below.

The first study on pyrolysis was done in order to convert Jatropha waste into more valuable products. In this study, pyrolysis under atmospheric condition was performed and the product yields and properties were compared with the previous study on pressurized pyrolysis. The following results could be obtained.

- Pyrolysis at atmospheric yielded more liquid product but less biochar and gaseous product than pressurized pyrolysis. However, the products from pressurized pyrolysis showed higher energy contents.
- The HHVs of biochar and bio-oil were significantly improved from Jatropha de-oiled cake. Other characteristics such as chemical compositions indicated the potential of using them as fuel replacement.

- The high carbon content found in biochar suggested the possible applications for activated carbon production or fuel substitute.
- High amounts of hydrocarbons contained in bio-oil indicated the possibility to use as transport fuel. However, with some oxygenates and nitrogenates found in bio-oil prevented it from being used as biofuel. This suggested the need of further upgrading process to remove the undesirable compounds.
- Mass and energy conversion efficiencies for both atmospheric and pressurized pyrolysis were not significantly different. For the atmospheric pyrolysis, 89.7% of mass recovery and 76.3% of energy recovery were achieved with the highest mass and energy portions coming from biochar.

Next study was to produce the activated carbon from the biochar obtained from pyrolysis. The response surface method was applied in order to evaluate the activation parameters (impregnation ratio, activation temperature, and time) on the activated carbon yields and characteristics. The results from this study were summarized below.

- The activated carbon yield was affected only by impregnation ratio and activation temperature; increasing biochar:KOH and decreasing temperature resulting in more yield. Therefore, highest yield (69.8%) was obtained at 600^{o}C with biochar:KOH of 1.8.
- The activated carbon properties such as carbon content, ash content, and surface area were significantly improved from the original biochar. All activation parameters (impregnation ratio, activation temperature, and time) had an effect on the carbon content.

- The highest surface area of activated carbon from this study was obtained at 285 m^2/g. This was substantially improved from the original biochar (1.51 m^2/g) but was still low compared to other studies. However, the adsorption ability of the highest surface area activated carbon showed a major improvement in removing the contaminants (Acetaminophen and Ibuprofen) from the solution over the original biochar.

The third study focused on the physical and chemical upgrading of liquid product from pyrolysis. The bio-oil and aqueous phase were first conducted the fractional distillation. Their distillate fraction yields and properties were analyzed and compared. Then the distillate from 100-230^oC was upgraded via catalytic hydrotreatment at different operating temperatures with Pd/C being used as a catalyst. The following conclusion was derived from this study.

- The fractional distillation showed the significant improvement in the bio-oil distillate fractions such as low moisture content, low acid number, and high energy content.
- The fractional distillation of aqueous phase indicated that the aqueous product mostly contained water, oxygenated, and nitrogenated compounds.
- Higher acid numbers of the distillates (from both bio-oil and aqueous) were observed at higher boiling point distillates. The water layer in BD1 had a lot higher acid number than the organic layer.

- More hydrocarbons were observed in the bio-oil distillates and the water was removed as a separate layer in BD1. More nitrogenates were found in higher boiling point distillates.
- The operating temperature of the catalytic hydrotreatment affected the upgraded product yield and quality. The upgraded bio-oil quality was improved from the distillate in terms of moisture content, acid number, and heating value.
- The upgraded bio-oil from 200^{o}C appeared to be the optimum condition based on the yield and quality such as highest yield (64.9%), highest heating value (41.3), highest hydrocarbons (75.7%), low moisture content (0.87) and low oxygen content (7.8%).
- In comparison to the commercial transport fuels, the organic phase in the first distillate fraction was similar to the biodiesel and gasoline while the hydrotreated distillate was close to the diesel properties.

The last study combined all energy conversion processes in the previous chapters. The mass and energy conversion efficiencies for the overall process were determined. The simple LCA was also conducted to investigate the environmental impact and the sustainability of the system. The result was summarized as shown below.

- More than half of the mass and energy contained in Jatropha waste meal was recovered in forms of other energy products, which were obtained from thermo-chemical and physico-chemical methods. The mass and energy conversion efficiencies were achieved at 74.3% and 54.5%, respectively.

- The CO_2 emissions due to the electricity consumed during the productions of activated carbon, bio-oil distillate (BD1), and the hydrotreated distillate were found at 4.3, 0.43, and 1.8 kg CO_2-eq., respectively
- The obtained positive values of NER and NEB for the energy products generated from Jatropha residue indicated the sustainable energy conversion process of the system.

The yields and energy contents of all products generated from the energy conversions of Jatropha de-oiled cake were summarized in Figure 6.1.

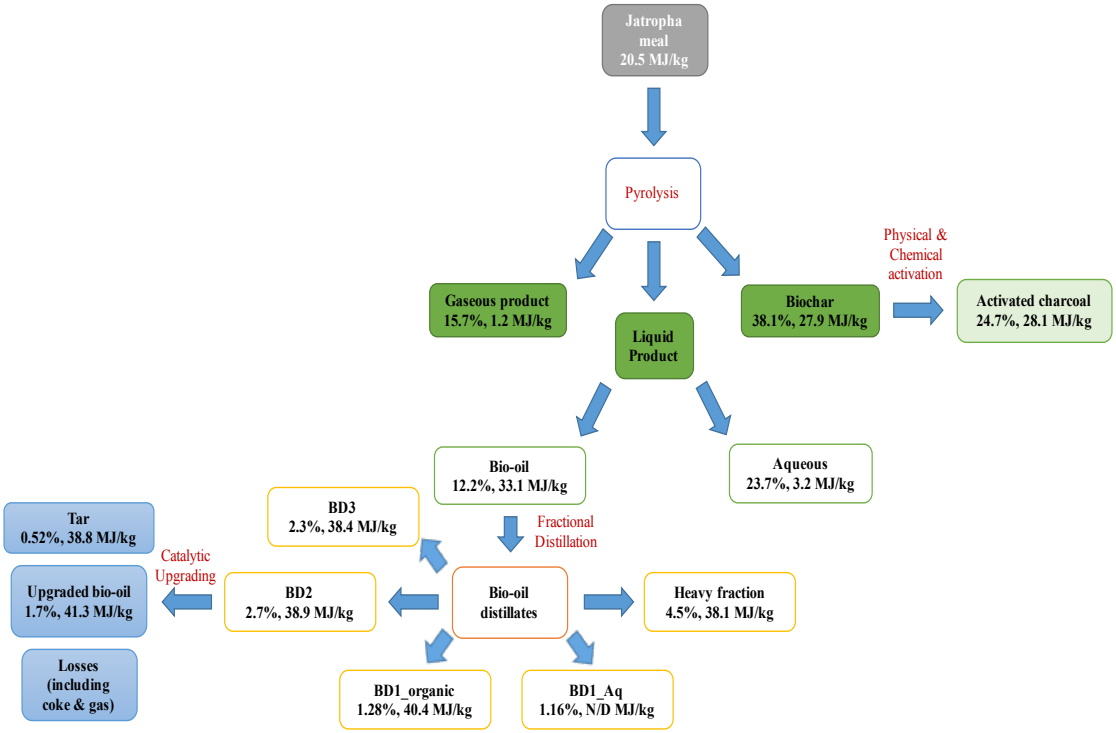

Figure 6.1. Summary of products from energy conversion process in this study.

According to the above conclusions, the following statements are recommended for further investigation of energy production from Jatropha de-oiled cake.

- The pyrolysis of Jatropha residue used in this study was a batch process, which could handle specific amount of feedstock and might not be economically effective. Therefore, a continuous system should be taken into account, along with the investigation of the product yields and characteristics for this system.
- The activated biochar obtained from this study still had a relatively low surface area. Further investigation may be done by changing the activation parameters based on the results obtained from this study. For instance, one might try increasing more impregnation ratio or activation temperature.
- Since the price of Pd/C catalyst is quite high, the cheaper catalysts such as the Ni/C or activated carbon can be used to study their effects on product yields and properties.
- The economics analysis of the energy conversion process can be done to evaluate the cost effectiveness of the system.

REFERENCES

[1] N. H. Afgan, D. A. Gobaisi, M. G. Carvalho and M. Cumo, "Sustainable energy development," *Renewable and Sustainable Energy Reviews,* vol. 2, no. 3, p. 235–286, 1998.

[2] S. Bilgen, "Structure and environmental impact of global energy consumption," *Renewable and Sustainable Energy Reviews,* vol. 38, p. 890–902, October 2014.

[3] BP, *BP Statistical Review of World Energy 2015*, London, Pureprint Group, 2015.

[4] M. M. Rahman, S. B. Mostafiz, J. V. Paatero and R. Lahdelma, "Extension of energy crops on surplus agricultural lands: A potentially viable option in developing countries while fossil fuel reserves are diminishing," *Renewable and Sustainable Energy Reviews,* vol. 29, p. 108–119, January 2014.

[5] B. E. Dale and R. G. Ong, "Energy, wealth, and human development: why and how biomass pretreatment," *Biotechnology Progress,* vol. 28, no. 4, p. 893–898, 2012.

[6] I. Dincer, "Renewable energy and sustainable development: a crucial review," *Renewable and Sustainable Energy Reviews,* vol. 4, no. 2, p. 157–175, 2000.

[7] P. McKendry, "Energy production from biomass (part 2): conversion technologies," *Bioresource Technology,* vol. 83, no. 1, p. 47–54, 2002.

[8] P. McKendry, "Energy production from biomass (part 1): overview of biomass," *Bioresource Technology,* vol. 83, no. 1, p. 37–46, May 2002.

[9] F. Ma and M. A. Hanna, "Biodiesel production: a review," *Bioresource Technology,* vol. 70, no. 1, p. 1–15, 1999.

[10] R. Manurung, D. Wever, J. Wildschut, R. Venderbosch, H. Hidayat, J. van Dam, E. Leijenhorst, A. Broekhuis and H. Heeres, "Valorisation of *Jatropha curcas L.* plant parts: nut shell conversion to fast pyrolysis oil," *Food and Bioproducts Processing,* vol. 87, no. 3, p. 187–196, September 2009.

[11] A. Agrawalla, S. Kumar and R. Singh, "Pyrolysis of groundnut de-oiled cake and characterization of the liquid product," *Bioresource Technology,* vol. 102, no. 22, p. 10711–10716, November 2011.

[12] Y. Chen, J. Duan and Y.-H. Luo, "Investigation of agricultural residues pyrolysis behavior under inert and oxidative conditions," *Journal of Analytical and Applied Pyrolysis,* vol. 83, no. 2, p. 165-174, November 2008.

[13] A. Demirbas, "Effects of temperature and particle size on bio-char yield from pyrolysis of agricultural residues," *Journal of Analytical and Applied Pyrolysis,* vol. 72, no. 2, p. 243-248, 2004.

[14] M. Azam, A. Waris and N. Nahar, "Prospects and potential of fatty acid methyl esters of some non-traditional seed oils for use as biodiesel in India," *Biomass and Bioenergy,* vol. 29, no. 4, p. 293–302, 2005.

[15] A. Atabani, T. Mahlia, I. A. Badruddin, H. Masjuki, W. Chong and K. T. Lee, "Investigation of physical and chemical properties of potential edible and non-edible feedstocks for biodiesel production, a comparative analysis," *Renewable and Sustainable Energy Reviews,* vol. 21, p. 749–755, 2013.

[16] K. Prueksakorna, S. H. Gheewalaa, P. Malakulb and S. Bonnet, "Energy analysis of Jatropha plantation systems for biodiesel production in Thailand," *Energy for Sustainable Development,* vol. 14, no. 1, p. 1-5, 2010.

[17] J. Portugal-Pereira, J. Nakatani, K. H. Kurisu and K. Hanaki, "Comparative energy and environmental analysis of Jatropha bioelectricity versus biodiesel production in remote areas," *Energy,* vol. 83, no. 1, p. 284-293, 2015.

[18] M. Mofijur, H. Masjuki, M. Kalam, M. Hazrat, A. Liaquat, M. Shahabuddin and M. Varman, "Prospects of biodiesel from Jatropha in Malaysia," *Renewable and Sustainable Energy Reviews,* vol. 16, no. 7, p. 5007–5020, 2012.

[19] C.-Y. Yang, Z. Fang, B. Li and Y.-f. Long, "Review and prospects of Jatropha biodiesel industry in China," *Renewable and Sustainable Energy Reviews,* vol. 16, no. 4, p. 2178–2190, 2012.

[20] G. Augustus, M. Jayabalan and G. Seiler, "Evaluation and bioinduction of energy components of Jatropha curcas," *Biomass and Bioenergy,* vol. 23, no. 3, p. 161-164, September 2002.

[21] V. Pandey, K. Singh, J. Singh, A. Kumar, B. Singh and R. Singh, "Jatropha curcas: a potential biofuel plant for sustainable environmental development," *Renewable and Sustainable Energy Reviews,* vol. 16, no. 5, p. 2870–2883, 2012.

[22] R. Banerji, A. Chowdhury, G. Misra, G. Sudarsanan, S. Verma and G. Srivastava, "Jatropha seed oils for energy," *Biomass,* vol. 8, no. 4, p. 277-282, 1985.

[23] N. Foidl, G. Foidl, M. Sanchez, M. Mittelbach and S. Hackel, "*Jatropha curcas L*. as a source for the production of biofuel in Nicaragua," *Bioresource Technology,* vol. 58, no. 1, p. 77-82, 1996.

[24] K. Openshaw, "A review of Jatropha curcas: an oil plant of unfulfilled promise," *Biomass and Bioenergy,* vol. 19, no. 1, p. 1-15, July 2000.

[25] F. Forson, E. Oduro and E. Hammond-Donkoh, "Performance of Jatropha oil blends in a diesel engine," *Renewable Energy,* vol. 29, no. 7, p. 1135-1145, June 2004.

[26] H. J. Berchmans and S. Hirata, "Biodiesel production from crude *Jatropha curcas L*. seed oil with a high content of free fatty acids," *Bioresource Technology,* vol. 99, no. 6, p. 1716–1721, April 2008.

[27] R. M. Jingura, D. Musademba and R. Matengaifa, "An evaluation of utility of *Jatropha curcas L*. as a source of multiple energy carriers," *International Journal of Engineering, Science and Technology,* vol. 2, no. 7, p. 115-122, 2010.

[28] J. Kongkasawan and S. C. Capareda, "Jatropha oil refining process and biodiesel conversion: mass and energy balance," *International Energy Journal,* vol. 13, no. 4, p. 169-176, December 2012.

[29] S. C. Capareda, "Chapter 9 Pyrolysis," in *Introduction to biomass energy conversions*, Boca Raton, CRC Press, 2014, p. 319-361.

[30] S. W. Kim, B. S. Koo, J. W. Ryu, J. S. Lee, C. J. Kim, D. H. Lee, G. R. Kim and S. Choi, "Bio-oil from the pyrolysis of palm and Jatropha wastes in a fluidized bed," *Fuel Processing Technology,* vol. 108, p. 118–124, April 2013.

[31] P. Basu, "Chapter 3 Pyrolysis and Torrefaction," in *Biomass Gasification and Pyrolysis*, Burlington, MA: Academic Press, 2010, p. 65–96.

[32] J. G. Speight, "Chapter 8 Fuels from Biomass," in *Synthetic Fuels Handbook: Properties, Process, and Performance*, New York, McGraw-Hill Companies Inc., 2008, p. 221-264.

[33] S. Antony Raja, Z. Robert Kennedy, B. Pillai and C. Lindon Robert Lee, "Flash pyrolysis of Jatropha oil cake in electrically heated fluidized bed reactor," *Energy,* vol. 35, no. 7, p. 2819–2823, July 2010.

[34] İ. Demiral and S. Şensöz, "The effects of different catalysts on the pyrolysis of industrial wastes (olive and hazelnut bagasse)," *Bioresource Technology,* vol. 99, no. 17, p. 8002–8007, November 2008.

[35] H. F. Gerçel, "The production and evaluation of bio-oils from the pyrolysis of sunflower-oil cake," *Biomass and Bioenergy,* vol. 23, no. 4, p. 307–314, October 2002.

[36] S. Ucar and A. R. Ozkan, "Characterization of products from the pyrolysis of rapeseed oil cake," *Bioresource Technology,* vol. 99, no. 18, p. 8771–8776, December 2008.

[37] J. Kongkasawan, H. Nam and S. C. Capareda, "Jatropha waste meal as an alternative energy source via pressurized pyrolysis: A study on temperature effects," *Energy,* vol. 113, p. 631-642, October 2016.

[38] H. Nam, S. C. Capareda, N. Ashwath and J. Kongkasawan, "Experimental investigation of pyrolysis of rice straw using bench-scale auger, batch and fluidized bed reactors," *Energy,* vol. 93, p. 2384–2394, 2015.

[39] D. L. V. Katz, "Chapter 4 Properties of Natural Gases and Volatile Hydrocarbon Liquids," in *Handbook of natural gas engineering*, New York, McGraw-Hill Companies Inc., 1959, p. 94-188.

[40] A. Kumar, L. Wang, Y. A. Dzenis, D. D. Jones and M. A. Hanna, "Thermogravimetric characterization of corn stover as gasification and pyrolysis feedstock," *Biomass and Bioenergy,* vol. 32, no. 5, p. 460–467, 2008.

[41] S. V. Mantilla, P. Gauthier-Maradei, P. Á. Gil and S. T. Cárdenas, "Comparative study of bio-oil production from sugarcane bagasse and palm empty fruit bunch: yield optimization and bio-oil characterization," *Journal of Analytical and Applied Pyrolysis,* vol. 108, p. 284–294, 2014.

[42] W. Tsai, M. Lee and Y. Chang, "Fast pyrolysis of rice husk: product yields and compositions," *Bioresource Technology,* vol. 98, no. 1, p. 22–28, 2007.

[43] H. Nam and S. Capareda, "Experimental investigation of torrefaction of two agricultural wastes of different composition using RSM (response surface methodology)," *Energy,* vol. 91, p. 507-516, 2015.

[44] W. Boie, "Fuel Technology Calculations," *Energietechnik,* vol. 3, p. 309-316, 1953.

[45] L. Prasad, P. Subbarao and J. Subrahmanyam, "Pyrolysis and gasification characteristics of Pongamia residue (de-oiled cake) using thermogravimetry and downdraft gasifier," *Applied Thermal Engineering,* vol. 63, no. 1, p. 379–386, 2014.

[46] V. Volli and R. K. Singh, "Production of bio-oil from mahua de-oiled cake," *Journal of Renewable and Sustainable Energy,* p. 1-9, 2012.

[47] V. Volli and R. Singh, "Production of bio-oil from de-oiled cakes by thermal pyrolysis," *Fuel,* vol. 96, p. 579–585, 2012.

[48] J. Kongkasawan, "Optimization of Jatropha oil extraction and its by-product utilization by pyrolysis method," MS Thesis. Texas A&M University, 2012.

[49] M. J. Antal and M. Grønli, "The art, science, and technology of charcoal production," *Ind. Eng. Chem. Res.,* vol. 42, p. 1619-1640, 2003.

[50] J. J. Manyà, F. X. Roca and J. F. Perales, "TGA study examining the effect of pressure and peak temperature on biochar yield during pyrolysis of two-phase olive mill waste," *Journal of Analytical and Applied Pyrolysis,* vol. 103, p. 86–95, 2013.

[51] W. S.-L. Mok and M. J. Antal Jr., "Effects of pressure on biomass pyrolysis. I. Cellulose pyrolysis products," *Thermochimica Acta,* vol. 68, no. 2-3, p. 155-164, 1983.

[52] M. C. C. Maguyon, "Technical feasibility study on biofuels production from pyrolysis of *Nannochloropsis oculata* and algal bio-oil upgrading," PhD Dissertation. Texas A&M University, 2013.

[53] C. F. S. Rombaldo, A. C. L. Lisbôa, M. O. A. Méndez and A. d. R. Coutinho, "Effect of operating conditions on scrap tire pyrolysis," *Materials Research,* vol. 11, no. 3, p. 359-363, 2008.

[54] E. S. Noumi, J. Blin, J. Valette and P. Rousset, "Combined effect of pyrolysis pressure and temperature on the yield and CO_2 gasification reactivity of Acacia wood in macro-TG," *Energy Fuels,* vol. 29, no. 11, p. 7301–7308, 2015.

[55] M. Brebu and C. Vasile, "Thermal degradation of lignin - a review," *Cellulose Chem. Technol.,* vol. 44, no. 9, p. 353-363, 2010.

[56] S. Maiti, S. Dey, S. Purakayastha and B. Ghosh, "Physical and thermochemical characterization of rice husk char as a potential biomass energy source," *Bioresource Technology,* vol. 97, no. 16, p. 2065–2070, 2006.

[57] K. Whitty, M. Kullberg, V. Sorvari, R. Backman and M. Hupa, "Influence of pressure on pyrolysis of black liquor: 2. Char yields and component release," *Bioresource Technology,* vol. 99, no. 3, p. 671–679, 2008.

[58] H. Zhang and T. H. Fletcher, "Nitrogen transformations during secondary coal," *Energy & Fuels,* vol. 15, no. 6, p. 1512-1522, 2001.

[59] C.-z. Li and P. Nelson, "An experimental study of the release of nitrogen from coals pyrolyzed in fluidized-bed reactors," *Symposium (International) on Combustion,* vol. 26, no. 2, p. 3205–3211, 1996.

[60] J. A. Capunitan and S. C. Capareda, "Assessing the potential for biofuel production of corn stover pyrolysis using a pressurized batch reactor," *Fuel,* vol. 95, p. 563–572, 2012.

[61] N. Mahinpey, P. Murugan, T. Mani and R. Raina, "Analysis of bio-oil, biogas, and biochar from pressurized pyrolysis of wheat straw using a tubular reactor," *Energy & Fuels,* vol. 23, p. 2736–2742, 2009.

[62] D. Kumar and K. K. Pant, "Production and characterization of biocrude and biochar obtained from non-edible de-oiled seed cakes hydrothermal conversion," *Journal of Analytical and Applied Pyrolysis,* vol. 115, p. 77–86, 2015.

[63] C. Wang, Z. Du, J. Pan, J. Li and Z. Yang, "Direct conversion of biomass to bio-petroleum at low temperature," *J. Anal. Appl.,* vol. 78, p. 438–444, 2007.

[64] S. A. Raja, Z. R. Kennedy, B. Pillai and C. L. R. Lee, "Flash pyrolysis of Jatropha oil cake in electrically heated fluidized bed reactor," *Energy,* vol. 35, no. 7, p. 2819–2823, 2010.

[65] R. Zanzi, K. Sjöström and E. Björnbom, "Rapid pyrolysis of agricultural residues at high temperature," *Biomass and Bioenergy,* vol. 23, no. 5, p. 357–366, 2002.

[66] K. Murata, Y. Liu, M. Inaba and I. Takahara, "Catalytic fast pyrolysis of Jatropha wastes," *Journal of Analytical and Applied Pyrolysis,* vol. 94, p. 75–82, 2012.

[67] S.-J. Kim, S.-H. Jung and J.-S. Kim, "Fast pyrolysis of palm kernel shells: Influence of operation parameters on the bio-oil yield and the yield of phenol and phenolic compounds," *Bioresource Technology,* vol. 101, no. 23, p. 9294–9300, 2010.

[68] Z. Qi, C. Jie, W. Tiejun and X. Ying, "Review of biomass pyrolysis oil properties and upgrading research," *Energy Conversion and Management,* vol. 48, p. 87–92, 2007.

[69] G. Duman, C. Okutucu, S. Ucar, R. Stahl and J. Yanik, "The slow and fast pyrolysis of cherry seed," *Bioresource Technology,* vol. 102, no. 2, p. 1869–1878, 2011.

[70] Z. Luo, S. Wang, Y. Liao, J. Zhou, Y. Gu and K. Cen, "Research on biomass fast pyrolysis for liquid fuel," *Biomass and Bioenergy ,* vol. 26, p. 455 – 462, 2004.

[71] S. Czernik and A. V. Bridgwater, "Overview of applications of biomass fast pyrolysis oil," *Energy Fuels,* vol. 18, no. 2, p. 590–598, 2004.

[72] S. Grierson, V. Strezov, G. Ellem, R. Mcgregor and J. Herbertson, "Thermal characterisation of microalgae under slow pyrolysis conditions," *Journal of Analytical and Applied Pyrolysis,* vol. 85, no. 1-2, p. 118–123, 2009.

[73] M. I. Jahirul, M. G. Rasul, A. A. Chowdhury and N. Ashwath, "Biofuels production through biomass pyrolysis —A technological review," *Energies,* vol. 5, p. 4952-5001, 2012.

[74] T. R. Brown, M. M. Wright and R. C. Brown, "Estimating profitability of two biochar production scenarios: slow pyrolysis vs fast pyrolysis," *Biofuels, Bioprod. Biorefin.,* vol. 5, no. 1, p. 54–68, 2011.

[75] L. Zhu, S. Yin, Q. Yin, H. Wang and S. Wang, "Biochar: a new promising catalyst support using methanation as a probe reaction," *Energy Science & Engineering,* vol. 3, no. 2, p. 126–134, 2015.

[76] A. M. Abioye and F. N. Ani, "Recent development in the production of activated carbon electrodes from agricultural waste biomass for supercapacitors: A review," *Renewable and Sustainable Energy Reviews,* vol. 52, p. 1282–1293, 2015.

[77] D. Montgomery, *Design and Analysis of Experiments*, 5th ed., New York, John Wiley & Sons Inc., 2001.

[78] D. Angin, "Production and characterization of activated carbon from sour cherry stones by zinc chloride," *Fuel,* vol. 115, p. 804-811, 2014.

[79] M. Gratuito, T. Panyathanmaporn, R.-A. Chumnanklang, N. Sirinuntawittaya and A. Dutta, "Production of activated carbon from coconut shell: Optimization using response surface methodology," *Bioresource Technology,* vol. 99, no. 11, p. 4887–4895, 2008.

[80] I. Tan, A. Ahmad and B. Hameed, "Preparation of activated carbon from coconut husk: Optimization study on removal of 2,4,6-trichlorophenol using response surface methodology," *Journal of Hazardous Materials,* vol. 153, no. 1-2, p. 709–717, 2008.

[81] G. Stavropoulos and A. Zabaniotou, "Production and characterization of activated carbons from olive-seed waste residue," *Microporous and Mesoporous Materials,* vol. 82, no. 1-2, p. 79-85, 2005.

[82] D. Angın, E. Altintig and T. E. Köse, "Influence of process parameters on the surface and chemical properties of activated carbon obtained from biochar by chemical activation," *Bioresource Technology,* vol. 148, p. 542–549, 2013.

[83] K. Açıkalın, F. Karaca and E. Bolat, "Pyrolysis of pistachio shell: Effects of pyrolysis conditions and analysis of products," *Fuel,* vol. 95, p. 169-177, 2012.

[84] B. Cagnon, X. Py, A. Guillot, F. Stoeckli and G. Chambat, "Contributions of hemicellulose, cellulose and lignin to the mass and the porous properties of chars and steam activated carbons from various lignocellulosic precursors," *Bioresource Technology,* vol. 100, no. 1, p. 292-298, 2009.

[85] D. Chen, X. Chen, J. Sun, Z. Zheng and K. Fu, "Pyrolysis polygeneration of pine nut shell: Quality of pyrolysis products and study on the preparation of activated carbon from biochar," *Bioresource Technology,* vol. 216, p. 629-636, 2016.

[86] A. C. Lua, T. Yang and J. Guo, "Effects of pyrolysis conditions on the properties of activated carbons prepared from pistachio-nut shells," *Journal of Analytical and Applied Pyrolysis,* vol. 72, no. 2, p. 279-287, 2004.

[87] M. Carrier, A. G. Hardie, Ü. Uras, J. Görgens and J. (. Knoetze, "Production of char from vacuum pyrolysis of South-African sugar cane bagasse and its characterization as activated carbon and biochar," *Journal of Analytical and Applied Pyrolysis,* vol. 96, p. 24–32, 2012.

[88] A. Aygüna, S. Yenisoy-Karakaş and I. Duman, "Production of granular activated carbon from fruit stones and nutshells and evolution their physical, chemical and adsorption properties," *Microporous and Mesoporous Materials,* vol. 66, no. 2-3, p. 189–195, 2003.

[89] H. M. Mozammel, O. Masahiro and B. SC, "Activated charcoal from coconut shell using ZnCl2 activation," *Biomass and Bioenergy,* vol. 22, no. 5, p. 397–400, 2002.

[90] G. Cruz, M. Pirilä, M. Huuhtanen, L. Carrión, E. Alvarenga and R. L. Keiski, "Production of Activated Carbon from Cocoa (Theobroma cacao) Pod Husk," *J Civil Environment Eng,* vol. 2, no. 2, p. 1-6, 2012.

[91] J. Park, I. Hung, Z. Gan, O. J. Rojas, K. H. Lim and S. Park, "Activated carbon from biochar: Influence of its physicochemical properties on the sorption characteristics of phenanthrene," *Bioresource Technology ,* vol. 149, p. 383–389, 2013.

[92] S. Xiu and A. Shahbazi, "Bio-oil production and upgrading research: A review," *Renewable and Sustainable Energy Reviews,* vol. 16, p. 4406–4414, 2012.

[93] H. Yang, J. Yao, G. Chen, W. Ma, B. Yan and Y. Qi, "Overview of upgrading of pyrolysis oil of biomass," *Energy Procedia,* vol. 61, p. 1306–1309, 2014.

[94] K. H. Altgelt, "Compositional Analysis: Dream and Reality," in *Composition and Analysis of Heavy Petroleum Fractions*, New York, CRC Press, 1993.

[95] ASTM Standards. D6751-12: *Standard Specification for Biodiesel Fuel Blend Stock (B100) for Middle Distillate Fuels.* West Conshohocken, Pa.: ASTM International. 2013.

[96] NREL, "Biodiesel Handling and Use Guide," 2009. [Online]. Available: http://www.nrel.gov/vehiclesandfuels/npbf/pdfs/43672.pdf. [Accessed 2016].

[97] G. C. Laredo, S. Leyva, R. Alvarez, M. Mares, J. Castillo and J. Cano, "Nitrogen compounds characterization in atmospheric gas oil and light cycle oil from a blend of Mexican crudes," *Fuel,* vol. 81, no. 10, p. 1341–1350, 2002.

[98] Z. Guo, S. Wang, Y. Gu, G. Xu, X. Li and Z. Luo, "Separation characteristics of biomass pyrolysis oil in molecular distillation," *Separation and Purification Technology,* vol. 76, no. 1, p. 52-57, 2010.

[99] G. W. Huber and A. Corma, "Synergies between bio- and oil refineries for the production of fuels from biomass," *Angewandthe Chemie,* vol. 46, no. 38, p. 7184-7201, 2007.

[100] Y. Huang, L. Wei, X. Zhao, S. Cheng, J. Julson and Y. Cao, "Upgrading pine sawdust pyrolysis oil to green biofuels by HDO over zinc-assisted Pd/C catalyst," *Energy Conversion and Management,* vol. 115, p. 8-16, 2016.

[101] X. Li, R. Gunawan, Y. Wang, W. Chaiwat, X. Hu, M. Gholizadeh, D. Mourant, J. Bromly and C.-Z. Li, "Upgrading of bio-oil into advanced biofuels and chemicals. Part III. Changes in aromatic structure and coke forming propensity during the catalytic hydrotreatment of a fast pyrolysis bio-oil with Pd/C catalyst," *Fuel,* vol. 116, p. 642-649, 2014.

[102] J. Wildschut, F. H. Mahfud, R. H. Venderbosch and H. J. Heeres, "Hydrotreatment of fast pyrolysis oil using heterogeneous noble-metal catalysts," *Ind. Eng. Chem. Res.,* vol. 48, no. 23, p. 10324–10334, 2009.

[103] N. Koike, S. Hosokai, A. Takagaki, S. Nishimura, R. Kikuchia, K. Ebitanic, Y. Suzukib and S. T. Oyama, "Upgrading of pyrolysis bio-oil using nickel phosphide catalysts," *Journal of Catalysis,* vol. 333, p. 115-126, 2016.

[104] W. B. U. Baldauf and M. Rupp, "Upgrading of flash pyrolysis oil and utilization in refineries," *Biomass and Bioenergy,* vol. 7, no. 1-6, p. 237-244, 1994.

[105] C. Lindfors, E. Kuoppala, A. Oasmaa, Y. Solantausta and V. Arpiainen, "Fractionation of bio-oil," *Energy Fuels,* vol. 28, no. 9, p. 5785–5791, 2014.

[106] J. A. Capunitan and S. C. Capareda, "Hydrotreatment of corn stover bio-oil using noble metal catalysts," *Fuel Processing Technology,* vol. 125, p. 190-199, 2014.

[107] R. Venderbosch, A. Ardiyanti, J. Wildschut, A. Oasmaa and H. Heeres, "Stabilization of biomass-derived pyrolysis oils," *J Chem Technol Biotechnol,* vol. 85, p. 674–686, 2010.

[108] Q. Bu, H. Lei, A. H. Zacher, L. Wang, S. Ren, J. Liang, Y. Wei, Y. Liu, J. Tang, Q. Zhang and R. Ruan, "A review of catalytic hydrodeoxygenation of lignin-derived phenols from biomass pyrolysis," *Bioresource Technology,* vol. 124, p. 470-477, 2012.

[109] J. Remón, P. Arcelus-Arrillaga, L. García and J. Arauzo, "Production of gaseous and liquid bio-fuels from the upgrading of lignocellulosic bio-oil in sub- and supercritical water: Effect of operating conditions on the process," *Energy Conversion and Management,* vol. 119, p. 14-36, 2016.

[110] X. Zhang, Q. Zhang, T. Wang, B. Li, Y. Xu and L. Ma, "Efficient upgrading process for production of low quality fuel from bio-oil," *Fuel,* vol. 179, p. 312-321, 2016.

[111] Z. Yuan, S. Cheng, M. Leitch and C. Xu, "Hydrolytic degradation of alkaline lignin in hot-compressed water and ethanol," *Bioresource Technology,* vol. 101, no. 23, p. 9308–9313, 2010.

[112] Z. Tang, Y. Zhang and Q. Guo, "Catalytic hydrocracking of pyrolytic lignin to liquid fuel in supercritical ethanol," *Ind. Eng. Chem. Res.,* vol. 49, no. 5, p. 2040–2046, 2010.

[113] D. C. Elliott, "Historical developments in hydroprocessing bio-oils," *Energy Fuels,* vol. 21, no. 3, p. 1792–1815, 2007.

[114] X. Huang, T. Korányi, M. Boot and E. Hensen, "Catalytic depolymerization of lignin in supercritical ethanol," *ChemSusChem.,* vol. 7, no. 8, p. 2276-88, 2014.

[115] S. Izhar, S. Uehara, N. Yoshida, Y. Yamamoto, T. Morioka and M. Nagai, "Hydrodenitrogenation of fast pyrolysis bio-oil derived from sewage sludge on NiMo/Al2O3 sulfide catalyst," *Fuel Processing Technology,* vol. 101, p. 10-15, 2012.

[116] A. Douglas, "Method to liberate hydrocarbon fractions from hydrocarbon mixtures". USA Patent US20030051989 A1, 20 Mar 2003.

[117] P. Duan and P. E. Savage, "Catalytic hydrotreatment of crude algal bio-oil in supercritical water," *Applied Catalysis B: Environmental,* vol. 104, no. 1-2, p. 136-143, 2011.

[118] W. Appleby, J. Gibson and G. Good, "Coke formation in catalytic cracking," *I&EC Process Design and Development,* vol. 1, no. 2, p. 102-110, 1962.

[119] Q. Dang, C. Yu and Z. Luo, "Environmental life cycle assessment of bio-fuel production via fast pyrolysis of corn stover and hydroprocessing," *Fuel,* vol. 131, p. 36-42, 2014.

[120] S. R. Fore, P. Porter and W. Lazarus, "Net energy balance of small-scale on-farm biodiesel production from canola and soybean," *Biomass and Bioenergy,* vol. 35, no. 5, p. 2234-2244, 2011.

[121] M. H. Rocha, R. S. Capaz, E. E. S. Lora, L. A. H. Nogueira, M. M. V. Leme, M. L. G. Renó and O. A. d. Olmo, "Life cycle assessment (LCA) for biofuels in Brazilian conditions: A meta-analysis," *Renewable and Sustainable Energy Reviews,* vol. 37, p. 435-459, 2014.

[122] R. Singh, D. Vyas, N. Srivastava and M. Narra, "SPRERI experience on holistic approach to utilize all parts of Jatropha curcas fruit for energy," *Renewable Energy,* vol. 33, no. 8, p. 1868-1873, 2008.

[123] J. Thiagarajan, P. Srividhya and E. Rajasakeran, "A review of thermo-chemical energy conversion process of non-edible seed cakes," *J. Energ. Biosci.,* vol. 4, no. 2, p. 7-15, 2013.

[124] P. Sirisomboon, P. Kitchaiya, T. Pholpho and W. Mahuttanyavanitch, "Physical and mechanical properties of Jatropha curcas L. fruits, nuts and kernels," *Biosystems Engineering,* vol. 97, no. 2, p. 201-207, 2007.

[125] M. Dhanya, N. Gupta, H. Joshi and Lata, "Biogas potentiality of agro-wastes Jatropha fruit coat," *International Scholarly and Scientific Research & Innovation,* vol. 3, no. 3, p. 70-74, 2009.